T.R.
GEBZE TECHNICAL UNIVERSITY
INSTITUTE OF NANOTECHNOLOGY

PREPARATION AND CHARACTERIZATION OF BORON NITRATE REINFORCED POLYMERIC HYDROGEL NANOBIOCOMPOSITES USING MICROFLUIDICS

Burak ERAYHAN
A THESIS SUBMITTED FOR THE DEGREE OF
MASTER OF SCIENCE
DEPARTMENT OF NANOSCIENCE AND NANOENGINEERING

GEBZE
2023

T.R.

GEBZE TECHNICAL UNIVERSITY

INSTITUTE OF NANOTECHNOLOGY

PREPARATION AND CHARACTERIZATION OF BORON NITRATE REINFORCED POLYMERIC HYDROGEL NANOBIOCOMPOSITES USING MICROFLUIDICS

Burak ERAYHAN

A THESIS SUBMITTED FOR THE DEGREE OF MASTER OF SCIENCE

DEPARTMENT OF NANOSCIENCE AND NANOENGINEERING

THESIS SUPERVISOR

ASSISTANT PROF. OSMAN EKSİK

GEBZE

2023

T.R.
GEBZE TEKNİK ÜNİVERSİTESİ
NANOTEKNOLOJİ ENSTİTÜSÜ

MİKROAKIŞKAN SİSTEM KULLANILARAK BOR NİTRAT TAKVİYELİ POLİMERİK HİDROJEL NANOBİYOKOMPOZİTLERİN HAZIRLANMASI VE KARAKTERİZASYONU

Burak ERAYHAN

YÜKSEK LİSANS TEZİ
NANOBİLİM VE NANOMÜHENDİSLİK

TEZ DANIŞMANI
DR. ÖĞR. ÜYESİ OSMAN EKSİK

GEBZE
2023

GEBZE TEKNİK ÜNİVERSİTESİ	YÜKSEK LİSANS JÜRİ ONAY FORMU

GTÜ Nanoteknoloji Enstitüsü Yönetim Kurulu'nun 30/01/ tarih ve 2023/… sayılı kararıyla oluşturulan jüri tarafından 17/05/2023 tarihinde tez savunma sınavı yapılan Burak ERAYHAN'ın tez çalışması Nanobilim ve Nanomühendislik Anabilim Dalında YÜKSEK LİSANS tezi olarak kabul edilmiştir.

JÜRİ

ÜYE
TEZ DANIŞMANI: DR. ÖĞR. ÜYESİ OSMAN EKSİK (Gebze Teknik Üniversitesi)

ÜYE : DR. ÖĞR. ÜYESİ NİHAN AYDEMİR (Gebze Teknik Üniversitesi)

ÜYE : PROF. DR. CEVAT SARIOĞLU (Marmara Üniversitesi)

ONAY

GTÜ Nanoteknoloji Enstitüsü Yönetim Kurulu'nun ……. tarih ve ……/…….. sayılı kararı.

İMZA/MÜHÜR

SUMMARY

The main purpose of this study is to produce boron nitrate (BN) added chitosan (CS) nanobiocomposite hydrogel tissue scaffolds (TS) that aim to be used in tissue engineering (TE) with the microfluidic method and their characterization. TE aims to regenerate damaged tissues with TS. A TS is biocompatible, biodegenerative, bioadhesive, and porous, ideally. The feasibility of popular methods in the production of TS is simple, but these methods lack equally dispersed porous structure formation. Hence, the use of microfluidics has been started. Hydrogel can be produced as a microfluidic bubble with a cross-linker reaction and can be used as an ideal TS. Even though CS has antimicrobial, anticancer, and antioxidant properties to produce hydrogel, its mechanical endurance is weak. Conventional works in the literature show that the addition of BN to CS hydrogel TS increases the compressive strength. However, there is no work in the literature that has been used BN in production of CS and TS via microfluidics. In this study, while BN adding, producing nanobiocomposite hydrogel TS with microfluidic, and characterizing them, comparing this result of characterization with the produced CS hydrogel with both microfluidic and conventional method was aimed. For the realization of these aims, the hydrogels were produced both with traditional methods and microfluidics; FTIR, DSC, TGA, XRD, and SEM characterizations were performed. According to these characterization results, BN adding developed to thermal and crystal structure of CS hydrogel. Our findings show that the novel microfluidic BN-CS hydrogel is promising as a TS in TE.

Keywords: BN, Chitosan, Nanobiocomposite Hydrogel, Microfluidic Method.

ÖZET

Bu çalışmanın temel amacı; doku mühendisliğinde (DM) kullanılması hedeflenen bor nitrür (BN) katkılı kitosan nanobiyokompozit hidrojel doku iskelelerinin (Dİ) mikroakışkan metotla üretilmesi ve karakterizasyonlarının yapılmasıdır. DM, Dİ ile hasar görmüş dokuların yenilenmesini amaçlamaktadır. İdeal olarak Dİ, biyouyumlu, biyobozunur, biyoadhesiv ve gözeneklidir. Dİ üretiminde yaygın yöntemlerin uygulanabilirliği basittir fakat eş düzey porlu yapıdan yoksundurlar. Bundan dolayı mikroakışkan sistemler kullanılmaya başlanmıştır. Mikroakışkan sistemle üretilen polimerik baloncukların bir çapraz bağlayıcıyla tepkimesi sağlanarak üretilen hidrojel, ideal Dİ olarak kullanılabilir. Her ne kadar kitosan, antimikrobiyal, antikanserojen ve antioksidan özelliklere sahip olsa da, mukavemeti zayıftır. Literatürdeki geleneksel çalışmalar yüksek biyouyumluluk, biyoadezyon, antimikrobiyal, termal ve mekanik kabiliyetli BN'e kitosan hidrojel Dİ'ne eklenmesinin basınç mukavemetini ve hücre çoğalmasını arttırdığını göstermektedir. Fakat, mikroakışkan yöntem kullanılarak kitosan Dİ üretiminde BN'lerin kullanıldığı bir çalışma literatürde bulunmamaktadır. Bu çalışmada BN ekleyerek nanobiyokompozit hidrojel Dİ'nin mikroakışkan sistemle üretilmesi ve karakterizasyonlarının yapılıp, bu sonuçların geleneksel bir yöntemle (çözücü dökümü) üretilen kitosan hidrojeller ile karşılaştırılması amaçlanmıştır. Bunun için kitosan ve BN ilaveli kitosan hidrojeller hem geleneksel yöntem ile hem de mikroakışkan sistemle elde edilip, FTIR, DSC, TGA, XRD, SEM karakterizasyonları yapılmıştır. Tüm bu karakterizasyon sonuçlarına göre BN ilavesinin kitosan hidrojelinde termal ve kristal yapı özelliklerini geliştirdiği gözlemlenmiştir. Bulgularımız, Dİ alanında kullanımı açısından BN katkılı kitosan nanobiyokompozit hidrojellerin mikroakışkan metodun kullanılması ile üretilmesinin umutlandırıcı olduğunu göstermektir.

Anahtar Kelimeler: BN, Kitosan, Nanobiyokompozit Hidrojel, Mikroakışkan Metot.

ACKNOWLEDGEMENTS

I would like to explain my pleasure to my supervisor, Asst. Prof. Dr. Osman Eksik, due to his support, suggestions, and encouragement in the ending period of time for my thesis work. Also, I would like to thank Assoc. Prof. Dr. Israfil Kucuk who is the first idea maker for my thesis due to his recommendations and philanthropic support. I also would like to thank Melda Elmas (MSc), Hasan Topaçlı, Ismail Bal and all other researchers who assisted me during my experimental setup preparations.

This thesis study was funded by Project Number 2020-A-101-13 from Gebze Technical University.

Finally, I want to thank my parents, my brother and his wife, and my close friends A. Burak ÖZTÜRK, Ata Barış SAKALLI, Baran UTAN, Denizhan ÇALIŞKAN, and Çağın TOK for their deep love and support.

TABLE of CONTENTS

LIST of ABBREVIATIONS and ACRONYMS

Abbreviations and Acronyms		**Explanations**
AA	:	Acetic Aside
B	:	Boron
BC1	:	0.05% w/v BN- 0.5% w/v CS - 0.5% v/v AA-1% v/v GA conventionally produced nanobiocomposite hydrogel
BC2	:	0.035% w/v BN- 0.5% w/v CS- 0.5% w/v AA – 1% GA conventionally produced nanobiocomposite hydrogel
BC3	:	0.025% w/v BN- 0.5% w/v CS- 0.5% v/v AA - 1% v/v GA conventionally produced nanobiocomposite hydrogel
BC4	:	0.015% w/v BN- 0.5% w/v CS- 0.5% v/v AA - 1% v/v GA conventionally produced nanobiocomposite hydrogel
BN	:	Boron Nitride
c-BN	:	Cubic BN
C=O	:	Carbonyl group
-COOH	:	Carboxyl group
CS	:	Chitosan
CS1	:	0.5% w/v CS- 0.5 % v/v AA- 0.5% v/v A conventionally produced polymeric hydrogel
CS4	:	0.5% w/v CS- 0.5 % v/v AA- 2% v/v GA conventionally produced polymeric hydrogel
CMC	:	Carboxymethyl cellulose
CVD	:	Chemical vapor deposition
DD	:	Degree of deacetylation
DSC	:	Differential Scanning Calorimeter
DW	:	Distilled water
ECM	:	Extracellular Matrix
EF	:	Electrostatic force
FDA	:	Food and Drugs Administration
CC	:	Face-centered cubic

FTIR	:	Fourier Transform Infrared Spectroscopy
GA	:	Glutaraldehyde
GAG	:	Glycosaminoglycans
GO	:	Graphene Oxide
GTU	:	Gebze Technical University
GMBC	:	0.05% w/v BN- 0.5% w/v CS- 0.5% w/v AA - 2% v/v GA microfluidic polymeric hydrogel
GMCS4	:	0.5% w/v CS - 0.5% v/v AA - 2 %v/v GA microfluidic polymeric hydrogel
H_3BO_3	:	Boric acid
h-BN	:	hexagonal BN
HCP	:	Hexagonal-closed-pack
-OH	:	Hydroxyl
m	:	Mass of the solution(g)
MP	:	Mega pixel
MF	:	Microfluidic
N_2	:	Nitrogen
$Na_2B_4O_7$	:	Sodium Borate
N-H	:	Imidogen
$(NH_2)_2CO$	:	Ammonia or urea
NSAIDs	:	Non-steroidal anti-inflammatory drugs
PBN	:	BN-powders
PCS	:	CS-powders
PDI	:	Polydispersity index
PLA	:	Polylactic aside
PMA	:	Polymethyl acrylate
PMMA	:	Polymethyl methacrylate
PEG	:	Polyethylene glycol
PGA	:	25% v/v GA solution
PVA	:	Polyvinylalcohol
r-BN	:	Rhombodhedral BN
SBN	:	1% w/v CS - 1% v/v AA BN added nanobiocomposite solution

SEM	:	Scanning Electron Microscopy
3D	:	Three Dimensional
TE	:	Tissue Engineering
TEM	:	Transmission Electron Microscopy
TGA	:	Thermogravimetric Analyzer
TS	:	Tissue scaffold
TiO	:	Titanium oxide
2D	:	Two Dimensional
3D	:	Three Dimensional
wBN	:	Wurtzite BN
XRD	:	X-Ray Diffraction
ZnO	:	Zinc oxide
c_1	:	Initial concentration (% v/v) of the solution
c_2	:	Final concentration (% v/v) of the solution
d	:	Density
davg	:	Average bubble diameter
m	:	Mass of the solution
ep	:	The mass of empty pycnometer
fp	:	mass of the pycnometer
σ	:	The standard deviation of the mean bubble
v_1	:	Initial concentration of the solution
v_2	:	Final concentration of the solution
v	:	Volume of the solution
v/v	:	Volume per volume
w/v	:	Weight per volume

LIST of FIGURES

LIST of TABLES

1. INTRODUCTION

The human body is an autonomous system composed of billions of molecular nanomachine that are built from DNA code. These nanomachines, which consist of the human body, regenerate certain type of cells, so they can repair damaged tissues. However, the healing capacity of these nanomachines is restricted by lots of factors, including cell type that comprises tissue, degenerative illness, traumatic events, age, and other factors that control the self-repairing mechanism of tissue [1].

On the other hand, according to results of Israni et al.'s recent work reports, the increasing demand for transplantation of tissue and organ is really high [2]. According to World Health Organization's recent data, deaths connected with acute illnesses like ischemic-coronary illness, have been increasing due to lack of tissue and organ donation. Therefore, tissue engineering (TE) has been developing as an engineering field with the ability to support the formation of tissue and organs equivalents or enhance the functionality of damaged tissue or organs while decreasing this restriction, developing tissue regeneration, and so playing a vital role in enhancing functional structures that can replace traditional medical applications [1]. In our country as well as worldwide, organ and tissue failure has been increasing, as have patients waiting to have tissue and organ transplantation who lose their lives while waiting for a proper organ from a corpse or a living donor. As for in vivid patients who are waiting to have tissue and organ transplantation, mitigation at physical activities and, due to their work performance, are affected by the blueprint of treatment that is being applied; work and salary losses or economic losses; dissipation of sexual life; and similar reasons cause hard times for patients and their families. For this reason, tissue engineering is tremendously important for tissue and organ damages and alleviation of correspondingly developing these social and psychological troubles [3].

Tissue engineering, which has been developing day by day, hosts biomaterials, cell biology, cell-material interactions, and the subfield of surface characterization in the structure, which is an interdisciplinary field [4]. Studies in this field basically aim to renew tissue properties and protection; they also consist of generally chosen and isolated cells, tissue scaffolds that build biomaterials, biochemical signal molecules such as proteins and growth factors, and bioreactors that function as support biological

environments, in other words, biomimetic extracellular matrix (ECM), in order to promote cell growth and differentiation [5,6].

A three-dimensional (3D) tissue scaffold (TS), which is a very important component of tissue engineering, plays the role of a platform that provides for the proliferation and attachment of cells with structural support during tissue regeneration. Adhesion of cells to the 3D tissue scaffold surface, being biocompatible with cells, resistible for all mechanic stress factors, and having basic features like biodegradability and porous structure are tremendously important during the tissue regeneration period with regard to cell growth and development [6].

In tissue engineering studies, the design and production of TS are tremendously important. The method that is going to be used in production of TS must both not change the biocompatibility of material and have sufficient sensibility and repeatability [1]. In addition, TS, in order to disperse on a material surface that consists of cells TS and support to grow, must be produce in both a 3D and a porous structural form. In order to produce such as TS, traditional methods such as freeze-drying, solvent casting, and gas foaming have drawbacks like not having proper porous size and geometry, a long production time, and, besides, not producing TS, which has a high deficiency [4].

In the literature, some recent methods such as electron spinning and 3D printing have been developed in order to gain 3D TS with proper tensile strength, which consist of monodisperse and homogeneous pores. With these recent production methods, TS, which has a high porous ratio and pores that have a suitable macro-micro length, can be produced. Tissue scaffolds, which were obtained from the electro spinning method, need to be developed because they do not protect 3D geometry. Furthermore, because production of TS with 3D printing technics requires the use of expensive devices and the control of these device, the production process takes a huge amount of time. In addition to this, produced tissue scaffolds biomolecular permeability, solubility, and adhesion of cells to TS are very weak, and the production of more functional tissue scaffold has different challenges. For all these reasons, studies on the production of TS, which provides the organization of cells that are specific to our tissues in micro-scale homogeneous pores and the alignment of these pores regularly, have maintained their importance as valuable research topics in recent days. With microfluidics, pores can be formed via gas-trapped foam-like bubbles. Obtaining these bubbles and pores

can be possible with microfluidics designs that have different geometric-shaped connection systems [7–9].

Microfluidics are widely used systems and advanced in the point of view that is currently receiving much attention for the producing of polymeric bubbles with narrow size distribution and bursting of the bubbles due to its attractive advantages such as environmental and cost effective preparation over the other methods aspect of easy and effective control of liquid flow and gas pressure [8,10].

In microfluidics, different shape of microfluidic (MF) platforms are used depending on the conjunction point where polymeric and gases meet, which are generally T-junction, V -Shaped, co-flow, and flow focusing. When the polymeric solution meets gas at the conjunction point, bubbling occurs, and polymeric bubbles are produced [11]. In the study of Kucuk et al, larger MF bubbles were produced by using T-Shaped MF [12]. These bigger bubbles have potential use as an ECM-like material when we crosslink and freeze-dry them [13,14]. Due to this reason, a T-shaped device was used in this thesis study.

Polymeric bubbles are two-phase lightweight materials that build up from gas-trapped polymeric solutions [15]. If these bubbles crosslink via a crosslinker agent, sponge-like porous hydrogels are produced. This hydrogel, which was recently designed and produced by microfluidics, constitutes proper structure for cells due to the formation of gelled bubbles, and these bubbles have monodisperse properties at the microscale. Also, in these monodispersly ordered pores structures, mechanical endurance is high due to the distributed pressure applied to the surface on the whole hydrogel surface [16,17].

All of these properties enable the use of MF hydrogels as high-performance tissue scaffolds. Hydrogels are materials that can be designed to have 3D geometry, be functional, and be reconstructible. These materials comprise hydrophilic polymers that are held together by intermolecular interaction. They can absorb a huge ratio of biological fluids that can swell easily without being dissolved. This related to the fact that these materials have high hydrophilic features, especially chemical groups of hydrophilic parts such as carboxyl, amide, amino, and hydroxyl, which were disturbed along with polymeric chain backbone [17].

Hydrogels are biochemically similar to extracellular fluidic that cover cells and are especially attractive as a tissue scaffold material for tissue engineers [18]. But

commonly used polymer-based hydrogels, due to their self-solid forms, especially in areas of use for hard tissues such as bone and cartilage, need improvement in their mechanical strength. Synthetic polymers such as polyethylene glycol (PEG), polyvinyl alcohol (PVA), poly methyl acrylate (PMA), poly lactic aside (PLA) or natural biopolymers such as alginate, cellulose, collagen and chitosan are preferred as TS platform in the production of hydrogel-based materials. However, synthetic polymers have a toxicity risk, and their bioadhesive talent is weak; nevertheless, the mechanical properties of natural biopolymers are weak according to synthetic polymers [19,20].

Chitosan polymer, which is a polysaccharide within natural biopolymers, has better mechanical properties. Besides, its bioadhesive talent is high [21,22].

Chitosan is a natural heteropolysaccharide that is produced partly or relatively deacetylated from chitin, which was first described in 19th century by Bradconnot. Chitin, which naturally occurs in shellfish's external skeletons like lobster, crab, and some cell membranes of bacteria and fungi cells, is known as the most abundant type of polysaccharide after cellulose in nature. Even though chitin can be produced from a variety of resources with easy productivity, which makes it convenient for usability as a biomaterial, chitin is needed to convert chitosan because it hardly dissolves in water solutions. Chitosan, which has especially high bioadhasive properties and is biocompatible and biodegradable and consists of glucosamine and N-acetyl glucosamine units copolymers linked with B-1,4 glycosidic links, is extensively used in drug, cosmetic, wound dressing, biochemical separation systems, and tissue engineering. Together with this advantage, other positive properties such as hydrophilic and net cationic charge make chitosan a more suitable polymer for the delivery of cell growth factors, steam cells, and other active components such as peptides [22,23]. But even chitosan polymers cannot meet the proper requirements for mechanical strength like other natural polymer materials. Prevention of this unwanted situation can be possible by providing the opportunity to make this material more resistant to mechanical stress via synthesizing two-dimensional (2D) ceramic materials as nanoparticles while applying nanoengineering methods and later via increasing the surface area on its porous surface [24–26].

In recent times, in order to produce TS, double-layered hydroxide, titanium oxide (TiO), graphene oxide (GO), zinc oxide (ZnO), black phosphor, boron nitride, and metal organic structure scaffolds have been used as 2D nanomaterials. All of these

materials have been shown to have suitable mechanical strength, cell adhesion, and biodegradable properties. However, 2D materials that include metal ions and graphene, which does not include metal ions, carry toxicity risks that have been noted [27,28].

Boron nitride (BN), known as ceramic, is composed of boron and nitrogen atoms and has superior electrical and thermal properties [29]. This compound has superior physical and chemical properties, and at the same time, it has been placed as a proper material for tissue engineering applications due to its antimicrobial, antioxidant, anticarcinogenic, biodegradable and bioadhesive properties [30–32]. For instance, in the work that done by Emanet et. al [24], they observed that the addition of BN increased mechanical strength of chitosan tissue scaffolds and also materialized that much more cells proliferated and attached to the surface of the TS in a better way.

It’s known that microfluidics provides important advantages in the usage of tissue engineering applications such as cell encapsulation and counting, controlled delivery of biochemistry, and production of TS. Although most TE applications have been done successfully with this method, the use of solutions with low viscosity makes it difficult to produce desired tissue scaffolds that have suitable mechanical properties due to nature of this method. As a parallel with this, reducing the time of biodegradation of tissue scaffold restricts usage, which requires high magnetic strength and a long healing time of tissue [7,9,33].

With this thesis, in order to minimize these restrictions, BN's, which were proven to support cell proliferation and biocompatibility with previous studies, will be dispersed in chitosan solution while dispersing nanobiocomposite foam with gas-based T-shaped microfluidics. After that, production of sponge-like TS platforms will be materialized while gelling with a crosslinking agent, which is glutaraldehyde (GA). Furthermore, with this method, tissue scaffolds platforms will be produced at a lower price, in less time, and in an environmentally friendly manner.

1.1. Tissue Engineering and Nanotechnology

Tissue engineering (TE) is an interdisciplinary discipline that focuses on the renewal of biological nanomachines (such as enzymes, proteins, and biomolecular signals) in order to integrate biology, engineering, nanoengineered materials, and

medical sciences, naturalize damaged tissue or organ functions, or give new functions to existing tissue or organs in future. This interdisciplinary engineering aim to renew, preserve, or make the tissue more functional [1,34]. This term was first described by Professor Robert Nerem in 1988 at UCLA Symposia on Molecular and Cellular Biology as *"the application of life sciences and engineering to develop a basic understanding of the functional and structural relationships of natural and pathologic mammalian tissues and the development of biological substitutes that can be utilized to restore, maintain, or improve tissues damaged or lost by various disease conditions"* [35].

Tissue engineering mainly consist of: 1. cells that proliferate and differentiate, such as stem cells and their precursors; 2. natural nanomachines that are bioactive molecules, such as growth factors, that provide these cells with the ability to differentiate and proliferate; and 3. tissue scaffolds that provide structural support for cells. Different tissue engineering approaches have been embarked on depending on whether these key components are applied alone or in combination. The key components of tissue engineering are shown in Figure 1.1. Different tissue engineering approaches were applied depending on these main components. These three main approaches that are used in tissue engineering are: isolated cells or cell substitution; tissue inducers such as growth and differentiation factors that send items to their intended destination; and cell implantation that grows in their dimensional structural scaffolds in order to develop cells that provide the necessary processes. These approaches were chosen based on damage to not properly functioning tissue in the applications. For instance, while cell treatment approaches can provide tissue repair in tissues with reduced function depending on cell deformations, they are not sufficient for tissue regeneration in situations where tissue damage is more prevalent. Using cytoskeleton structure from three structure generally produces more successful results. In this approach, tissue scaffolds have tremendous importance [5,36].

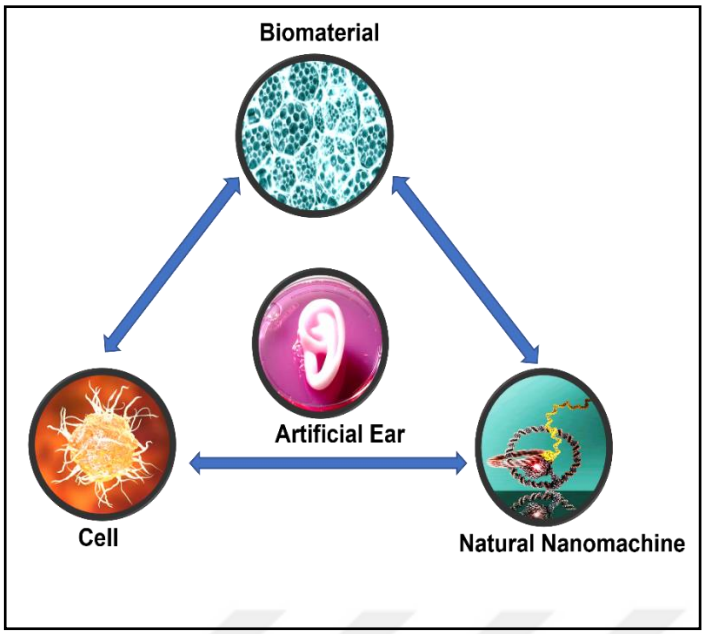

Figure 1.1. Main components of tissue engineering [1, 122, 123,124,125].

Our cells are surrounded by extracellular matrix (ECM), which is characterized by a natural network of hierarchically arranged with nanomachines (such as proteins, biosignal molecules and enzymes) and nanostructures. Integration of these nanostructures provides biomechanical and biochemical support for the cell, determines cell behaviour, and specifies the cell behaviour with the ECM [1,22]. On the other hand, creating a natural ECM like a biomimetic nanoengineered environment in order to promote cell growth, proliferation, and migration is essential in the TE applications. In this concept, the integration of nanostructures provides support for the cell and determines the cell's behaviour with the extracellular matrix. Nanomaterials play an important role in stimulating cell growth and tissue regeneration [1, 36, 37].

1.1.1. Extracellular Matrix

Living tissues consist of cells and their surrounding nanostructured protein-based matrix. This surrounds a nanostructured protein-based matrix called extracellular matrix (ECM). In order to produce biomimetic nanobiocomposite material for tissue engineering application, molecular structure, biomechanical, physicochemical events in ECM must be well known due to providing a proper biomolecular and biomechanical environment for cell growth [38]. ECM can be

thought of as the steel and concrete of a skyscraper that provide mechanical strength to buildings; however, unlike the static structure of skyscraper, ECM is regularly degraded, synthesized, and produced by cells in both healthy and diseased conditions [39, 40].

The cells sense mechanical forces of ECM by their transmembrane receptor protein, termed integrin. Integrins are composed of two α and β subunits, which are heterodimeric proteins that connect the ECM to the cell's actin cytoskeleton. This issue regulates cell life processes from adhesion, differentiation, proliferation, and migration in order to realize programmed cell death due to the extensive network of matrix components and their interaction with signalling factors and cell membrane receptors [39].

The ECM is composed of more than 300 proteins, but it is mainly composed of collagen, elastin, proteoglycans and glycoproteins. Collagen account for 30% of all proteins in vertebrates and is a major ECM components composed of three same (homotrimers) or different (heterotrimers) polypeptide chains. Because of their biomolecular organisation, fibrillar and non-fibrillar collagens are distinguished. Non-fibrillar collagens constitute shorter helical domains interspersed with so-called telopeptides, i.e., non-helical domains. Collagens play an important role in cell adhesion (as ligands of cell receptors), cell migration (contact guidance), and tissue reconstruction and remodelling. Even though collagens are present in most body tissues and affect their mechanical properties, their distribution varies. For instance type 1 collagen is mostly seen in bone, skin and tendon [20, 36, 40].

The ECM also constitutes a hydrophobic fibrillar protein, which is elastin. It owes its characteristic elastic properties to extensive covalent cross-linking of the structure. They are commonly secreted from fibroblast, smooth muscle cells, endothelial cells, respiratory epithelial cells, keratinocytes and chondrocytes. Elastin forms by cross-linking the reaction of lysine and allysine residues with trophoblastic molecules by Schiff base reaction or the aldol condensation of two allysine residues. This fiber protein plays an important role in the stretching of tissues, which are also important component of blood vessel walls, skin, lungs, heart, bladder, tendons, ligaments, and elastic cartilage tissue [14, 36, 41].

Proteoglycans are macromolecules of a complex 3D structure that are composed of a protein core covalently linked to one or more chains of glycosaminoglycans

(GAGs), a type of unbranched, linear heteropolysaccharides. Their chains are built by repeating disaccharide units, where one residue is uronic acid. In addition, GAGs alters the type of monosaccharide residues, the geometry of the linkages between the constituent units (α and β glycosidic linkages), the degree of sulfation of the polysaccharide backbone, and the position of this substitution. Heparan/heparan sulfate, keratan sulfate, chondroitin sulfate/dermatan sulfate, and hyaluronic acid are four basic groups of GAGs according to the chemical structure of the chain. Unlike other GAGs, hyaluronic acid does not form covalent bonds with proteins. Hyaluronan has excellent water retention. It is abundant in the skin, cartilage, brain, synovial fluid, vitreous body,and umbilical cord, which shows remarkable viscoelasticity [20, 36, 39].

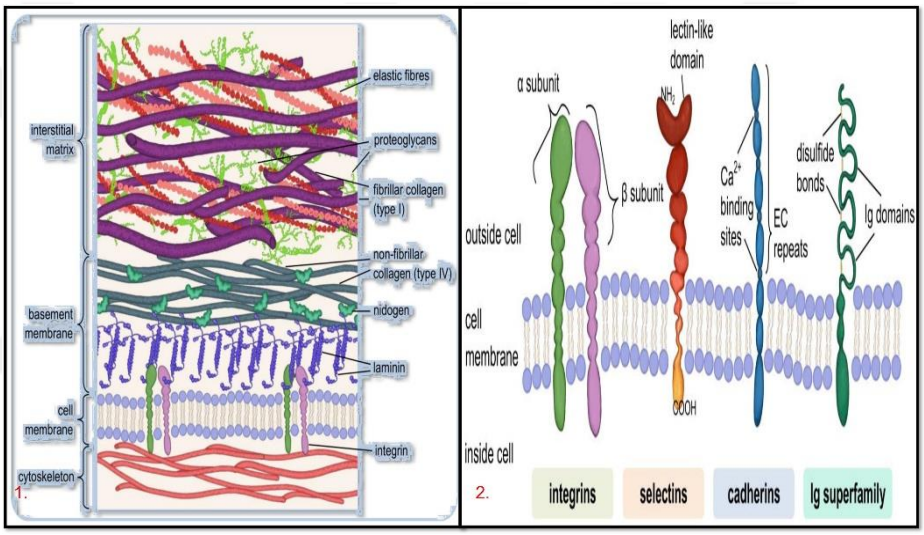

Figure 2.1. 1. Basic ECM and its nanostructure, **2**. Main cell membrane proteins [39].

Glycoproteins are composed of covalently linked protein and carbohydrate parts, of which the saccharide is much shorter, does not contain repeating units, and is usually branched according to proteoglycans. This protein family often act as connectors in the ECM, as they have functional groups capable of binding other proteins, growth factors, or receptors. Their existence is important for many biological processes: immune, fertilization, inflammatory response, blood coagulation, and wound healing. Fibronectin and laminin are the most important types of glycoproteins [14, 36].

1.1.2. Tissue Scaffolds

Developing three-dimensional (3D) structural or matrix structures that stimulate cells is one of the main goals of TE in order to create functional tissues. 3D tissue scaffolds aid cell adhesion and proliferation during tissue regeneration by providing structural support to cells. This tissue scaffold substantially provides a physical environment in order to provide a porous structure for tissue development and cell growth. In addition to this, TS must provide an environment where cells can protect their phenotypes and synthesize their proteins and molecules. For this reason, TS production must be different according to each type of tissue and cell [3,45].

In tissue engineering studies, while producing TS, economic and commercialization potential are also important, as are providing biomimetic structural features. In this concept, an ideal TS for TE applications must improve or allow cell viability, cell adhesion, cell proliferation, tissue differentiation, and other features. All of general features of TS for tissue regeneration are listed in Table 1.1 [37].

Table 1.1. General features of TS for tissue regeneration [40].

Tissue Scaffold for Tissue Regeneration			
Biological talents	**Composition**	**Manufacturing**	**Structural Features**
Non-toxic	Ceramics	**Conventional**	Biomimetic
Biocompatible	Polymeric	Freeze-Drying	Customize shape
Biodegradable	Composites	Solvent casting	High porosity
Non-immunogenic		Gas Foaming	Pore interconnection
Bioactive		**Advanced:**	
		Electrospinning	
		3D printing	Mechanical Properties
		Microfluidic	Surface Topography

1.1.2.1. Biocompatibility

Biocompatibility as a word has two roots: bio, *"a word-forming element meaning life''* and compatibility, which means capable of existing in harmony. Recently, the word *"biocompatibility"* was defined as *"the ability of a material to locally trigger and guide the proteins and cells of the host toward a non-fibrotic vascularized reconstruction and functional tissue integration.''* by Crawford et al. [42].

In our body, our cells and tissues organized in 3D micro-and nanoarchitecture. For this reason, an ideal TS must be similar to the natural environment where our cell live. In this concept, TS must be biocompatible first [43]. The cells must attach to the surface of the TS and must properly grow and migrate before the formation of new ECM. After implantation, TS must cause an inflammatory reaction as well as rejection from the body, which may reduce healing [1, 44].

1.1.2.2. Biodegradability

In order to cure tissue or organ loss or damage, non-degradable implants are used in general medicine. But non-degradable materials tend to have adverse effects such as irritations and infections. Also, removing the temporary implants requires secondary surgery. Thus, recent research interest has emphasized biodegradable materials, showing promising aspects for surgeons by allowing the patient to reduce the cost of device retrieval and physical pain [45].

Biodegradation talent is of unique importance in nano-engineered tissue scaffold since it must be coordinated with tissue generation in order to build up enough to effectively sustain the mechanical stresses in the tissue environment. Significantly, the by-product of biomaterial degradation must not be toxic to get rid of an immune response and be extractable through our body's functions. The biodegradation rate of TS is therefore of utmost importance because it is connected with tissue viability. Specifically, if biodegradation of TS occurs faster than native tissue regeneration, the cells could lack biomimetic ECM-like structure, the formed tissue will be unfeasible and defective, or the produced by-products cannot be expeditiously ejected from the body. At same time, too slow TS degradation may result in scaffold encapsulation,

poor integration, or rejection from the host tissue, triggering an immune response [44, 46].

In addition to all these, implant location and patient's age, gender, and other illness also affect the rate of TS degradation. The degradation rate of polymeric TS is highly parallel with the material composition, the polymer molecular architecture (e.g., aromatic groups, side groups, double or triple bonds, and crosslinking), and the fabrication method (e,g., blending and copolymerization), which control the degree of chain scission and modulate it in TE applications. Crosslinking of polymer reduces the biodegradation rate of TS. Incorporation of nanoengineered material into TS plays the role of bioactive sites and increases the degradation rate, although some studies have shown the opposite effect [1,47]. All of factors which effect biodegradation mechanism of TS are shown in Figure 1.3.

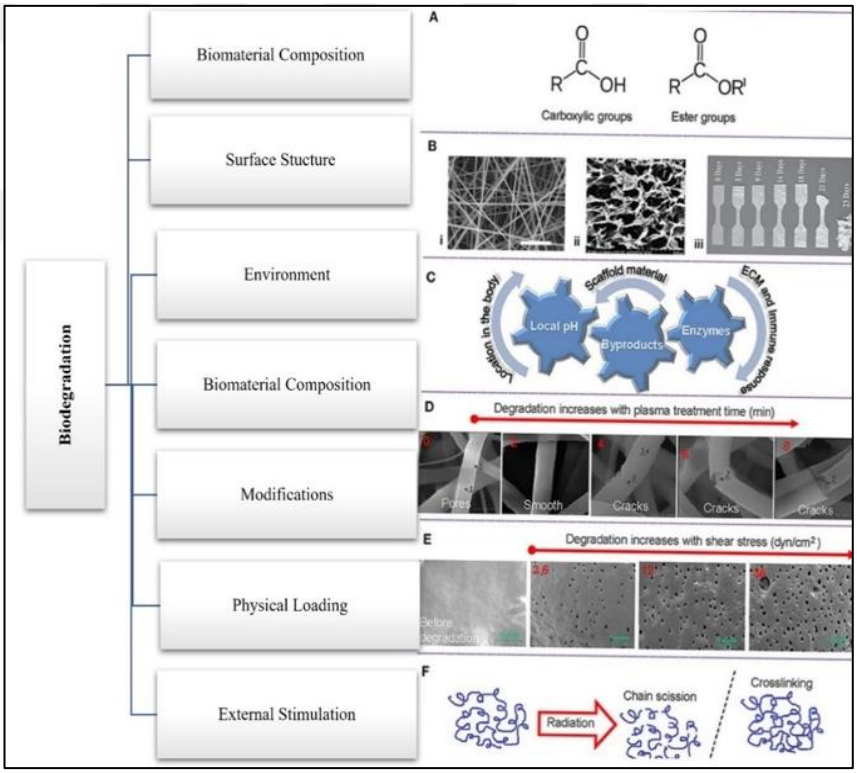

Figure 1. 1. Important factors which effects biodegradation mechanism of TS [1].

1.1.2.3. Porosity

In a recent review, Hernandez et al. defined porosity as *"the voids of material"*. Porosity is characterized by the throats, or interconnections, between pores and the walls or struts of the medium, which forms the 3D structure. Properties of throats, pores, or struts are classified by their organization, shape, size, homogeneity, and density. Conventionally, the pore scale is described as microporous when greater than 50 nm, mesoporous between 2 nm and 50 nm, and microporous when smaller than 2 nm. Also, the term "nanoporosity" is used to delineate materials within the range of nanoscale, with diameters of pores between 1 and 100 nm. In common porous materials, tubular, spherical, and random pore structures are commonly observed, in spite of novel fabrication methods continuing to develop complex, high-resolution geometries and even materials with transforming topologies. The geometry of these pores and their interconnection zones is further defined as either open, closed, or blind-ended [13].

Porosity, void and struts size, and pore geometry tremendously effect the mechanical properties of materials such as TS. Compressive strength, which is defined as "the capacity of a material or structure to withstand load bearing", highly depends on the porosity and geometry of voids. An increase in porosity decreases the strength of the material. From the point of view of pore geometry, the triangular pore of TS possesses the highest surface area and highest compressive strength, whereas the scaffold with high porosity has the lowest compressive strength, which is the circular pore of TS. But the highest specific strength (strength-to-weight ratio) value of TS is observed in hexagonal geometric shapes. This shows that TS that possess hexagonal voids can resist more bending force, which means that hexagonally shaped porous TS provide the best biomechanical platforms for cells and natural nanomachines for TE studies [48, 49]. In tissue engineered TS, pores are characteristically intended to facilitate the entrance of oxygen and nutrients to cells, cell migration, and the expulsion of metabolic wastes[1,13]. For this reason, the porosity and voids of the porous structure of TS must be well balanced. In more detail, larger void sizes decrease intercellular interactions and thus cell proliferation. On the contrary, inadequate void size causes weak cell permeability, preventing the transport of nutrients and metabolic waste and the formation of blood vessels [50]. For example, in the study of Xie and

co-workers, small pores in TS have three times the cell proliferation capacity of large pores in TS [51]. Void size and distribution have not only key importance for well-cellular behaviour but also play an important role in the secretion of ECM. ECM secretion greatly depends on pore size. For this reason, each TS possess a critical pore size range that can change depending on cell type and tissue type [43]. For instance, the optimal pore size for skin cell is 20-125 μm, for fibrocartilaginous tissue ,150-300 μm, for smooth muscle tissue cells, 60-150 μm, and for osteogenic cells, 100-150 μm, respectively [52].

Porosity improves tissue healing responses and decreases scar tissue growth. Protein absorption is highly dependent on the utilized material but is also increased by surface roughness. The increased rate of absorption is also parallel with the surface area to volume ratio of TS. Therefore, greater porosity may induce greater protein adhesion [13]. For instance, in the study of Jansson and co-workers, titanium surfaces with pores between 0.2-0.3 μm absorbed two to eleven times more protein (albumin and IgG) than smooth titanium surfaces [53]. However, this effect can be different at the scale of protein size, as was shown in a study by Richert and co-workers. In their study, titanium-based nonporous surfaces with a mean pore diameter of 0.011μm promoted different enzymes and proteins (lysozyme, fibrinogen and human growth/differentiation factor 5) binding and decreased absorbance of bovine serum albumin, IgG, fibronectin, and collagen as compared to nonporous surfaces [54].

The porosity of TS also may affect immune response. When the pore and strut size increase, more immune cells (macrophages) attach to the surface of TS. But the reduced pore size, reduces the attachment of immune cells. For instance, in the study of Garg and co-workers, polydioxanone materials with randomly conformed pore diameter averaging between in 2 μm, 22 μm, and 30 μm, which increase with strut diameter, resulted in greater immune cell attachment (M2 macrophage attachment) [55].

1.1.3. Production Method of Tissue Scaffolds

1.1.3.1. Solvent Casting/Particle Leaching

Solvent casting is technique of preparing porous TS by dissolving particles of different sizes and particle numbers. As pore-forming agents, sodium chloride particles, sugar-particles, ice particles, and paraffin microspheres have been used. This traditional solvent casting/particle leaching method is a popular one that controls the porosity and pore size structures by dissolving different numbers and sizes of particles. Solvent casting or particle leaching does not require specialized equipment and is a simple process. But this method is often difficult with large or thick volumes of materials. Also, it is difficult to choose a particle size for high-porosity TS, and it is difficult to maintain good mechanical properties. Even more, the pores in the TS are not connected, the TS thickness is limited, and there are residual particles in the TS that produce pores [50,52].

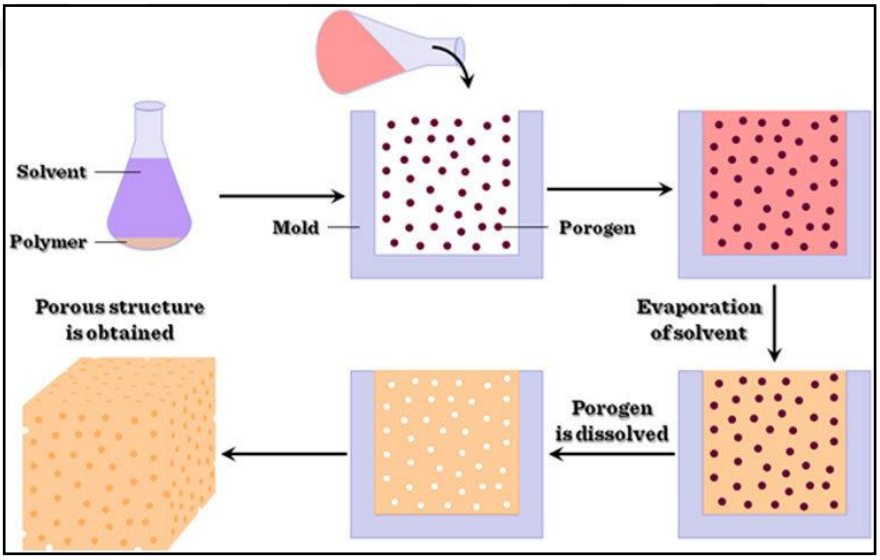

Figure 1.4. Systemic illustration of solvent casting/particle leaching method [52].

1.1.3.2. Freeze-Drying

The freeze-drying method is commonly used in the producing of TS, which has porous structures. This method can eliminate the drawbacks of restricted thickness and unconnected pores in solvent casting and particle leaching [50].

Freeze-Drying (or lyophilization) transforms solutions into sponge-like solid materials, as sl in Figure 1.5, in four steps: pre-treatment, freezing, primary drying, and secondary drying. In the first phase, treatments are applied in order to improve the precursors' stability while the process is being realized, preparing the prepared precursors to be ready for the freezing steps. In this concept, a polymer solution is cooled down to below the triple point of the solvent crystals, and the polymer provides a controlled network within the interstitial voids. The final phase is divided into two steps in which the solvent in frozen and unfrozen components is removed by sublimation as a first step and evaporation as a second. Pressure and temperature cycles are accurately controlled during the whole process to avoid structural damages of the produced TS and achieve an interconnected porous structure [56].

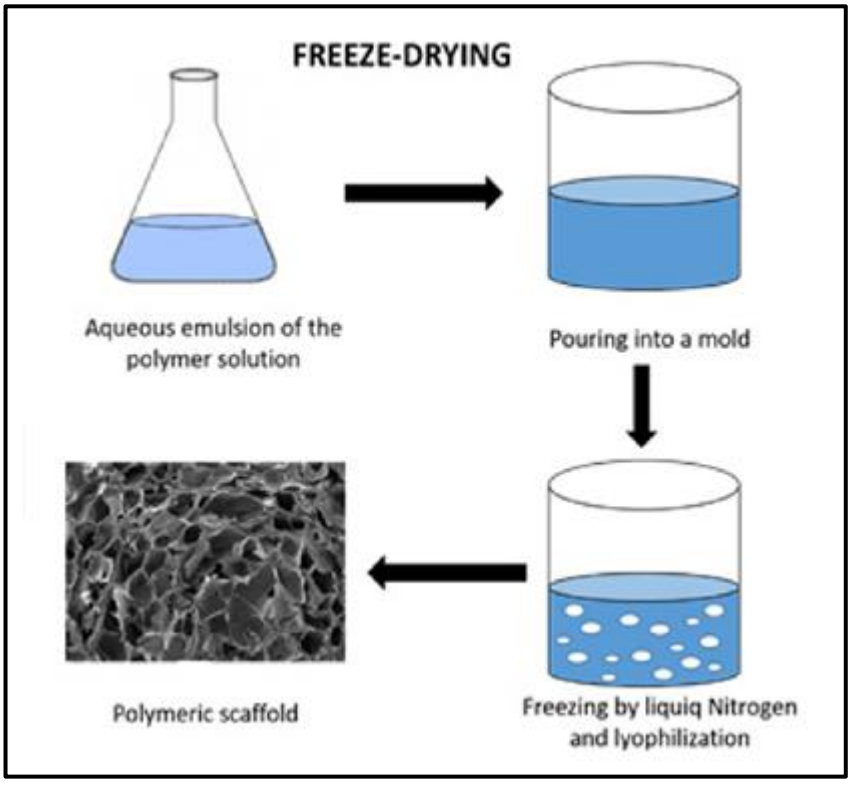

Figure 1.5. Systemic illustration of Freeze-Drying method [56]**.**

The pore structure of freeze-dried TS can be designed and customized by controlling the formation of ice crystals during cooling. With this method, the distribution, size, shape and density of ice crystals can be controlled by changing the freezing parameters, which means that the void size, gradient, porosity, and shape of the freeze-dried TS can be customized. With this method, porous sponge-like TS can be produced. Freeze-dried porous TS have uniform pore size, high water absorption, high porosity, retention capacity, and proper degradation rates. This TS can protect pore structure during the whole process, providing effective cell support and attachment for tissue healing [50,52].

Freeze-drying production of the TS allows customisation of the aperture, gradient, shape, and porosity. The porous structure of the TS can be adjusted by changing the freeze-drying temperature, used material and its concentration, and freezing speed [56]. However, the produced pore structure is not regular as desired, and freeze-dried TS is weak for more complex biomimetic vascular structures in terms of porosity [50,57].

1.1.3.3. Gas Foaming

Gas foaming is an efficient, green method to produce porous materials; CO_2 and N_2 are inexpensive and readily available, with no residue after foaming. This is a method, where it is possible to avoid organic solvents and pores, which are produced by gas dilation. As pyrogen gases, CO_2 and NH_2 are commonly used. Even though this method affords highly porous foam (pore size of 100 μm) with a porosity of up to 93%, the pore interconnection, especially on surface of TS, is low, at only 10%-30%. Open-pored TS can be produced by using the gas foaming/salt leaching method. With a combination of these two methods, macroporous TS structures with interconnected pores of 100-500 μm may be produced where cells can be seeded and their viability is high [50].

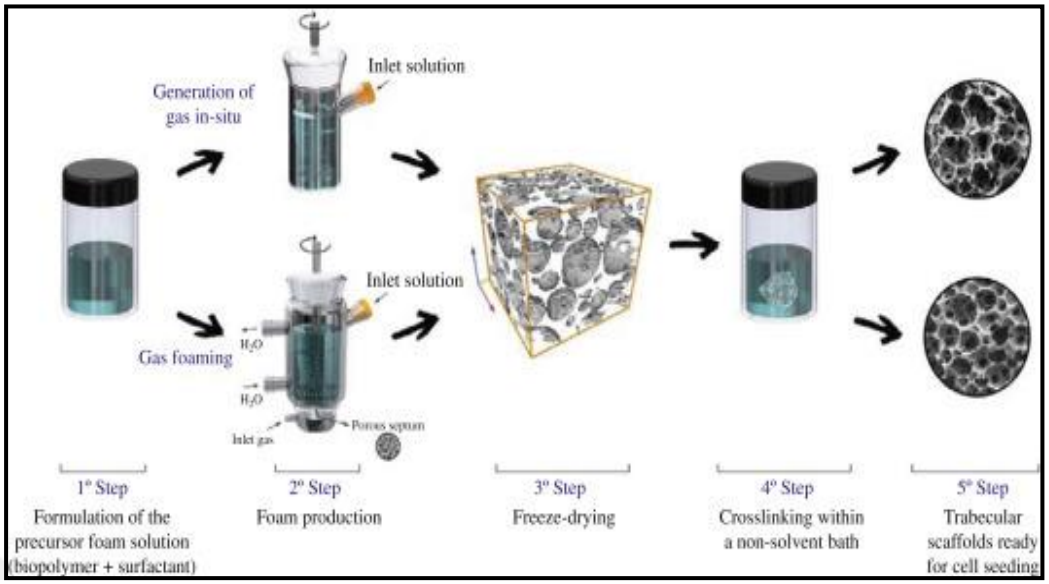

Figure 1.4. Systemic illustration of gas foaming method [52].

1.1.3.4. Electrospining

Electrospinning is an extensively used method in many research fields, especially in the TE fields; it can generate fibres from millimetres to nanometres in diameter that have a high surface area to volume ratio and a swelling talent. The electrospinning system uses a strong electric field to process polymer solutions into thin and continuous polymer fibers [50,58].

This technique take advantage from the ability of using a high electric field to produce ultra-fine polymeric fibres. A electro-physical activity between the electrostatic force (EF) and the polymeric solution is the main mechanism behind this technology. In electrospinning, a high-voltage electric field is generated between the injection needle and the collecting screen using a electrodes and power supply. After forcing out of the polymer solution, a hemispherical solution droplet is shaped at the tip of the needle. This droplet lengthens into a conical form, and the surface charge of the polymer droplets increases with time by increasing the voltage. Than a polymeric jet starts to for suddenly after overcoming the surface charge of the polymer droplet. After vaporizing the solvent in the jet, the surface charge on the jet increases, and so destabilizes. This polymeric jet is geometrically segregated, initially into two jets and, eventually, into a large number of jets, to counterbalance for the instability. The EF,

which affects the constantly splitting polymer droplets causes the nanofiber patterning. Besides, a spinneret with a metallic needle, a syringe pump, a high-voltage power supply, and a grounded collector are the major constituents of a standard electrospinning system [58].

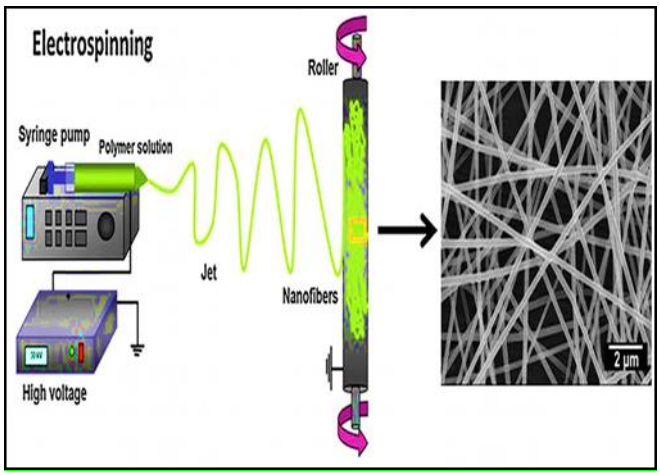

Figure 1.6. Systemic illustration of electrospinning method [58].

With this methods, nanofibrous TS can be produced, which is quite surprisingly similar to the ECM microstructure. Also, these advanced nanofibrous TS possess cell attachment, proliferation and differentiation properties. Considering these properties, electrospun nanofibrous scaffolds are capable of providing a wide range of functions needed for TE applications. Sadly, this method has drawbacks. This technology needs high-voltage apparatus. Also, used solvents may be toxic. In addition, the pore size of nanofibers is too small, and the pore structure is not regular for tissue formation [11, 58].

1.1.3.5. Three Dimensional Bioprinting

3D printing technology has high intelligence processing, good controllability, and a fine structure when compared with traditional method. 3D-printed porous structures requires a CAD model to be designed in advance; the morphology characteristics, size, and porosity can be designed according to the requirements of the designing software, as shown in Figure 1.8. 3D bioprinting technology is an important branch of 3D printing technology, but it involves extra complexity, including cell

types, bio-inks, the selection of bioactive molecules, and technical challenges correlated with the sensitivity of living cells and complex tissue structures. Inkjet, micro-extrusion, and laser-assisted are the main types of bioprinting method. 3D bioprinting is a new technology for cell delivering from polymer gels to damaged tissues [50].

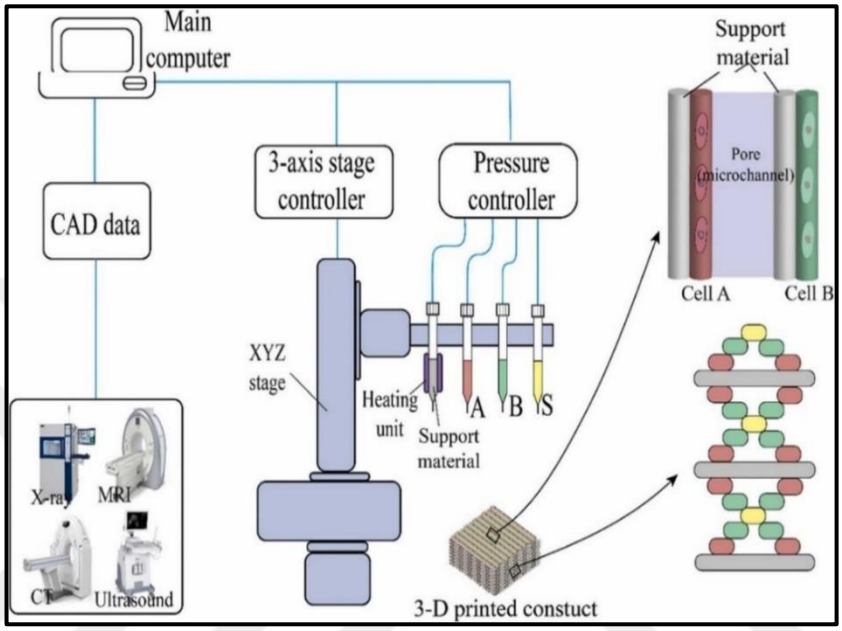

Figure 3.8. Main parts of 3D Bioprinting [50].

The bioprinting variables must be distinctly adjusted during the bioprinting process to produce the best product. The variables include nozzle diameter, extrusion pressure, dispensing speed, printing speed, and bio-manufacturing time. Bio-manufacturing time determines the embedding of cells in bioprinting according to the printing needs of bio-inks, which are determined by their mechanical properties, cross-linking mechanism, and 3D bioprinting parameters. The deposition of bioinks is adjusted with micron-scale precision in order to form tissue ultrastructure; 3D bioprinting provides an ideal spatial distribution of cell-loaded tissue scaffolds [50].

3D bioprinting, when compared with other techniques, has the clear advantage that TS can be designed precisely in terms of the pore shape, pore size, arrangement, and form, as the final pore structure is not dependent on an emulsion, thermodynamics (the matrix pore forming agent distribution), fluid mechanics, or a random event (gas foaming and electrostatic spinning). However, the 3D bioprinting process has few

adverse effects on cell survival. CAD may only design regular microporous forms, whereas our tissues are irregular, with a variety of porous forms in different locations. Sadly, large solid particles are challenging in practice [50]. Also, this method requires control of expensive device, and production of TS takes much longer according to other method [11].

1.2. Microfluidic Technology

Microfluidics is defined as "the science of fluid mechanics at the microscale, guides microfluidic device design and its applications in biology, chemistry, and physics" in the critical review of Li and co-worker [33]. Contrasted with the other method the novel microfluidic (MF) technology shows unique advantages in assisting the fabrication of natural polymer based materials, which provides the controllable production of various microstructures with controllable size, shape and functions. Specifically, MF usually relates to a technology for manipulating and processing tiny fluids (generally $1x10^{-9}$ L ~$1x10^{-18}$ L) with channels of ten to several hundred micrometres or nanometres in size. Due to the large specific surface area, small size, and high mass transfer and heat transfer performance of the microchannels and MF porous products, MF technology possess plenty of advantages, such as less reagent or sample consumption, high mixing efficiency, fast response, and precise control of fluid physicochemical properties, that can help overcome disadvantages involved in conventional fabrication methods. This technology is widely used in important fields such as food engineering, material science, aerospace science, and even forensic science [59–61]. Besides, the fabrication environment can be biocompatible, so MF technology shows great promises in developing various biomaterials with different structures and functions. In other words, MF devices have been widely used in bio-applications of diagnostic and detection thanks to their significant advantages, such as low reagent consumption, fast analysis, and high capillary electrophoresis separation efficiency, associated with their inherent miniaturization, portability, integration, and automation [62, 63].

1.2.1. Producing Tissue Scaffolds Based on Microfluidic Technology

There are plenty of ordered porous TS, such as 2D films and 3D foams, nanofibers, and microparticles. This thesis mainly introduces 3D foams. 3D foam-like TS are actually sponge-like solids with an open-pore structure, which are produced by the solidification of liquid polymeric foams. Foaming platforms are usually used to prepare the solid foams, and the geometrical structure of platforms is of key importance for the foams, as shown in Figure 1.9 [11].

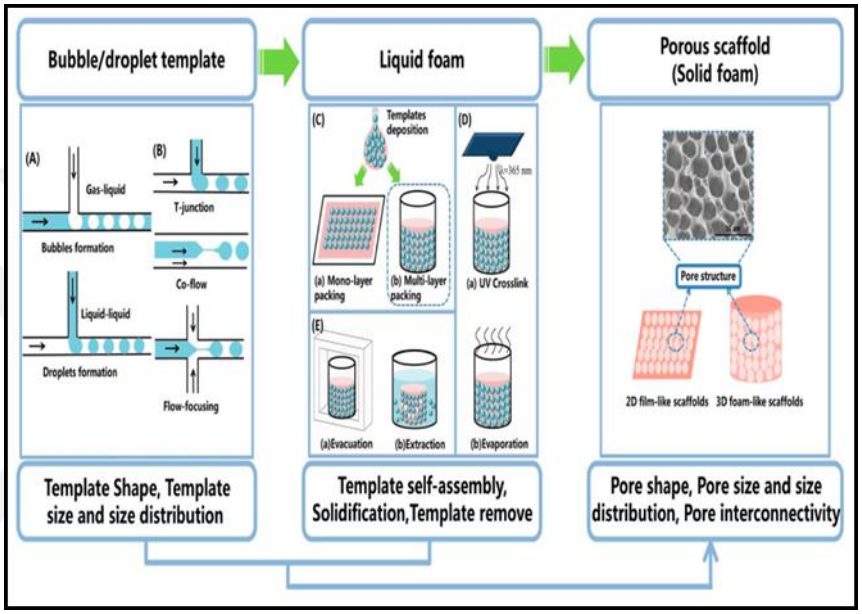

Figure 1.9. Demonstrating **1.** Bubble/droplet formation, **2.** Liquid foaming, **3.** Solid foam forming [11].

The primary superiority of the MF platform is its monodispersity, and the production of these platforms is exactly adjusted in a passive or active manner, which is a key point to well-ordered porous TS preparation, especially for TS with unique structure requirements. Depending on the flow behaviours (surface tension, viscosity and contact angles) of polymeric solution, the general principles used in microfluidics in order to produce TS are divided into gas-liquid interface segmented flow and liquid-liquid segmented flow, which respectively format the MF bubble template and the MF droplet template. T-junction, co-flow, and flow-focusing are common MF channel geometries that are used and described to produce monodisperse polymeric bubble clusters (polymeric foams). In these micro-sized channels, the continuous gas phase

squeezes the dispersed phase, causing foam template formation. Then, the template accumulates in a assay tube or beaker, and the foams spontaneously self-assemble into crystal-like structures. After solidification of the foams, a sponge-like TS with the desired porous structure is produced. This desired porousness of the TS was tailored accurately by the foam template size and volume fraction. The general anatomical shape of TS was directly fabricated with a cylindrical foam due to its templating in a tube or beaker. This template-assembly- based TS is easily reproduced and practical, and the final morphology of TS meets the requirements of TE [11].

1.2.2. Formation of Liquid Foam Structures From Bubbles

When there is a high density of bubbles in MF system, they come together and nucleation occurs, thereby forming foams in the micro-channel outlet [11]. Ostwald ripening, drainage, and coalescence are the main principal mechanisms involved in the generation of MF foams. Briefly, Ostwald ripening refers to the diffusion of smaller gas bubbles into larger once; drainage refers to the flow of liquid through the foam films; and coalescence refers to breaking of the thin film between two bubbles, as showed in Figure 1.10 [64–66]. In general, where sizes are monodisperse, bubbles expeditiously self-assemble in a regularly ordered structure, whose arrangement depends on the gas and liquid flow. Foam structures and different lattices, from face-centered cubic (FCC) circular bubbles to hexagonal-closed-pack (HCP) structures, can easily be tuned by increasing the gas pressure, as explained in Figure 1.11 [67].

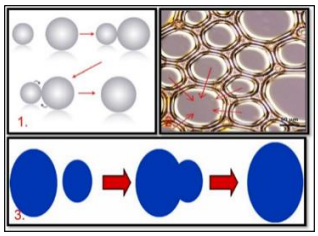

Figure 1.10. Main mechanism of MF foam forming 1. Ostwald Ripening 2. Coarsening 3. Coalescence [68].

Generally, the stability of foam exposed to deformation is affected by the interplay of different aging phenomena: the decrease of the liquid volume fraction under gravity (drainage), the rupture of the films separating the bubbles (coalescence),

and gas transfer between bubbles (coarsening). These deformation effects can occur simultaneously, ameliorating one another and causing the breaking of the foam structure. To get rid of these mechanisms, the use of stabilizing agents, which are surfactants (such as SDS), polymers (such as PEG), proteins, or particles, can also be useful for some specific applications, especially in TE [15,17].

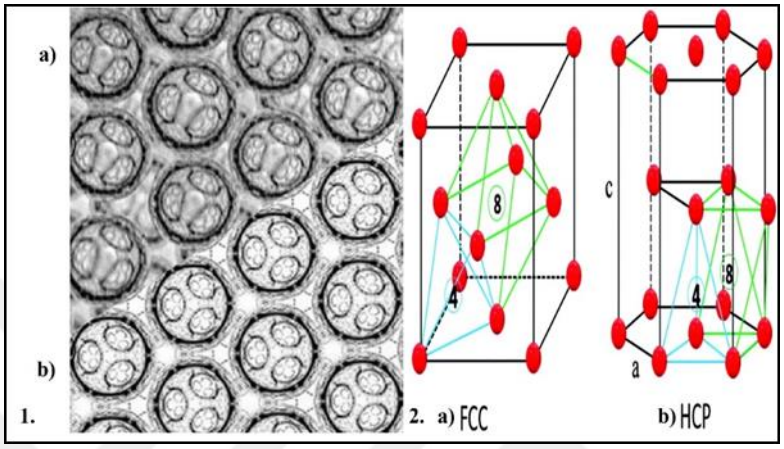

Figure 1. 2. Two main cage structures of MF foam. **1.** a) microscopic image of MF FCC packed foam; b) microscopic image of MF HCP packed foam [69]., **2.** Representative cage structures of a) FCC packed foam b) HCP packed foam.(Red spheres refer to bubbles) [70].

1.3. Hydrogel

Hydrogels are 3D synthetic or natural polymer-based networks in which the liquid constituent is water. Many parts of our body consist of hydrogels in the form of ECM, mucous, collagen, gelatin, cartilage, epidermis, meniscus, and tendons. The high water content of hydrogel TS possesses similar features to our body in the concept of flexibility and elasticity, which provide biomechanical, biochemical, and structural support to the surrounding cells, making hydrogels a novel biomaterial for TE applications [71,72].

However, this novel biomaterial still possess challenges in integrating TE application, including the toxicity risk of common polymers, weak biomechanical properties, and non-regular porous structure [19,22]. In order to minimize these unwanted properties of hydrogel, nanoceramic can be added the polymer structure to

ameliorate the mechanical properties [18]. And also, with the MF method, the porous structure can be significantly regulated. Besides the mechanical properties, they can also be slightly enhanced [17,67].

1.3.1. Microfluidic Hydrogel Foams

Hydrogel foams are a unique type of porous material in which the dispersed phase is a gas and the continuous phase is a hydrogel. Hydrogel foams possess key importance in many different areas, the most popular being the biomedical, sanitary, agricultural, and food sectors. They possess huge usage potential in TE rather than simple polymeric material due to their elastic and flexible structure, their high biocompatibility, the ease of adding therapeutic biomolecules within their network, their stimuli-responsive features, or their talent for combining other properties of different polymers or nanoceramics [17,18,43].

Hydrogel foams are a sub-group of macroporous hydrogels that consist of enough gas so that the pores touch each other. Beyond the porosity, it is their structure that makes hydrogel foam a unique, elastic, sponge like porous biomaterial. When pore sizes are larger than 10 μm, the pore shapes are dictated by the surface tension of the polymeric solution. In a nutshell, hydrogel foam production consists of generating a stable polymer solution and subsequently cross-linking the continuous phase to obtain a solid polymer foam whose structure has been adjusted by the equilibrium of forces in the liquid state and by the solidification procedure. At the beginning, the wet hydrogel foam can be subsequently dried via methods such as freeze drying [15,17].

In order to produce hydrogel foam, a kitchen blender and the paddle-stirrer based mechanical foaming, batch foaming, and chemical foaming method can be used. But these methods do not provide a well-ordered porous structure. Due to this reason, the MF method has huge potential to produce well-ordered ordered porous hydrogel structures. In the concept of producing MF hydrogel foam, porous polymer-based liquid foam is cross-linked with a cross-linker agent in order to protect foam stability. The polymer foam can be meet outside of MF system in a gelling dish or in the MF chip channel. Latter gelling occur. After that, the produced hydrogel foam can be subjected to a freeze-dry or heating process in order to sustain well-ordered MF foam, as shown in Figure 1.12 [15,17].

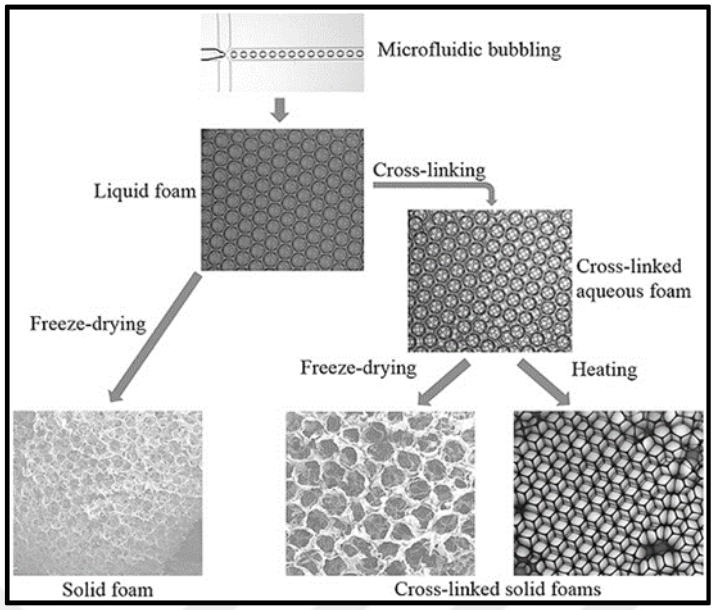

Figure 1.12. Basic presentation of producing MF hydrogel [73].

During gelling of MF polymeric solution, each bubble cannot be cross-linked in a well-ordered form because of the nature of bubble coarsening, coalescence, and drainage. And also, the bottom bubble cannot tolerate the mechanical stress of the upper bubble in a tubular gelling dish. Because of these reasons, MF hydrogel foams raise many interesting and challenging scientific questions: 1. How do the foam effects from the gelation process and the final gel properties compare to a bulk gel made with the same formulation?, 2. Which mechanisms arrange the pore opening process in hydrogel foams? 3. How can the mechanical features of foams be predicted? 4. How are foam structure and gel properties coupled in the freeze-drying and absorption process? How can they be optimised? [15,17].

1.4. Polymer-Based Nanobiocomposites

Recently, polymer-based nanobiocomposites have received much interest in the field of nanobiotechnology. Although synthetic polymers have been broadly employed in composite products over the last half -century, their poor biodegradability has made them a key source of waste disposal problems. The synthetic polymers are not only non-compatible with our environment but also not biocompatible and poorly biodegradable with our cells. Hence, special attention has been given to replacing traditional synthetic polymers with substances based on biopolymers, such as biodegradable proteins, polyesters, or polysaccharides such as cellulose, kitin, or proteins. Nanobiocomposites are a type of hybrid material composed of biopolymers and inorganic solids with at least one dimension in 1- 100 nm. The incorporation of nano-sized inorganic fillers leads to modification and enhancement of biopolymers features. Due to their being eco-friendly, biodegradable, cost-effective, and easy to prepare [73,74].

Polysaccharides possess key importance due to their recyclable and renewable nature and biodegradability among all biopolymers. Chitosan is one of the most extensively used polysaccharides in a multitude of applications due to its features that are affected by environmental variables such as ionic strength, pH, and electric field. However, chitosan-based nanobiocomposites are considered non-toxic and possess a remarkable affinity for biomolecules such as proteins. Because of their exceptional biochemical activity, biocompatibility, nontoxicity and biodegradability, these nanobiocomposites have gained huge popularity in biological sciences such as TE and bioengineering [74].

1.4.1. Chitosan

Chitosan ($C_6H_{11}O_4N$) is an FDA (Food and Drugs Administration)-approved cationic biopolymer composed of N-acetyl-D-glucosamine and β-1,4-linked 2-amino-2-deaoxy- β-D-glucose (deacetylated D-glucosamine) units less crystallinity and less molecular weight (MW) than chitin. Chitin (β-(1-4)-poly-N-acetyl-D-glucosamine) is the most abundant biopolymer, which can be found in the exoskeletons of crabs and shrimps, the cuticles of insects, and cell walls of fungi. In order to be used in

biomedical applications, chitin is converted to its deacetylated derivative, chitosan, by enzymatic or chemical hydrolysis, as shown in Figure 1.13 [74].

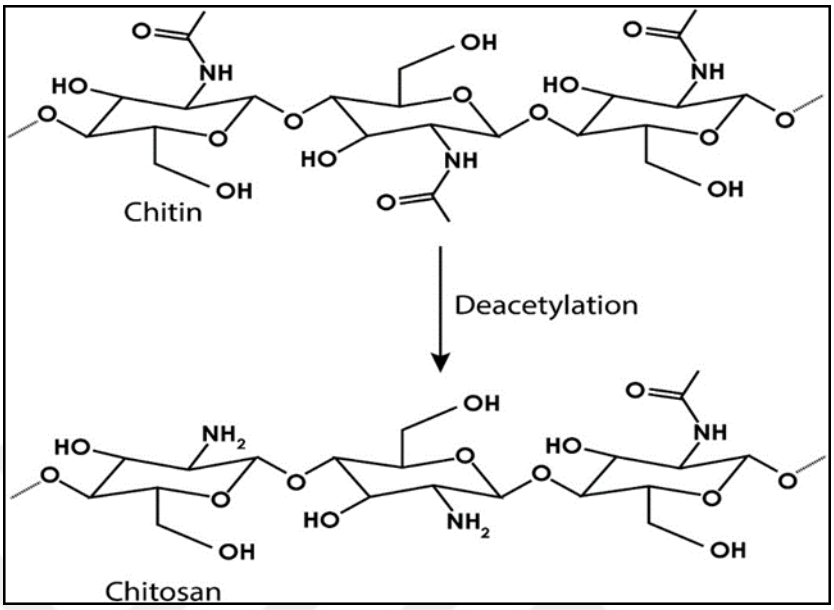

Figure 1.13. Chitosan from chitin by deacetylation [75].

Generally, chitosan possesses viscosity, chelation, mucoadhesive, and polyelectrolyte behaviours. It was found that the linear form of CS possesses excellent viscosity; the viscosity of CS can be modified by changing the deacetylation conditions. The physicochemical talents of CS are effected by degree of deacetylation (DD), crystallinity, MW, and methods of degradation. It was discovered that the degradation rate of CS is related to DD and is also dependent on the distribution and order of acetyl groups. A higher DD shows a significantly lower biodegradation rate, while a lower DD shows a higher biodegradation rate. Chitosan possesses three reactive positions, one amino group and two hydroxyl groups in every glycosidic residue. Among all the group, the amino group possesses key importance as it is pH-sensitive and responsible for the cationic nature of CS and the regulation of its various physicochemical characteristics. The solubility of CS depends on the pH-responsive amino groups protonated at lower pH, permitting CS to dissolve and form cationic polymers, which means the amino group becomes deprotonated at a pH of more than 6, making CS insoluble [74].

In terms of biological talents, CS possesses an outstanding anti-bacterial effect on a wide range of disease-causing bacteria because of the cationic nature, which permits the interaction between negatively charged proteins and lipids present in the bacterial cell wall. Besides, CS also possesses anti-fungal talent due to its electrostatic reaction with the cell membrane's negatively charged phospholipids. When the fungus cell membrane is disrupted, CS may penetrate the cell and prevent RNA and DNA synthesis, thus causing cell death [74].

It has been shown that CS exhibits anti-inflammatory and analgesic properties by reducing the release of inflammatory signals from immune cells. Chitosan has an advantage over NSAIDs (the conventional medications for inflammatory conditions), because it does not cause gastric side effects due to free amino groups that generate a defensive shield over the stomach. This polymer also absorbs proton ions released at the inflammatory site to control pain. Besides, CS can also heal damaged connective tissues. When CS undergoes acid hydrolysis, glucosamine monosaccharides are generated, forming the proteoglycan structural components of connective tissues and cartilage's ECM, thus providing tissue repair. Eventhough the precise mechanism is not clear, CS also shows anti-tumor activity. Despite possessing desired physiochemical and biological talents, certain disadvantages in the molecule pose significant challenges and restricts its application. It has low solubility due to physiological pH, which could cause restriction in the TE. The European Food Safety Authority does not support CS, even though the FDA has approved it as a food-contact material. The high elasticity of CS-based nanobiocomposites is another drawback that limits their applications. Difficulties in regard to drug release effectiveness, drug loading capacity, degradation rate of nanobiocomposite materials, delivery duration, and many others. Finally, industrial manufacture centres still have an economic problem to introduce commercial availability of sustainable nanobiopolymer in the real market [74].

1.4.1.1. Synthesis of Chitosan

There are plenty of techniques used to synthesize chitosan. These techniques includes microwave-assisted, chemical, electrochemical, pulsed electric field, microbial fermentation, enzyme-assisted, and ultrasound-assisted approaches. The conventional synthesis of chitin using a chemical procedure requires huge volumes of chemicals, which are subsequently released into our environment. In the chemical synthesis process of CS, the protein components have not been recovered in a better way. Recently, biological synthesis (microbial fermentation) techniques, enzyme-assisted synthesis, electrochemical, and microwave-assisted green synthesis methods have been used in order to produce chitosan polymers. But green methods are still lacking due to long-term production and being not commercially available [75].

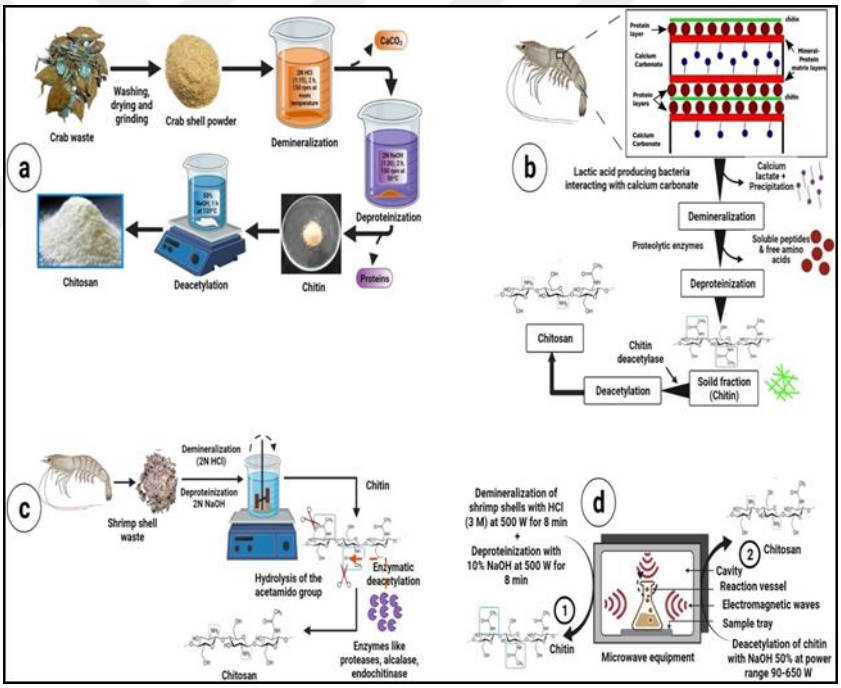

Figure 1.14. Schematic diagram of a) chemical synthesis of CS; b) biological synthesis of CS; and c) enzyme-assisted synthesis of CS d) microwave-assisted synthesis of CS [84].

As shown in Figure 1.14.a. in common CS synthesis, the raw material of shells (shrimp, crap, insects, etc.) are washed, crushed, and ground to powder with demineralization of some components, such as calcium carbonate, by chemical

extraction with dilute hydrochloric acid with stirring at room temperature. After demineralization process, the deproteinization process is performed by applying a dilute basic sodium hydroxide solution. Proteins can be recovered by lowering the pH to 4.0 and then drying the precipitate. Chitosan is produced by deacetylation of produced chitin in sodium hydroxide solution, but in an environment without oxygen [76]. Even though chemical methods are commonly used in order to produce CS, these methods could affect the physicochemical and biochemical properties of chitin and chitosan. Hence, biological, enzyme-assisted and microwave- assisted methods possess value-added chitosan in the greener approach [75].

The greener aim of conducting deproteinization using proteolytic (breaking down of proteins into smaller polypeptides or amino acids) fermentation was found to be a sustainable method. The microbial fermentation or biological synthesis is shown in figure 1.14.b. For instance, shrimp heads were used in order to produce protease (an enzyme which break downs protein) using a bacterium (Paenibacillus mucilaginosus). In addition, a combination of other bacteria (Serratia marcescens and L. Plantarum) ameliorated deproteinization and demineralization activity. Briefly, the proteolytic enzymes produced by bacterial communities exhibited better yield, and it is one of the promising biological synthesis process when compared to alkali reaction [75].

Also, the enzymatic-assisted synthesis method is gaining popularity due to its environmentally friendly nature. Besides, this synthesis method is fast in action and, more specifically, reduces the use of energy, chemicals, and/or water compared to conventional processes, which provide the recovery of high-value added products. Enzymatic synthesis of CS is realized by specific enzymes such as chitosanases and nonspecific enzymes such as carbohydrates and proteases. In this method, washed and ground shrimp shells are treated with mild alkali solutions. The shell waste is deproteinized by the enzymes and demineralized with 10% HCL solution. Later, a suspension of the demineralized shells is subjected to protein hydrolysis at 55 ^{o}C and a pH of 8.5 with an enzyme. Finally, produced chitin is deacetylated, and chitosan is synthesized. In the microwave-assisted method, washed and ground shrimp shells demineralize and deproteinize in microwave device, and CS is produced as shown in Figure 1.15.c [75] .

1.4.1.2. Chitosan Hydrogels

Chitosan hydrogels are special type of natural hydrogels that are formed via cross-linking or being interconnected by different interactions of a 3D bulky structure or injectable form of chitosan. These hydrogels are one of the smart materials that are capable of responding to external stimuli including temperature, light, pH, solvents, pressure, ionic strength, electromagnetic radiation, and magnetic fields [77, 78].

Chitosan-based hydrogels that possess certain responses to different pH or temperature conditions are synthesized by various methods, such as chemical cross-linking and physical cross-linking [23,79]. According to their synthesized method, they can be classified as chemicals and physical hydrogels. In the physical method, hydrophobic and electrostatic interactions with hydrogen bonds result in the formation of entangled networks. As to ionic interactions, ionic strength and pH possess key importance in hydrogel formation because CS interacts with ions, small molecules, or macromolecules bearing opposite charges in a typical pH range of 4-6. As shown in Figure 1.15. Simply put, hydrogel formation occurs when CS undergoes a cross-linking reaction with another synthetic (PEG and PVA) or natural (alginate and cellulose) chain of its own. In the chemical method, chitosan hydrogels are formed by the covalent bonding of chitosan monomers. Hydroxyl and amines groups of CS chains play important role when chemical crosslinking is realized. In addition, this cross-linking can occur via photopolymerization reaction. Hence, when synthesizing CS hydrogels, cross-linker agents such as sodium tripolyphosphate, glyoxal, genipin and glutaraldehyde are used [22]. Among them, glutaraldehyde is mostly used as a crosslinker agent while producing CS hydrogel. Because this chemical is not only cheaper than others and but also cross-links into a better 3D bulky structure [80].

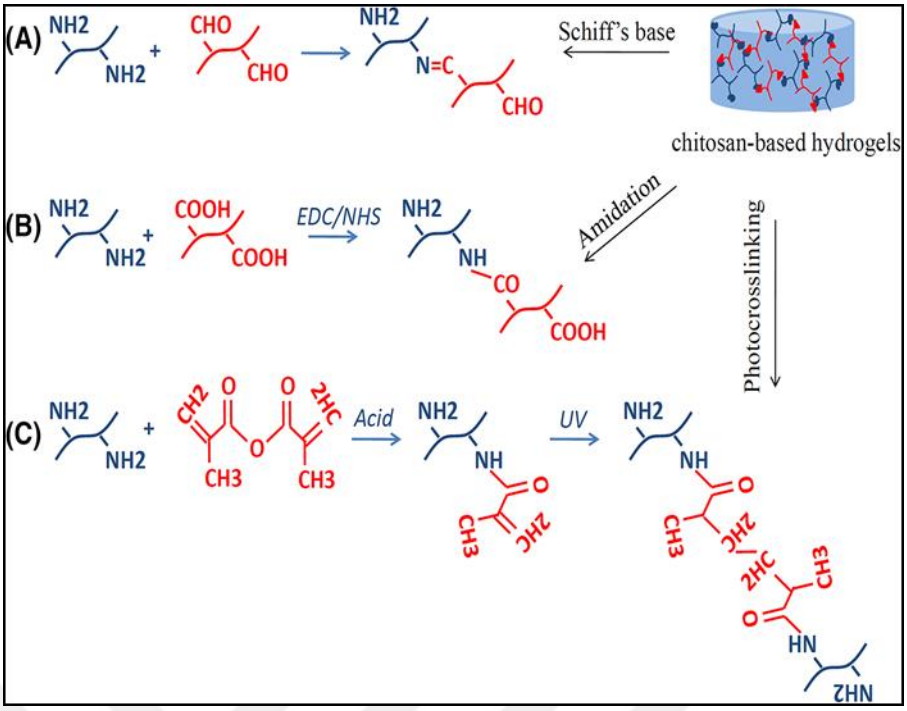

Figure 1.45. The general strategies to synthesize CS hydrogels. (a) Schiff's base reaction, (b) Amidation reaction, and (c) Photocrosslinking [25].

1.4.1.3. Application Area of Chitosan Hydrogel

Chitosan and chitosan-based hydrogels possess huge potential for usage in many technological fields due to their cationic and ionic conductivity, multiple stimuli (pH, magnetic field, temperature), viscoelasticity, high swelling, and bio- and eco-friendly degradation mechanism. For example, CS can be crosslinked via Li^+ or Ag^+ ions, and so CS hydrogel can be used as a good electric storage device. Similarly, CS hydrogel can be also used in wearable electronic devices and soft robotics as an eco-friendly material [81].

Chitosan hydrogel is not only used in electrical engineering and the energy storage industry, but it can also be used in agriculture engineering and food packing industry. Chitosan shows antipestisit, antimicrobial and antifungal properties, so it protects agricultural products and increases efficacy without polluting the soil. Besides, these hydrogels can protect food due to their antibacterial and antifungal properties, so they also possess huge usage potential in the food packaging industry [82,83] .

Chitosan hydrogel also possesses huge usage potential in TE because plenty of amino groups existing in this hydrogel can interact with the negatively charged tissue surface and anionic biomolecules, such as sialic acid, and the glycosaminoglycans abundantly present in ECM. Hence, CS has become an ideal candidate as a tissue adhesive. Besides, this hydrogel degrades with a natural enzyme called lysozyme. All of these properties of these hydrogels have been appealed to by tissue engineers [84] .

Although CS hydrogels possess usage in many areas, their mechanical properties, thermal properties, electronic properties, and degradation properties are still lacking. This issue can be eliminated by increasing crosslinking concentration; however, this may decrease viscoelasticity and cause toxicity. Also, in order to enhance mechanical properties, synthetic polymers can be used, but this also causes toxicity. Lastly, CS concentration can be increased, but this is associated with decreasing viscoelasticity [22,24].

1.4.2. Two Dimensional Nanomaterials

As stated in ISO (2017), nanomaterials are defined as *" the materials with any external dimension in the nanoscale (1-100nm) or have internal/surface structure in the nanoscale."* The physical features of nanomaterials have a direct correlation with their shape and size. Commonly, bulk materials range above 100 nm in all dimensions, and their physical features are independent of size. In an interesting way, decreasing the size to the nanoscale range creates quantum confinement, which fosters novel physio-chemical features [85].

Two-dimensional (2D) nanomaterials are layered nanomaterials with high anisotropy and planar architecture. This planar architecture of 2D nanomaterials provides desirable characteristics for many applications, including a very high surface-to-volume ratio, good mechanical properties, and excellent functionalization capabilities. Compared to other dimensional nanomaterials, 2D nanomaterials possess the highest specific surface area, resulting in high number of surface atoms. The existence of a large number of surface atoms provides high surface energy and can also provide a high number of surface anchoring sites. This unusual characteristics results in enhanced interactions of 2D nanomaterials with biological moieties, which consist of cells, cellular components, and biochemical molecules [85].

1.4.2.1. Boron Nitride

BN is a 2D ceramic that contains an equal number of boron (B) and nitrogen (N) atoms. This nanoceramic is isostructural to graphite; however, the B atoms, the N atomic nucleus and B atoms combine sp^2 orbitals to form a strong bond. In addition, BN presents a partially ionic feature due to the electron pairs in sp^2 hybridized B-N and weak van der Waals bonds between B and N atoms of adjacent layers, hence catering to anisotropic features. BN possesses four main crystalline structures: cubic BN (c-BN), hexagonal BN (h-BN), wurtzite BN (w-BN) and rhombohedral (r-BN). Hybridization of these structures creates the main difference: r-BN and h-BN are dense phases with sp^2 hybridization, whereas c-BN and w-BN are low-density phases with sp^3 hybridized B-N bonds as shown in Figure 1.16. Hexagonal BN is particularly interesting due to its structural analogy with hexagonal graphite [86].

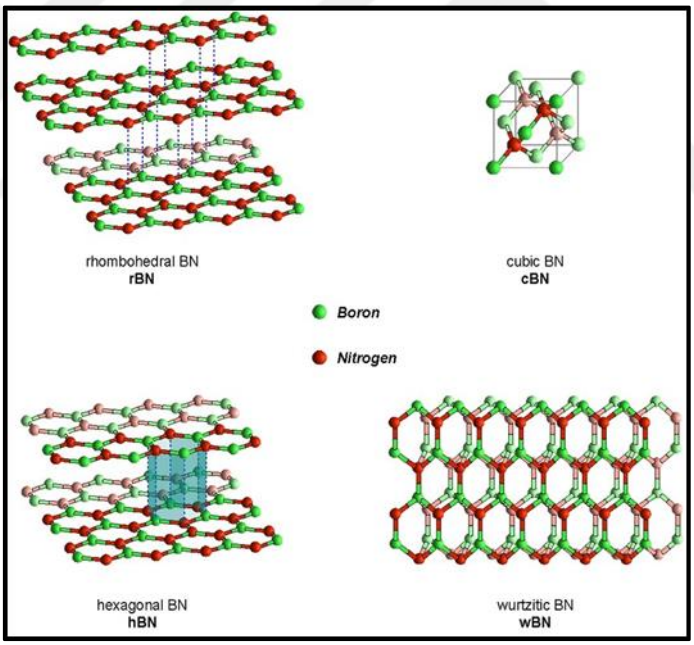

Figure 1 16. Different form of 2D BN [91].

BN ceramic can be zero-dimensional (eg.nonospheres), one-dimensional (e.g. nanofibers, nanotubes and nanoribbons), two-dimensional (nanosheets and thin films), or three-dimensional (nanostructured porous materials) [87]. Among the BN forms, hBN is the most stable form, which is available in fullborene, nanotube (BNNT), and

nanosheet (BNNS) forms. The atomic structure of hBN is similar to graphene due to fact that B-N atoms are bonded with a strong covalent bond in a honeycomb configuration [86].

Important properties, including crystal structure parameters of bulk BN, few-layer BNNS, BNNT, and graphene nanomaterials, are showed in Table 1.17. The fracture strength, Young's modulus, and crystallographic structure properties of BN materials are similar to graphene. However, BN possesses a tremendously higher electronic bandgap and better thermal stability compared to graphene, thus making it suitable for use in electrical insulation applications. Eventhough most of the properties are comparable for all three forms of BN nanomaterials (bulk BN, few-layer BNNS, and BNNT), few-layer BNNS possess a very high surface area ($2600 m^2 g^{-1}$) compared to bulk BN ($10 m^2 g^{-1}$) and BNNT (212-254 $m^2 g^{-1}$). Also, the thermal conductivity of BNNS shows significantly higher values (2000 $Wm^{-1}K^{-1}$) compared with bulk BN materials (390 W $m^{-1}K^{-1}$). In 2D structure, BNNS possess a high aspect ratio which facilitates high surface area for interfacial molecular interaction within matrix [86].

Table 1.2. Physicochemical, mechanical, thermal, and electrical properties of bulk BN, BNNS, BNNT, and graphene nanomaterials [93].

Properties	Bulk BN	BNNS	BNNT	Graphene
Chemical bonding	B and N are boned with covalent and bond length is 1.44 A. Layers of BN are bonded with van der Waals force			Carbons are bonded with covalent and the bond length is 1.42 A
Crystallographic parameters	'a' = 0.25 nm, 'c' = 0.666 nm, and interlayer distance = 0.333 nm			'a' = 0.246 nm, 'c' = 0.670 nm, and interlayer distance = 0.335 nm
Colour	White			Black
Specific surface area (m^2/g)	<10	~2600	212-254	2630
Hydrophobicity	Partial hydrophilicity to super hydrophobic			Both hydrophilic and hydrophobic depending on the substrate
Cytotoxicity	Low cytotoxic			Very less cytotoxic
Surface energy (mJ/m^2)	35-37 (in polar solvent)			83 (in water), 115 (single layer in nitrogen), 119 (few layers in nitrogen)
Young's modulus	Elastic modulus 0.811 TPa	Young's modulus 0.8 TPa and elastic modulus 220-510 N/m	Young's modulus 0.784-0.912 TPa and tensile strength 33 GPa	1.0 TPa
Fracture stress (GPa)	N/A	165	133	130
Thermal conductivity at room temperature (W/m-K)	390	300-2000	1700-2000	3000-5000
Thermal stability in air and vacuum	Stable up to 800-900°C in air and 1400 °C in vacuum			Depends on the synthetic method, usually 500-600 °C
Thermal expansion coefficient at 300 K (K^{-1})	N/A	-2.72 x 10^{-6} (axial direction)	2 x 10^{-6} (axial direction)	Single-layer -0.8 ± 0.7 x 10^{-6} (298 K)
Bandgap (eV)	5-6			Zero bandgap
Work function (eV)	3.5	3.65	5.3	4.49

1.4.2.2 Boron Nitride Synthesis

BN was synthesized in 1840s by W.H. Balmain using molten boric acid and potassium cyanide; however, this new ceramic wasn't stable, and many attempts were required to synthesize a stable form of BN. Approximately 100 years later, in the 1950s, Carborundum and Union Carbide achieved in synthesising BN on an industrial

scale and processed the shaped BN parts with advanced hot pressing techniques in proper commercial applications [88].

Those days, in the general synthesize of BN powder, boric acid (H_3BO_3) or borax such as sodium borate ($Na_2B_4O_7$) and nitrogen-containing compounds such as ammonia or urea ($(NH_2)_2CO$) form a BN bond when heated together [88].

In order to synthesize BN nanostructures, top-down exfoliation and down-top synthesis methods are applied. An appealing top-down method, named mechanical peeling, was commonly applied to produce atomic-thin nanosheets from bulk crystals. This method uses adhesive tape to attach the h-BN single crystal. The BN-nanostructured nanosheets were peeled and transferred to target substrates [87].

Among the different synthesis method, solid-phase exfoliation by ball milling is one of the most intriguing methods for synthesising gram-scale BN nanostructure powder and high-concentration colloidal dispersion. In this method, a planetary mill is used to mix and roll the balls, raw materials, and milling agents to reduce the thickness of 2D materials by shear force [89].

The liquid-phase strategy in exfoliation of BN is available in solvents, consisting of distilled water, organic solvents, ionic liquids, and aqueous surfactant solutions. Commonly, the raw materials were dispersed in an aqueous solution and sonicated. Later, the 2D crystallites were synthesized into nanosheet. After this synthesis, polymer solvents were used to stabilize the colloidal solution through electrostatic repulsion [87].

As a bottom-up approach, the chemical vapor deposition (CVD) method provides h-BN films with large domains. In this method, BN powder interfere with ammonia gas flow at high temperature value (1200 ^oC) with $FeS/Fe_2/O_3$ as catalyzing agent [90].

1.4.2.3. Application Area of Boron Nitride

The superior thermal and physicochemical stability, along with some unique properties such as low dielectric loss and high thermal conductance, provide the practicability of BN nanostructures in electronics and energy applications. The BN layer can satisfy both high-performance dielectrics and insulators, thus being widely applied for in-plane microelectronics [91]. In addition, the large band gap properties

of BN-based nanostructures enable them, especially BNNTs, to emit ultraviolet luminescence light when they are excited with phonons or electrons [92]. This luminescence property and also the transparent properties of BN nanostructures provide tremendous opportunity for analyzing cell substitutes, cells, cell-cell integrations, anatomies, and physiology of natural nanomachines [93, 94].

BN-based nanostructures have been employed in widespread research to lower cytotoxicity unless used in excess concentrations. Moreover, having low infrared light absorption, BNNTs do not cause damage or overheat biomolecule cargo. Also, these nanostructures have been employed as carrier molecules or a nanoenhancements to improve biological functionality. Being able to generate strong hydrogen bonding with proteins in addition to van der Waals interactions, BNNTs are designed as important nanoplatforms for drug targeting [92].

BN-based nanostructures are particularly attractive for use in biomedical applications because of the biocompatibility of both hydrogels, which mimic the nanostructure of tissue and BN. Also, BN possesses biodegradable properties, and the boron that is produced during its degradation can enhance wound healing and the treatment of prostate cancer. Besides, the biochemical activity of BN-containing materials has also been demonstrated to promote tissue healing by promoting hydroxyapatite (main inorganic fraction of bone and teeth). Hence, BN-based nanocomposites possess key importance in tissue engineering applications [95].

BN-based nanostructures not only possess biodegradable, biocompatible, and anticarcinogenic properties but also show antibacterial properties and increase the adhesive and mechanical properties of materials. Unsaturated borons placed at the surface or edge of BNNS cause bacterial death [96]. In terms of mechanical properties, a high surface-to-volume ratio of BN makes it more resistant to mechanical stress when incorporated with any material [90] .

LITERATURE REVIEW

Kisku et al. were prepared CS/BN nanobiocomposites by solution method using $CuSO_4$ /glycine chelate complex as the catalyst with BN loading. The dispersion of BN with the CS was achieved with sonication. The chemical interactions of CS and BN were examined by Fourier transform infrared spectroscopy. The structure of composite investigated by transmission electron microscopy (TEM) and X-Ray diffraction analysis (XRD). According to their produced result, BN were dispersed with the CS matrix through intercalation. The quantitative determination of composites was examined by energy dispersive X-ray spectroscopy and selected area electron diffraction. The thermal properties of CS/BN nanobiocomposites were studied by thermogravimetric analysis. It was observed that the thermal stability of CS/BN nanobiocomposites was increased compared with a pristine CS matrix. The oxygen barrier properties of CS/BN nanobiocomposites were measured with a gas permeameter. A reduction in oxygen permeability was observed with increasing BN concentrations, which suggests that the synthesized composite materials may be applicable in packing industry [25].

Emanet et al. reported that hydroxylated BN nanotubes were included in CS scaffolds and tested for their swelling behaviour, biodegradability and mechanical strength. The results show that incorporation of BNNTs-OH into the CS scaffold increases the mechanical strength and pore size to values optimal for high cellular adhesion and proliferation. Besides, the CS/BNNT-OH scaffold was found to be non-toxic to human dermal fibroblast cells due to its slow biodegradation rate. Cell proliferation and adhesion were increased as compared to the CS-only scaffold, as observed by SEM and fluorescent microscopy images [24].

Chen et. al. reported the high-efficiency synthesis of a few layers of h-BN nanosheets by homogenizer. Then, the h-BN nanosheets and chitosan microspheres are finally synthesized by mixing h-BN nanosheets with CS under alkaline conditions. The h-BN nanosheets dispersion is examined by UV-vis spectrophotometer and TEM. Also, they use SEM and laser particle size analyzers in order to characterize the microscopic and macroscopic morphology of h-BN nanosheets and chitosan composites. Raman spectroscopy and specific surface area testing are also used to determine the intrinsic properties of h-BN-CS. The TGA result shows that composites

with a high content of h-BN nanosheets possess higher thermal stability. The results show that BN nanosheets are dispersed in the network of CS microspheres, and the higher rate of centrifugation, the fewer h-BN nanosheets are dispersed in the microspheres. The CS microspheres are composite with pore diameters in the range of 1.7-2.9 nm [26] .

Dhanavel et. al. synthesized a CS/hydroxylated BN nanocomposites matrix composite in order to use in a drug delivery system for cancer treatment. In their study, curcumin and 5-fluorouracil were loaded into the matrix nanobiocomposite individually and in conjugated form (5-fluorouracil + curcumin). The synthesized nanobiocomposites were analyzed using various characterizations. The synthesized nanobiocomposites showed high encapsulation efficiencies of 85.4% and 91.2% for 5-fluorouracil+curcumin, respectively. Also, in vitro experiments on human colorectal cancer cells were carried out, and as a results, the administration of drug-loaded OH-BN nanobiocomposites with 5-fluorouracil and curcumin showed anticancer activity on human colorectal cancer cells [97].

Zou et. al. reported novel eco-friendly CS microspheres and hydroxyl-functionalized h-BN nanobiocomposites with a honeycomb network morphology. Using their significant difference in scales, the nanobiocomposite is arranged between each CS microsphere so that the morphology is closely similar to the honeycomp: CS microspheres were honeycomb cores, and the nanostructures were honeycomb networks. Compared with the routine-structure BN/CS composites, the thermal conductivity of honeycomb-structured BN/CS showed a significant enhancement. The thermal conductivity of BN/CS nanobiocomposites reaches 5.66 ± 0.32 $Wm^{-1}K^{-1}$ with hexagonal network 50 wt% OH-h-BN nanobiocomposites, revealing 502 % higher than other nanobiocomposite (0.94 ± 0.02 $Wm^{-1}K^{-1}$) and closely 1914% higher than that of pure CS (0.28 ± 0.01 $Wm^{-1}K^{-1}$). According to TGA results, the thermal stability of the nanobiocomposites increased with the increasing content of BN [98].

With this thesis, in order to minimize these restrictions, BN's, which were proven to support cell proliferation and biocompatibility with previous studies, will be dispersing in chitosan solution while dispersing nanobiocomposite foam with gas-based T-shaped microfluidics. After that, production of sponge-like TS platforms will be materialized while gelling with a crosslinking agent, which is glutaraldehyde (GA).

Furthermore, with this method, tissue scaffolds platforms will be produced at a lower price, in less time, and in an environmental friendly manner.

As a summary, the aim of this thesis work is to:

- A polymeric chitosan solution will be prepared. The solution behaviour of chitosan particles will be observed in a water solution that contains acetic aside (AA). Chitosan and acetic aside concentration/ratio optimization studies will be done, and physical characterizations (density, viscosity, surface tension, etc.) of these solution will be materialized in a triumphant manner.

- Chitosan solutions that have different concentration of chitosan will be cast with a traditional solvent casting method with gelling via GA, which is a cross-linker agent, and optimization studies in concentration will be performed. An accurate concentration of CS and GA will be indicated in order to produce the best bulky chitosan hydrogels. These polymeric hydrogels will be characterized (scanning electron microscopy (SEM), XRD, Fourier transform infrared spectroscopy(FTIR), differential scanning calorimetry (DSC) and thermogravimetric analysis (TGA)).

- A BN-added chitosan nanobiocomposite solution will be prepared, and optimization studies of BN concentration will be performed. Nanobiocomposite solutions, which contain different concentration of BN, will be characterized (density, viscosity and surface tension). Later with these solutions, in order to produce chitosan hydrogel with the best GA concentration and GA content, gelling with solvent casting method, nanobiocomposite hydrogels will be produced, and characterizations of these produced nanobiocomposite hydrogels will be made (SEM, XRD, FTIR, DSC and TGA).

- Setting up this T-Shaped MF system will materialize. With this system, polymeric and nanobiocomposite bubbles will be produced. MF-based polymeric and nanobiocomposite-based hydrogels will be produced while gelling the MF bubbles in GA and will be characterized. The characterization results of hydrogels were compered, which were produced with microfluidics and traditional methods by us.

3. MATERIALS AND METHOD

This Chapter includes the materials and devices used in this thesis study and the experimental methods performed. The preparation procedures of both chitosan hydrogel and boron nitride/chitosan hydrogel nanobiocomposites by using two different production ways; solvent casting method and the microfluidic device technique were described in detail. Experimental procedures, preparation, and characterization methods for producing chitosan polymeric hydrogels and boron nitride/ chitosan hydrogel were described.

3.1. Materials

The main materials used in the experimental work are shown in Table 3.1. Chitosan(CS) used as an extracellular matrix (ECM) material like bulky hydrogel tissue scaffolds. Acetic acid (AA) was also used for enhancing dissolution of CS in distilled water(DW) due to the complex chemical form of CS, having a degree of deacylation of 75%, is not water-soluble; hence, AA (glacial) was added to the CS polymer solution as mentioned in Chapter 3.2.1.1 in detail. To prepare chitosan polymer-based nanobiocomposite hydrogels, chitosan polymer was dissolved in AA and DW solvent and immediately gelation agent was poured into the liquid polymeric solution. To form nanobiocomposite hydrogels, boron nitride (BN) nanoceramic powders with ~1μm particle size as an enhancement agent were added into chitosan solution then subsequently gelation agent was deposited in the nanobiocomposite solution. BN is known as a nanoceramic material, which enable to enhance mechanical properties of chitosan based-polymeric hydrogel scaffolds. The prone sonication technique was used to disperse BN nanoceramic particles throughout the polymeric solution for an achievement of homogenous solution form. Glutaraldehyde (GA) solution (25% v/v) was used as a gelling agent to transform polymeric solution to hydrogel form. A ready gelation solution was a gelling agent to transform polymeric solution to hydrogel form. A ready gelation solution was added to both polymeric and nanobiocomposite solutions to generate bulk hydrogel scaffolds as described in Chapters 3.2.4 and 3.2.5.

Table 3.1. Materials used in whole experimental work of this thesis research.

Material	Brand	City/Country
Shrimp-derived chitosan (CS) (%75≥ deacetylated)	Sigma-Aldrich	Shnelldorf/Germany
Boron nitride (BN) nanoceramic powders with ~1μm particle size	Sigma-Aldrich	Shnelldorf/Germany
Glutaraldehyde (GA) Solution 25% v/v	Sigma-Aldrich	Shnelldorf/Germany
Acetic Acid (glacial)	TEKKİM	Bursa/Turkey

Table 3.1. presented boron nitride (BN) nanoceramic powders with ~ 1μm particle size were purchased from Sigma Aldrich. Acetic acid (AA, glacial) with the purity of %99-%100 from Tekim Company, shrimp-derived chitosan (CS) (%75 deacetylated), and liquid glutaraldehyde (GA) solution at 25% v/v were purchased from Sigma Aldrich. Distilled water (DW) collected from Sartorius device which is available in Institute of Nanotechnology at Gebze Technical University (GTU), Turkey.

3.2. Method

Preparation and optimization of only chitosan solution and BN/chitosan nanobiocomposite solutions as well as their solution characterization were presented in this section. Also, the raw materials used, conventional method (the solvent casting) and the microfluidic device technique engineered only chitosan or boron nitride reinforced chitosan nanobiocomposite hydrogels and their structural thermal and chemical characterization procedures by using FTIR (to observe chemical structure), DSC and TGA (to observe thermal behaviour), XRD (to observe crystallographic properties), SEM (to observe structural properties) were presented in detail.

3.2.1. Preparation of Boron Nitride Added Chitosan Nanobiocomposite Solutions

In this part of thesis, only chitosan and chitosan based-nanocomposite polymeric solution preparation and the optimization of their preparation parameters were explained in detail.

3.2.1.1. Preparation of Chitosan Solution

0.11g (2.2% w/v) CS polymer powders were dissolved in 5 ml DW and 0.05 ml (2% v/v) AA solvent mixture under 1000 rpm at 37°C for an hour, then a speed of magnetic stirrer was changed at 1500 rpm in 37 °C to accelerate dissolution process and thus two hours later clear solution was successfully achieved. A view of the solutions obtained was captured by using the smart phone (Vestel, Venus V7, Turkey) with 13 mega pixel(MP) + 2 MP rear camera and a 52 MP resolution.

3.2.1.2. Optimization of Acetic Acid Concentration in Chitosan-Acetic Acid-Water Solution

The average pH value of the human body amends between 7.35 to 7.45 [99]. The pH value for the chitosan in acidic solutions is measured below from 6 presented in the literature. It is well-known in the literature that polymeric scaffolds produced by using chitosan solutions with high acetic acid concentration are not biocompatible due to their level of acidity [100, 101]. Therefore, optimization of AA concentration in the solution was studied.

0.11 g of CS was dissolved in 5ml DW and 0.025 ml of AA at 1500 rpm for 24 hours by magnetic stirring and the 0.5% v/v AA-2.2% w/v CS solution resulted in. This solution appeared as solution number 1 in Table 3.2. However, very tiny amount of chitosan polymer was not still dissolved, and a reduction in an amount of chitosan concentration was adjusted as well. Therefore, 0.075 g CS was dissolved in 0.035ml AA and 5ml DW at 1500 rpm at 37°C for 24 hours by magnetic stirring and the 0.8% v/v AA-1.5% w/v CS solution obtained that indicated as number 3 in Table 3.2. 0.075

g CS was dissolved in 0.050 ml AA and 5 ml DW at 1500 rpm at 37°C for 24 hours by magnetic stirring and the 1% v/v AA-1.5% w/v CS solution achieved depicted as number 4 in Table 3.2. A view of the solutions obtained was captured by using the smart phone (Vestel, Venus V7, Turkey) with 13 (MP) + 2 MP rear camera and 52 MP resolution.

Table 3. 2: Only chitosan solutions which optimized for AA concentration and their amounts and parameters amounts and parameters.

Solution Nu	Solution	Amounts			Parameters		
		CS(g)	AA(ml)	DW(ml)	Time(s)	Mix. Velocity(rpm)	Temp. (°C)
1	0.5% v/v AA-2.2% w/v CS	0.11	0.025	5	24	1500	37
2	0.7% v/v AA-1.5% w/v CS	0.075	0.035	5	24	1500	37
3	0.8% v/v AA-1.5% w/v CS	0.075	0.040	5	24	1500	37
4	1% v/v AA-1.5% w/v CS	0.075	0.050	5	24	1500	37

3.2.1.2. Optimization of Chitosan Concentration in Chitosan-Acetic Acid-Water Solution

Chitosan solutions were prepared with different concentrations, ranging between 0.3 to 1 wt. % in this thesis study, as shown in Table 3.3.**Error! Reference source not found.** in order to determine suitable CS solutions to utilise them through to the microfluidic device technique used in this thesis work. 0.05g CS was dissolved in 5ml DW and 0.05 ml of AA at 1500 rpm for 24 hours by magnetic stirring and the 1% w/v CS- 1% v/v AA solution achieved depicted as number 1 in Table 3.3. 0.035g CS was dissolved in 5ml DW and 0.05 ml of AA at 1500 rpm for 24 hours by magnetic stirring and the 1% w/v CS- 0.7% v/v AA solution achieved depicted as number 2 in Table 3.3. 0.025 g CS was dissolved in 5ml DW and 0.05 ml of AA at 1500 rpm for 24 hours by magnetic stirring and the 0.5% w/v CS- 1% v/v AA solution achieved depicted as

number 3 in Table 3.3. 0.015 g CS was dissolved in 5ml DW and 0.05 ml of AA at 1500 rpm for 24 hours by magnetic stirring the 0.3% w/v CS- 1% v/v AA achieved depicted as number 4 in Table 3.3. A view of the solutions obtained was captured by using the smart phone (Vestel, Venus V7, Turkey) with 13 mega pixel (MP) + 2 MP rear camera and 52 MP resolution.

Table 3. 3: Optimization of Chitosan solution concentration.

Solution Number	Solution	Amounts			Parameters		
		CS (g)	AA(ml)	DW (ml)	Time(s)	Mix. Velocity(rpm)	Temp. (^{O}C)
1	1% w/v CS- 1% v/v AA	0.05	0.05	5	24	1500	37
2	0.7% w/v CS- 1% v/v AA-	0.035	0.05	5	24	1500	37
3	0.5% w/v CS - 1% v/v AA	0.025	0.05	5	24	1500	37
4	0.3% w/v CS - 1% v/v AA	0.015	0.05	5	24	1500	37

3.2.2. Physical Characterization of Chitosan Solutions

Homogeneous chitosan solutions at optimized CS concentrations of 1% w/v, 0.7% w/v, 0.5% w/v and 0.3 w/v were prepared in 40 ml 1% (v/v) AA aqueous solutions. Physical characterization studies were performed to evaluate the most desired polymer solution to use in microfluidic.

0.12g CS dissolved in 40 ml DW and 0.4 ml AA at 600 rpm, 37^{o}C for 12s by magnetic stirring and the 0.3% w/v CS -1% v/v AA solution achieved depicted as number 4 in Table 3.4 . 0.2g CS dissolved in 40 ml DW and 0.4 ml AA at 600 rpm, 37oC for 12s by magnetic stirring and the 0.5% w/v CS -1% v/v AA solution obtained presented as number 3 in Table 3.4. 0.28g CS dissolved in 40 ml DW and 0.4 ml AA

at 600 rpm, 37oC for 12s by magnetic stirring and the 0.7% w/v CS -1% v/v AA solution obtained shown as solution number 2 in Table 3.4. 0.4 g CS powder dissolved in 40 ml DW and 0.4 ml AA at 600 rpm, 37oC for 12s by magnetic stirring and the 1% w/v CS -1% v/v AA solution obtained indicated as solution number 1 in Table 3.4. Finally, a view of the solutions obtained was captured by using the smart phone (Vestel, Venus V7, Turkey) with 13 mega pixel (MP) + 2 MP rear camera and 52 MP resolution.

Table 3.4. Preparation parameters of the CS solution in order to characterize them.

Solution Number	Solution	Amounts			Parameters		
		CS(g)	AA(ml)	DW(ml)	Time(s)	Mix. Velocity (rpm)	Temp.(^{O}C)
1	1% w/v CS- 1% v/v AA	0.4	0.4	40	12	600	37
2	0.7% w/v CS- 1% v/v AA-	0.28	0.4	40	12	600	37
3	0.5% w/v CS -1% v/v AA	0.2	0.4	40	12	600	37
4	0.3% w/v CS -1% v/v AA	0.12	0.4	40	12	600	37

Values of viscosity for each chitosan-based polymeric solutions were determined by using a turning fork principle via an immersion of the probes in the beaker (SV-10, Vibro Viscometer, A&D, Japan) at room temperature environment. A 35 ml of each CS solutions poured into viscosity cape and the probe was placed into the cape for a measurement. Accurate placing of the probes into the accurate level of chitosan-base polymeric solution in cape is significant due to the correct data allocation (See in Figure 3.1.). After arranging the probes, the viscometer was switched on and a measurement kicked off. At least triplicate of the viscosity measurement was performed to collect data for statistical analysis. Finally, average viscosity values of the samples were calculated and presented.

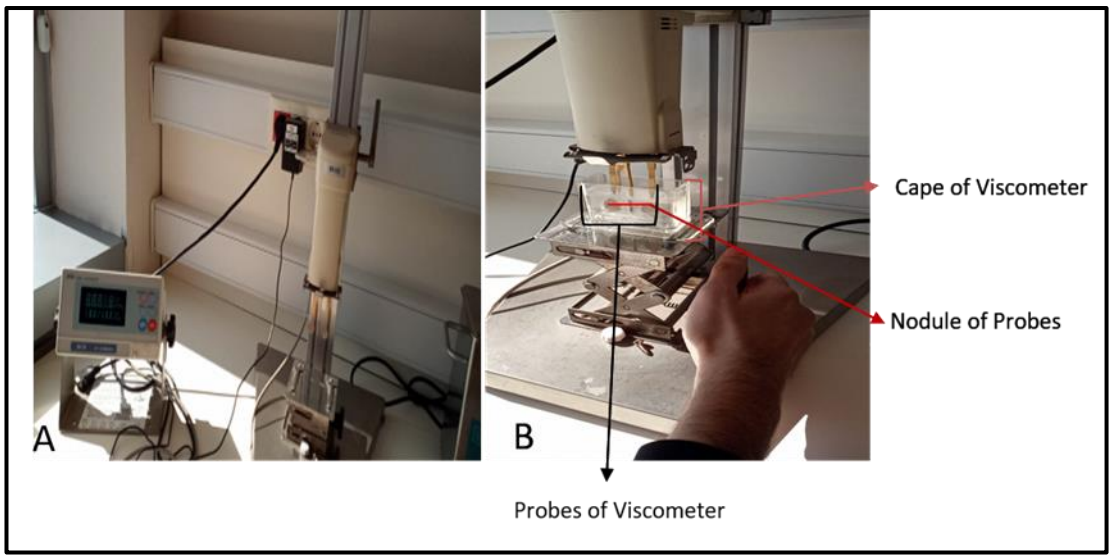

Figure 3.1. Viscometer device and it's parts which was used in viscosity measuring.

In order to measure the density of the CS solutions, a pycnometer (Pycnometer Density Bottle Meter, ISOLAB, Germany) was used. Empty weight of the pycnometer used was recorded as 29.38 g and then, each 25 mL solutions were poured into the beaker separately to determine values of viscosity per each sample. As seen in Table 3.1, 54.957 g was obtained as total weight of the pycnometer with 0.3% w/v CS-1% v/v AA solution, 55.0805 g was obtained as total weight of the pycnometer with 0.5% w/v CS-1% AA solution, 55.0755 g was obtained as total weight of the pycnometer with 0.7% w/v CS-1% AA solution, 54.978 g was obtained as total weight of the pycnometer with 1% w/v CS-1% AA solution. Results of density for each CS based composite solutions were calculated according to Eq.3.1 and Eq.3.2.

$$d = \frac{\mathrm{m}}{\mathrm{v}} \tag{3.1}$$

Here, d is density (g/cm^3), m is the mass of the solution (g), and v is volume (cm^3). Using Eq. 3.1, the density of the chitosan solutions was evaluated as shown in Eq. 3.2:

$$d = \frac{\mathrm{m}}{\mathrm{v}} = \frac{\mathrm{fp} - \mathrm{ep}}{v} \tag{3.2}$$

Here, fp is total mass of pycnometer with solution (g), ep is the mass of empty pycnometer (g), and v is the volume of pycnometer (cm^3). Using Eq. 3.2, we calculated density of each the CS solution as shown in Table 3.5.

Table 3.5. The CS solutions and their density calculating.

Solution	Fp(g)	ep(g)	Volume (cm^3)	Calculation	Density (g/cm^3)
0.3% w/v CS-1% v/v AA solution	54.957			d= (54.957-29.838)/25	1.0048
0.5% w/v CS-1% AA solution	55.0805	29.838	25	d=(55.0805-29.838)/25	1.0097
0.7% w/v CS-1% AA solution	55.075			d = (55.075-29.838)/25	1.0095
1% w/v CS-1% AA	54.978			d = (54.978-29.838)/25	1.0056

The surface tension of each CS based nanocomposite polymeric solutions was measured by using a contact angle device (Attention/Theta Life, Sweden) with measurement sensitivity of approximately 0.1 mN/m. The needle of the device was used to determine the surface tension of the CS based nanocomposite polymeric solutions. When the drop falling from the tip of the needle burst, a cross-sectional area was created and the surface tension was measured by calculating the gap at the burst.

3.2.3. Preparation of Nanobiocomposite Solution

Preparation of CS based nanobiocomposite solution includes couple of steps like mixing surfactant agent and BN ceramic nano powders in water environment and sonication the for a determined period of timed. Carboxymethyl cellulose (CMC) was used as a surfactant agent in order to disperse BN ceramics well in CS polymeric solutions during a preparation of BN added chitosan based nanobiocomposite solutions. So, firstly, 0.04 g BN and 0.08g carboxymethyl cellulose (CMC) were mixed in 40 ml DW by magnetic stirring at 600 rpm for 15 min at ambient temperature (23±2°C). After mixing, the mixture was sonicated (BANDELIN SONOPULS HD 2070, Germany) at 750W power for 15 minutes in order to provide well-dispersion of BN powders, and 40 ml 0.1% w/v BN-0.02% w/v CMC solution was prepared. Meanwhile, 1% w/v CS- 1% v/v AA solution was prepared as described in chapter

3.2.2. 2 ml of 0.1% w/v BN-0.02% w/v CMC solution was added slowly in a stirring 2 ml 1% w/v CS- 1% v/v AA solution at 1000 rpm and it was mixed in a magnetic stirrer for 15 min as stated in Table 3.6. 4ml 0.05% w/v BN- 0.01% w/v CMC-0.5% w/v CS- 0.5% v/v AA nanobiocomposite solution was obtained. However, CS and CMC were crosslinked rapidly as in undesired structure. So then, a use of CMC was desisted.

Table 3.6 Preparation of CMC added BN-Chitosan solutions; amounts, concentration and parameters used in the present work.

MF Device	Material from which is produced /Brand-Model	Function
T-Shaped Chip	Polymethylmethacrylate (PMMA)	Bubble formation by combining the solution gas solution with the gas at a T-Junction point
N_2 Gas Tank	Yıldız-N1-230	Inert gas source for bubble
Microtubes	Fluoroethylene polypropylene (FEP)	Provide to T-Shaped chip solution which is coming from syringe pump and gas transmission, provide to leaving bubbles from system
Syringe pump	Inovenso/IPS-14-RS	Provide arrival of solution with syringe to Microfluidic systems

The CS based nanobiocomposite solutions were prepared without CMC. For example, 0.04 g BN and 0.4 g CS were mixed at 800 rpm in 40 ml of DW and 0.4 ml of AA together for 12 h at 37 ^{o}C by magnetic stirring. Then, this mixture was sonicated (BANDELIN SONOPULS HD 2070, Germany) at 750W power for 15 minutes to provide dispersion of BN powder as shown in Table 3.7.

Table 3. 7. Parameters of BN added nanobiocomposit solution**.**

Material	Concentration and Amount	Parameters
BN	0.1%0.04g	**Magnetic Stirrer** 800rpm 12h 37ºC
CS	1%0.4g	**Sonication**
AA	1%0.4ml	750 Watt 15m
DW	40ml	

3.2.3.1. Optimization of Boron Nitride Concentration in Nanobiocomposite Solution

Chitosan based nanobiocomposite solutions were homogenously prepared with different ratios of Boron nitride nano ceramic powders with 0.1% w/v, 0.07% w/v, 0.05% w/v and 0.03 w/v respectively. These aqueous polymeric solutions were consisting of constant ratios of 1% v/v AA and 1% w/v chitosan polymer. For example, 0.04g BN ceramic powders and 0.4 g CS polymer were blended in 0.4 ml AA blended 40 ml DI water solution until appearing a homogeneous solution view for 12s, at 800 rpm, 37ºC by magnetic stirring and 0.1% w/v BN-1% w/v CS-%1 v/v AA nanobiocomposite solution was obtained. For example, details of solution content prepared was indicated as solution number 1 in Table 3.8. 0.028g BN and 0.4 g CS were mixed in 40 ml DW with 0.4 ml AA until appearing a homogeneous solution view for 12s, at 800 rpm, 37ºC. 0.07% w/v BN-1% w/v CS-%1 v/v AA nanobiocomposite solution was obtained which indicated as solution number 2 in Table 3.8. 0.02g BN and 0.4 g CS were mixed in 40 ml DW and 0.4 ml AA until appearing a homogeneous solution view for 12s, at 800 rpm, 37ºC by magnetic stirring. 0.05% w/v BN-1% w/v CS-%1 v/v AA nanobiocomposite solution was obtained which indicated as number 3 in Table 3.8. 0.012g BN and 0.4 g CS were mixed in 40 ml DW and 0.4 ml AA until appearing a homogeneous solution view for 12s, at 800 rpm, 37ºC by magnetic stirring. 0.03% w/v BN- 1% w/v CS-%1 v/v AA nanobiocomposite solution was obtained which indicated as number 4 in Table 3.8. In the present work, digital view of nanobiocomposite solutions prepared were captured by using a smart phone (Vestel, Venus V7) with 13 MP+2 MP rear camera and 52 MP resolution.

Table 3.8. Nanobiocomposite solutions which optimized of BN concentration and their preparation parameters.

Solution Nu	Solution	Amount				Parameters
		CS (g)	BN(g)	AA(ml)	DW(ml)	
1	0.1% w/v BN-1% w/v CS-%1 v/v AA	0.4	0.04	0.4	40	Magnetic Mixing: 800rpm 12h 37°C
2	0.07% w/v BN-1% w/v CS-%1 v/v AA	0.4	0.028	0.4	40	Sonication: 750 Watt 15 mins
3	0.05% w/v BN-1% w/v CS-%1 v/v AA	0.4	0.02	0.4	40	
4	0.03% w/v BN- 1% w/v CS-%1 v/v AA	0.4	0.012	0.4	40	

3.2.3.2. Physical Characterization of Nanobiocomposite Solutions

Physical characterization studies were carried out to assess to find out the most suitable BN added and only CS based solution for processing them through the T-shaped microfluidic device technique.

Viscosities of chitosan based nanobiocomposite solutions were measured at room temperature with the turning fork method by immersing the probes in the device (SV-10, Vibro Viscometer, A&D, Japan). 35 ml of the each nanobiocomposite solutions were poured into viscosity vial and probes of viscometer were arranged, separately. Setting up the probes and vials for reaching the nanobiocomposite solution on nodules of the probes was significant due to a collection of correct results. After the probes arranged, the viscometer was switched on and measurement of viscosity for a solution was achieved. The value of solution viscosity was measured repeatedly on three different occasions using viscometer screen and probable error of each mean value was calculated then the mean viscosity value of the three sets of measurements were determined.

In order to measure the density of the chitosan based nanobiocomposite solutions, a pycnometer (Pycnometer Density Bottle Meter, ISOLAB, Germany) was used. Table 3.9 presented data set of densities achieved for the chitosan based nanobiocomposite solutions. Weight of the pycnometer used was recorded as 29.838 g and subsequently 25 mL of chitosan based nanobiocomposite solutions were poured into the beaker, respectively to determine weight of the solution used. For example; 55.208 g was obtained as the total weight of the pycnometer for 0.1% w/v BN-1% w/v

CS-1% v/v AA solution; 74.338 g was obtained as the total weight of the pycnometer for 0.07% w/v BN - 1% w/v CS-1% AA solution; 55.68 g was obtained as the total weight of the pycnometer for 0.05% w/v BN - 1% w/v CS-1% AA solution; and 55.818 g was obtained as the total weight of the pycnometer for 0.03% w/v BN - 1% w/v CS-1% AA solution. As seen in Table 3.9, differences on weight between the topped up pycnometer(fp) and the empty pycnometer(ep) were taken and density of nanobiocomposite solutions used was calculated according Eq. 3.1 and Eq. 3.2.

Tablo 3.9. Data of densities achieved for the CS based nanobiocomposite solutions.

Solution	fp(g)	ep(g)	Volume(cm^3)	Calculation	Density (g/ cm^3)
0.3% w/v CS-1% v/v AA	54.957g	29.838g	25	d = (54.957-29.838)/25	1.0048
0.5% w/v CS-1% AA	55.0805g			d= (55.0805-29.838)/25	1.0097
0.7% w/v CS-1% AA	55.0755g			d= (55.075-29.838)/25	1.0095
1% w/v CS-1% AA	54.978g			d= (54.978-29.838)/25	1.0056

3.2.4. Production of Chitosan Hydrogels

Production of hydrogels using chitosan polymer needs a cross-linking known as gelation process to form hydrogel scaffolds. In the present work, 0.3% w/v CS-1% v/v AA, 0.5% w/v CS-1% v/v AA, 0.7% w/v CS-1% v/vAA and 1% w/v CS-1% v/vAA polymeric solutions were firstly prepared as detailed in part 3.2.1.2 in chapter 3. Then, gelation process was achieved via using one of a glutaraldehyde (GA) gelation solution as an agent with a volume ratio of 1:1 (CS:GA) to form chitosan hydrogel scaffolds. Optimization of CS and GA concentration studies were applied to determine accurate ratio between them in order to produce most better bulky CS hydrogels in mechanical stability.

3.2.4.1. Optimization of Glutaraldehyde Gelation Agent

In order to optimize concentration of Glutaraldehyde (GA), 0.1% v/v GA, 0.2% v/v GA, 0.3% v/v G, 0.6 % v/v GA, 0.9% v/v GA, 1% v/v GA, 2% v/v GA, 4% v/v GA, 6% v/v GA and 12.5% v/v GA aqueous solutions were prepared respectively. To achieve the above-mentioned concentrations, 25% v/v GA aqueous solution was used as stock solution and it was diluted by using DW. Using the equation 3.3, volume of the necessary stock solution calculated.

$$c_1 v_1 = c_2 v_2 \tag{3.3}$$

Here, c_1 is initial concentration (% v/v) of solution, v_1 is initial volume (ml) of the solution, c_2 is final concentration (% w/v) of the solution and v_2 is final concentration of the solution. There are details of chitosan gelation by using various concentrations of GA to achieve chitosan hydrogel scaffolds below;

- 0.4 ml 25% v/v GA added to 9.96 ml DI water and mixed at 600 rpm for 2 minutes by magnetic stirring at ambient temperature (23±2°C) to obtain 10 ml 0.1% v/v GA solution. For covalent cross-linking gelation, 2 ml 0.1% v/v GA solution was added to 2 ml 0.3% w/v CS- 1% v/v AA solution by the drop-by-drop method and stayed for 30 minutes at 37 ºC.

- 2. 0.08 ml 25% v/v GA added to 9.92 ml DI water and mixed at 600 rpm for 2 minutes by magnetic stirring at ambient temperature (23±2°C) to obtain 10 ml 0.2 % v/v GA solution. For covalent cross-linking gelation, 2 ml 0.2% v/v GA solution was added to 2.5 ml 0.3% w/v CS- 1% v/v AA solution by the drop-by-drop method and stayed for 30 minutes at 37 ºC.

- 3. 0.12 ml 25% v/v GA added to 9.88 ml DW and mixed at 600 rpm for 2 minutes by magnetic stirring at ambient temperature (23±2°C) to obtain 10 ml 0.3 % v/v GA solution. For covalent cross-linking gelation, 2 ml 0.3% v/v GA solution was added to 2ml 0.3% w/v CS- 1% v/v AA solution by the drop-by-drop method and stayed for 30 minutes at 37 ºC.

- 4. 0.24 ml 25% v/v GA added to 9.76 ml DW and mixed at 600 rpm for 2 minutes by magnetic stirring at ambient temperature (23±2°C) to obtain 10 ml 0.6 % v/v GA solution. For covalent cross-linking gelation, 2 ml 0.6% v/v GA solution was added to 2.5 ml 0.3% w/v CS- 1% v/v AA solution by the drop-by-drop method and waited for 30 minutes at 37 ºC.

- 5. 0.36 ml 25% v/v GA added to 9.64 ml DW and mixed at 600 rpm for 2 minutes by magnetic stirring at ambient temperature (23±2°C) to obtain 10 ml 0.9 % v/v GA solution. For covalent cross-linking gelation, 2 ml 0.6% v/v GA solution was added to 2 ml 3% w/v CS- 1% v/v AA solution by the drop-by-drop method and waited for 30 minutes at 37 ºC.

- 6. 0.4 ml 25% v/v GA added to 9.6 ml DW and mixed at 600 rpm for 2 minutes by magnetic stirring at ambient temperature (23±2°C) to obtain 10 ml 1% v/v GA solution. For covalent cross-linking gelation, 2 ml 1% v/v GA solution was added to 2 ml 0.3% w/v CS- 1% v/v AA solution by the drop-by-drop method and waited for 30 minutes at 37ºC.

- 7. 0.8 ml 25% v/v GA added to 9.6 ml DW and mixed at 600 rpm for 2 minutes by magnetic stirring at ambient temperature (23±2°C) to obtain 10 ml 2% v/v GA solution. For covalent cross-linking gelation, 2 ml 2% v/v GA solution was added to 2 ml 0.3% w/v CS- 1% v/v AA solution by the drop-by-drop method and waited for 30 minutes at 37ºC.
- 8. 1.6 ml 25% v/v GA added to 8.4 ml DW and mixed at 600 rpm for 2 minutes by magnetic stirring at ambient temperature (23±2°C) to obtain 10 ml 4% v/v GA solution. For covalent cross-linking gelation, 2 ml 4% v/v GA solution was added to 2 ml 0.3% w/v CS- 1% v/v AA solution by the drop-by-drop method and waited for 30 minutes at 37ºC.

- 9. 2.4 ml 25% v/v GA added to 7.6 ml DW and mixed at 600 rpm for 2 minutes by magnetic stirring at ambient temperature (23±2°C) to obtain 10 ml 6% v/v GA solution. For covalent cross-linking gelation, 2 ml 6% v/v GA solution was added to 2

ml 0.3% w/v CS- 1% v/v AA solution by the drop-by-drop method and waited for 30 minutes at 37ºC.

- 5 ml 25% v/v GA added to 5 ml DW and mixed at 600 rpm for 2 minutes by magnetic stirring at ambient temperature (23±2°C) to obtain 10 ml 6% v/v GA solution. For covalent cross-linking gelation, 2 ml 6% v/v GA solution was added to 2 ml 0.3% w/v CS- 1% v/v AA solution by the drop-by-drop method and stayed for 30 minutes at 37ºC.

3.2.4.2. Optimization of Chitosan content in Hydrogel Scaffolds

Optimization of chitosan content in hydrogel scaffold is required because of a direct relationship exists between gelation agent and polymer's amount. So, various concentration of chitosan polymer in aqueous solution like; 1% w/v CS- 1% v/v AA, 0.7% w/v CS - 1% v/v AA and 0.5% w/v CS - 1% v/v AA were prepared and details of this process was mentioned in section 3.2.1.2 on the Chapter 3. Furthermore, different concentration of gelation agent such as, 0.1% v/v GA, 0.2% v/v GA, 0.3% v/v GA, 0.6 % v/v GA, 0.9% v/v GA, 1% v/v GA, 2% v/v GA, 4% v/v GA, 6% v/v GA and 12.5% v/v GA were prepared and detailed in section 3.2.4.1 on the Chapter 3. To achieve a successful gelation of chitosan polymer, 2 ml of GA solution added to each 2ml of chitosan based-solutions by the drop-by-drop method and stayed for 30 minutes at 37ºC.

3.2.5. Production of Boron Nitride/Chitosan Nanobiocomposites Hydrogels by using the Conventional Method

In order to evaluate effect of boron nitrite on nanobiocomposite hydrogel scaffold structures, a preparation of BN enriched chitosan based-nanobiocomposites solutions were prepared with ratios as follows; a) 0.1% w/v BN-1% w/v CS-%1 v/v AA, b) 0.07% w/v BN- 1% w/v CS-%1 v/v AA, c) 0.05% w/v BN- 1% w/v CS-%1 v/v AA and d) 0.03% w/v BN- 1% w/v CS-%1 v/v AA as described in section 3.2.3.1 on the chapter 3. To investigate an effect of gelation agent, glutaraldehyde, solutions were prepared with ratios as follows; 0.1% v/v GA, 0.2% v/v GA, 0.3% v/v G, 0.6 %

v/v GA, 0.9% v/v GA, 1% v/v GA, 2% v/v GA, 4% v/v GA, 6% v/v GA and 12.5% v/v GA as previously mentioned in section 3.2.4.1 on the chapter 3. The nanobiocomposite hydrogels were prepared by combining BN enriched CS based-solutions with a GA solution at a volume ratio of 1:1. Optimization of GA concentration and BN concentration studies were applied to determine suitable solution to use it in microfluidics system in order to achieve bulky BN enriched CS based nanobiocomposites hydrogel scaffolds.

Hydrogel formation appeared with a covalent interaction between a positively charged NH_2 group of chitosan solution and negatively charged group of the aldehydic in GA solution. After gelation by covalent interaction, the resultant nanobiocomposite hydrogels were freeze dried in lyophilization device (TK 252, Nuve, Turkey). The produced nanobiocomposite hydrogels were kept in freezer at -80 °C during a night before a lyophilization process. The frozen nanobiocomposite hydrogels were treated for a day, until pressure reach to 6.11 mbar in the lyophilization device.

3.2.5.1. Boron Nitride Optimization Studies in Production of Boron Nitride/Chitosan Nanobiocomposites Hydrogels

40 ml of a) 0.1% w/v BN-1% w/v CS-%1 v/v AA, b) 0.07% w/v BN- 1% w/v CS-%1 v/v AA, c) 0.05% w/v BN- 1% w/v CS-%1 v/v AA and d) 0.03% w/v BN- 1% w/v CS-%1 v/v AA solutions were prepared as described in section 3.2.3.1on Chapter 3. 2 ml of the each nanobiocomposite solutions were added onto 2ml of a) 0.1% v/v GA, b) 0.2% v/v GA, c) 0.3% v/v G, d) 0.6 % v/v GA, e) 0.9% v/v GA, f) 1% v/v GA, g) 2% v/v GA, h) 4% v/v GA, i) 6% v/v GA and k) 12.5% v/v GA by the drop-by-drop method and stayed for 30 minutes at 37^{o}C.

3.2.6. Production of Only Chitosan and Boron Nitride/Chitosan Nanobiocomposite Bubbles and Hydrogel by using the T-Shaped Microfluidic Junction Device Method

Microfluidic bubble production was delivered using the home-made polymethylmethacrylate (PMMA) T-shaped microfluidic device with dimensions of 30mm× 30mm × 15mm. The set-up for the generation of monodisperse polymeric and

nanobiocomposite bubbles was shown in Figure 3.2. These microfluidic device elements which forms set-up, the material from which devices are made and the function of these devices are stated in Table 3.10.

Table 3. 10. MF and its devices and functions.

MF Device	Material from which is produced /Brand-Model	Function
T-Shaped Chip	Polymethylmethacrylate (PMMA)	Bubble formation by combining the solution gas solution with the gas at a T-Junction point
N_2 Gas Tank	Yıldız-N1-230	Inert gas source for bubble
Microtubes	Fluoroethylene polypropylene (FEP)	Provide to T-Shaped chip solution which is coming from syringe pump and gas transmission, provide to leaving bubbles from system
Syringe pump	Inovenso/IPS-14-RS	Provide arrival of solution with syringe to Microfluidic systems

The chitosan polymer (1% w/v CS-1% v/v AA) based solution was prepared as previously described in section 3.2.1.1 on Chapter 3. Later, this solution was filtered with a 0.45-μm syringe filter (PTFU, GVS, UK) to eliminate agglomerated CS particles and thus, clogging successfully prevented while feeding the polymer solution into the micro-scale channels. The polymer solution was filled in a 10-mL BD plastic syringe (Becton Dickinson, USA) and placed in syringe pump (IPS-14-RS, Inovenso, USA). The polymer solution flow with 200±10 μm/minute flow rate was supplied into the side-inlet of the T-shaped microfluidic junction device. N_2 gas pressure with 10 psi was supplied into upper side-inlet of the T-shaped microfluidic junction device. Both polymer solution and N_2 gas, mixed in the T junction point of the T-shaped microfluidic device. Subsequently, production of polymeric bubbles was carried out. These resultant polymeric bubbles were then guided down the bottom side of T-Shaped microfluidic junction device and polymeric bubbles were collected in the beaker for gelation which was filled with 2% v/v GA solution (Figure 3.2). The mix of 2% v/v GA and polymeric bubble cluster was cross-linked at 37^{o}C for 30 minutes.

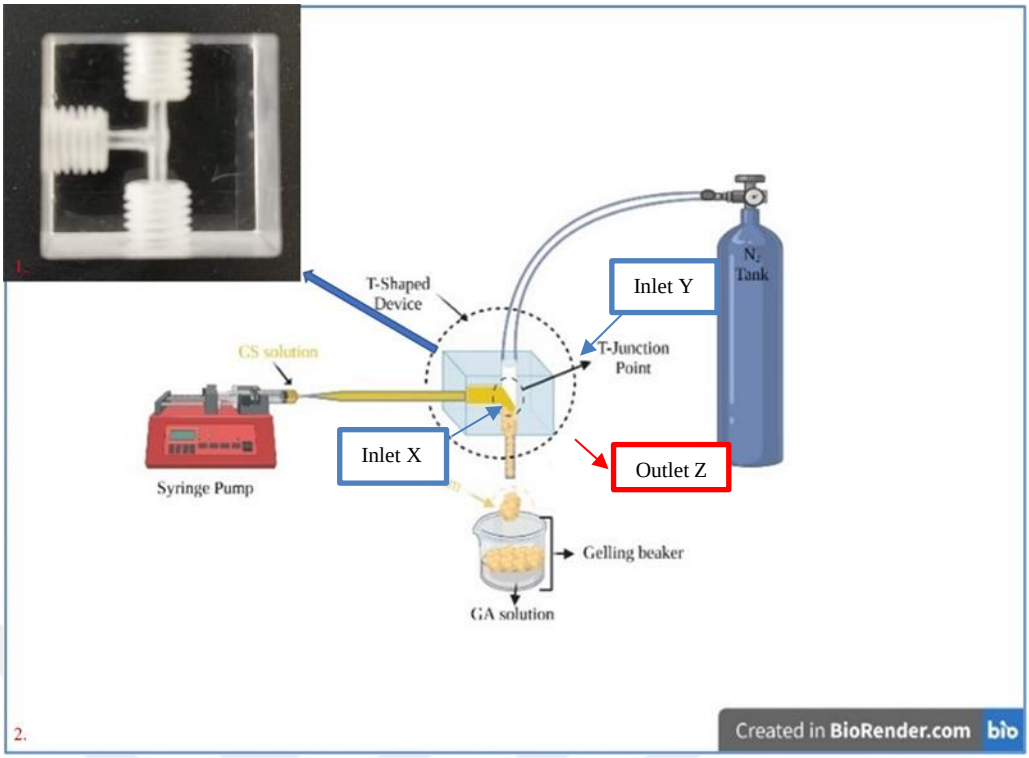

Figure 3. 2. (a) Real image of T-Shaped Chip. (b) Representative image of T-Shaped microfluidic system and producing polymeric foams with this system.

The nanobiocomposite (0.1% w/v BN- 1% w/v CS-1% v/v AA) solution prepared as described in Chapter 3.2.3. Later the nanobiocomposite solution was filtered with a 0.45-µm syringe filter (PTFU, GVS, UK) to eliminate agglomerated CS and BN particles. The nanobiocomposite solution was added a 10-mL BD plastic syringe (Becton Dickinson, USA) and placed in syringe pump (IPS-14-RS, Inovenso, USA). The nanobiocomposite solution flow is supplied into the inlet X of T-Shaped chip with an 200±10 µm/minute flow rate. N_2 gas pressure is supplied into the inlet Y of T-Shaped with 10 psi. Both nanobiocomposite solution and N_2 gas, mixed in the T junction point of the chip. Subsequently, production of nanobiocomposite bubbles were carried out. These resultant bubbles were then guided down an outlet Y of T-Shaped chip and nanobiocomposite foams were collected at the beaker (Figure 3.2).

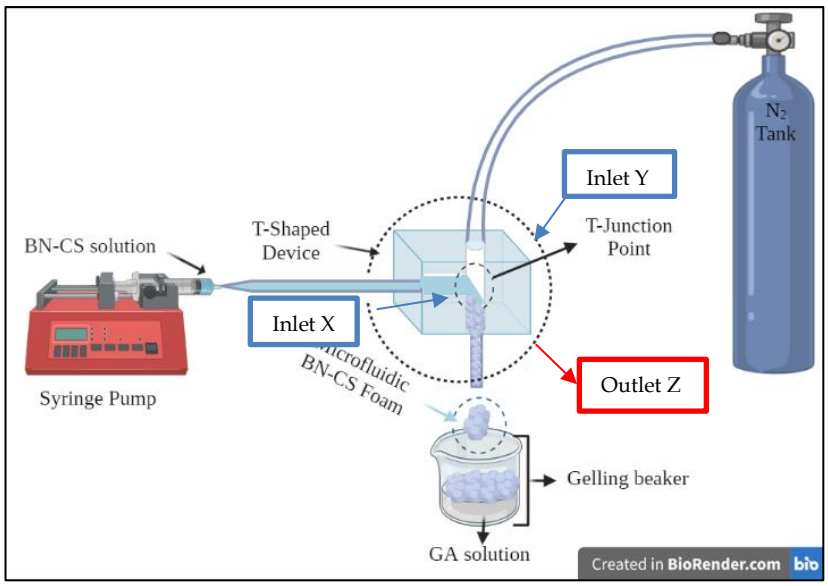

Figure 3. 3. Representative image of T-Shaped microfluidic system and producing nanobiocomposite foams with this system.

3.2.7. Determination of the Size and Size Distribution of the Produced Chitosan, Boron Nitride, and Chitosan Foam

The morphology of the chitosan and BN added nanobiocomposite foams produced by the T-junction microfluidic device was evaluated using an optical microscope (Nikon-Eclipse LV 150N). The polymeric and nanobiocomposite foams were produced as described in chapter 3.2.6. A few drop of freshly generated CS and BN added nanobiocomposite microbubbles were collected on microscopy slayd at the outlet channel of the T-junction microfluidic chip. The size measurement of microbubbles was done afterwards producing them from the microchannel. In order to precise evaluation of the images, 5X and 10X objective lenses were used for magnification. Later, the bubble diameters of foam were determined and their images were recorded. Micrographs were obtained at 5x and 10X magnification, microbubble diameters were calculated using ImageJ program. Polydispersity index (PDI) of microbubbles was calculated using equation 3.4.

$$PDI(\%) = \frac{\sigma}{davg} x100 \qquad 3.4$$

Here σ is standard deviation of the mean bubble and davg is average the bubble diameter.

In addition, produced these polymeric and nanobiocomposite foam imaged with cell phone (Vestel, Venus V7, Turkey) which have 13 MP+2 MP rear camera and 52 MP resolution.

3.1.6. Characterization of Produced Chitosan, Boron Nitride /Chitosan Nanobiocomposite Solutions and Hydrogels

Sample of BN added nanobiocomposite solution 0.1% w/v BN- 1% w/v CS - 1% v/v AA (SBN), polymeric solution 1% w/v CS -1 % v/v AA (CG), acetic acid (PAA), 25% v/v GA solution (PGA) conventionally produced polymeric hydrogel 0.5% w/v CS- 0.5 % v/v AA- 0.5% v/v GA (CS1), conventionally produced polymeric hydrogel 0.5% w/v CS- 0.5 % v/v AA- 2% v/v GA (CS4), microfluidic polymeric hydrogel 0.5% w/v CS - 0.5% v/v AA - 2 %v/v GA (GMCS4), conventionally produced nanobiocomposite hydrogel 0.05% w/v BN- 0.5% w/v CS - 0.5% v/v AA - 1% v/v GA (BC1), conventionally produced nanobiocomposite hydrogel 0.035% w/v BN- 0.5% w/v CS- 0.5% w/v AA – 1% GA (BC2), conventionally produced nanobiocomposite hydrogel 0.025% w/v BN- 0.5% w/v CS- 0.5% v/v AA - 1% v/v GA (BC3), conventionally produced nanobiocomposite hydrogel 0.015% w/v BN- 0.5% w/v CS- 0.5% v/v AA - 1% v/v GA (BC4) and microfluidic nanobiocomposite hydrogel 0.05% w/v BN- 0.5% w/v CS- 0.5% w/v AA - 2% v/v GA (GMBC) were coded as stated in Table 3.7.

The samples characterisations which Fourier Transform Infrared Spectroscopy (FTIR), Differential Scanning Calorimeter (DSC), thermal gravimetric analysis (TGA), X-Ray Diffractometer (XRD) and Scanning Electron Microscopy (SEM) were done. Each characterization method explained in Chapter 3.1.6.1., 3.1.6.2, 3.1.6.3, 3.1.6.4. and 3.1.6.5 in detail.

Table 3.11: Characterized samples code, content, and produced methods**.**

Sample Code	Sample Content	Type	Procured Method
PBN	Pure BN powder	Chemical	Purchased
PCS	Pure CS powder	Chemical	Purchased
PAA	Acetic acid (Food Type)	Chemical	Purchased
PGA	25% v/v GA	Chemical	Purchased
CG	1% w/v CS -1 % v/v AA	Polymeric Solution	Magnetic Mixing
CS1	0.5% w/v CS- 0.5 0.5% v/v AA- 0.5%0 v/v GA	Polymeric Solution	SolventCasting+ lyophilised
CS4	0.5% w/v CS - 0.5 % v/v AA- 2% v/v GA	Polymeric Solution	Solvent Casting+ lyophilised
GMCS4	0.5% w/v CS - 0.5 %v/v AA - 2 %v/v GA	Polymeric Solution	Microfluidic+ lyophilised
BC1	0.05% w/v BN- 0.5% w/v CS – 0.5% v/v AA - 1% v/v GA	Nanobiocomposite Hydrogel	Solvent Casting + lyophilised
BC2	0.035% w/v BN- 0.5% w/v CS- 0.5% w/v AA - %1 GA	Nanobiocomposite Hydrogel	Solvent Casting + lyophilised
BC3	0.025% w/v BN- 0.5% w/v CS - %0.5 v/v AA - %1 GA	Nanobiocomposite Hydrogel	Solvent Casting + lyophilised
BC4	0.025% w/v BN- 0.5% w/v CS- 0.5% v/v AA - 1% v/v GA	Nanobiocomposite Hydrogel	Solvent Casting+ lyophilised
GMBC	0.05% w/v BN- 0.5% w/v CS - 0.5% w/v AA - 2% v/v GA	Nanobiocomposite Hydrogel	Microfluidic+ lyophilised
SBN	0.1% w/v BN- 1% w/v CS - 1% v/v AA	Nanobiocomposite Hydrogel	Magnetic Mixing+Sonication

3.1.6.1. Chemical Structural Analysis Of The Raw Materials Used And The Resultant Chitosan-Based Hydrogel Nanobiocomposites via Fourier Transform Infrared Spectroscopy

PBN, PCS, BN added nanobiocomposite hydrogel tissues scaffolds and polymeric tissue scaffolds which were produced with both solvent casting and microfluidic method, were subjected to FTIR analysis to determine functional group changes by observing the shifts in wavenumbers. Nearly 2 mg of each sample was

placed in the spectroscopy chamber (Spectrum 100, PerkinElmer, USA) and wavenumber measurements were performed in the range of 400-4000 cm^{-1}.

3.1.6.2. Differential Scanning Calorimeter Analysis

In order to indicate heat flow and glassy heat transmission temperature of PBN, PCS, polymeric hydrogels and BN added nanobiocomposite hydrogels samples were analysed with a differential scanning calorimeter (DSC 404 C Pegasus, Netzsch-Gerätebau GmbH, Germany) in different temperature. All samples entangled to analysis in dry state and their phase changes and temperatures were measured with a heating/cooling rate of 10°C/min in the temperature range from -25°C-300°C.

3.1.6.3. Thermal Gravimetric Analysis

In order to indicate thermal degradation and thermal stability of BN added nanobiocomposite hydrogels, polymeric hydrogels, PBN and PCS powders were analysed with a thermal gravimetric analysis device (TGA Linseis STA 1600 HP, Germany). The dry samples were examined in 25-800°C temperature range with a heating/cooling rate of 10°C/min. The temperature was increased with dynamic N_2 gas with a flow of 50ml/min.

3.1.6.4. X-Ray Diffractometer Analysis

In order to indicate the crystal structure properties of PBN, PCS, polymeric hydrogel tissue scaffolds and BN added nanobiocomposite tissue scaffolds hydrogels, XRD analysis were done (Bruker, AXS Discovery, USA). All samples were examined at Cu K_α radiation l= 0,154 nm and range of 2Θ = 5-90°, 2°/minute examine flow.

3.1.6.5. Scanning Electron Microscopy Analysis

BN added nanobiocomposite tissue scaffolds hydrogels, polymeric hydrogel tissue scaffolds, pure BN powder and chitosan particles cross structure, surface morphology and pore magnitude with pore size distribution analysis were carried out

with using SEM (Win10 FEI (Philips) XL30 microscope, USA) device. Sputter-coating of all samples were carried out (SC7620 Mini Sputter Coater Operating Manual, Quorum Technologies, UK) with gold for 1 min before examining through a SEM with an accelerating voltage of 5 kV.

4. RESULT AND DISCUSSION

4.1. Results of Chitosan Solution Preparation Studies

The chitosan solution (2.2% w/v CS-2% v/v AA) was presented in Figure 4.1 This solution had transparent image. But bubbles were observed in the solution. The bubble formation can be related with harsh magnetic stirring and it can be reduce by mild magnetic stirring. But mild magnetic stirring may result with long time of CS dissolving. As alternative, stove or homogenizer device can be use to eliminate the bubbles.

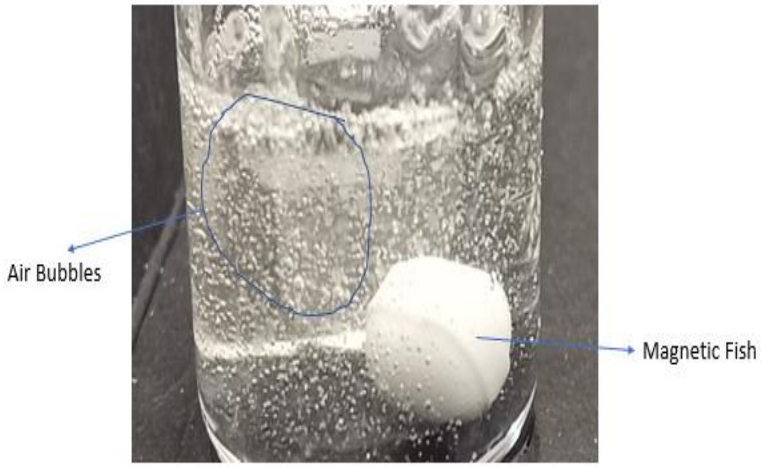

Figure 4. 3. 2.2% w/v CS- 2% v/v AA solution.

4.1.1. Results of Optimization of Acetic Acid Concentration in Chitosan-Acetic Acid-Water Solution

The digital image of 0.5% v/v AA- 2.2% w /v CS, 0.7% v/v AA- 1.5% w /v CS, 0.8% v/v AA- 1.5% w /v CS and 1.5% w /v CS 4. 1% v/v AA- 2.2% w /v CS solutions which AA concentrations were optimized, presented in Figure 4.2 respectively as numbered. As shown in the Figure 4.2, 1. solution had a very blurry appearance. The blurry appearance is due to the fact that the cationic NH_2 group of CS molecules were not protonated by negative charged acetic acid. It was observed that a certain amount of CS particles accumulated at the bottom of the beaker in 2. Solution. 2. Solution was possess less blurry image than 1. Solution. It was observed that a certain amount of CS

particles accumulated at the bottom of the beaker in 2. Solution and it was possess less blurry image than 2. Solution. Very few CS particles were observed in 3. Solution and no undissolved CS particles were observed in 4. Solution. The turbidity increased with increasing AA concentration. It was concluded that CS particles were best dissolved in 4. Solution with 1% v/v AA concentration among all these AA optimized solutions.

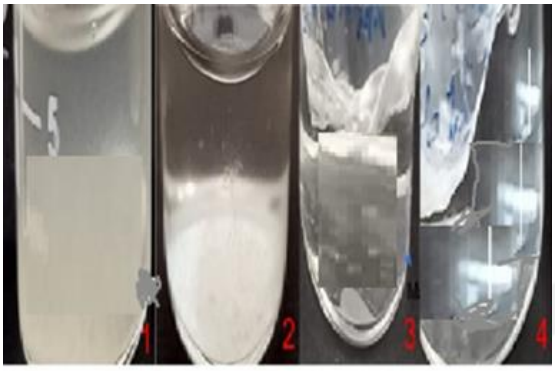

Figure 4. 4. Chitosan solutions which their AA concentrations were optimized. 1. 0.5% v/v AA- 2.2% w /v CS 2. 0.7% v/v AA- 1.5% w /v CS 3. 0.8% v/v AA- 1.5% w /v CS 4. 1% v/v AA- 2.2% w /v CS.

4.1.2. Results of Optimization of Chitosan Concentration in Chitosan-Acetic Acid-Water Solution

The digital image of 0.3% w/v CS-1% v/v AA, 0.5% w/v CS-1% v/v AA, 0.7% w/v CS-1% v/v AA and 1% w/v CS-1% v/v AA solutions which their CS concentrations were optimized, presented in Figure 4.3 respectively as numbered. 3. polymer solution was possess the blurriest image. Colour of the solutions were getting yellowish when CS concentration increased. The most transparent solution was 0.3% w/v CS-1% v/v AA.

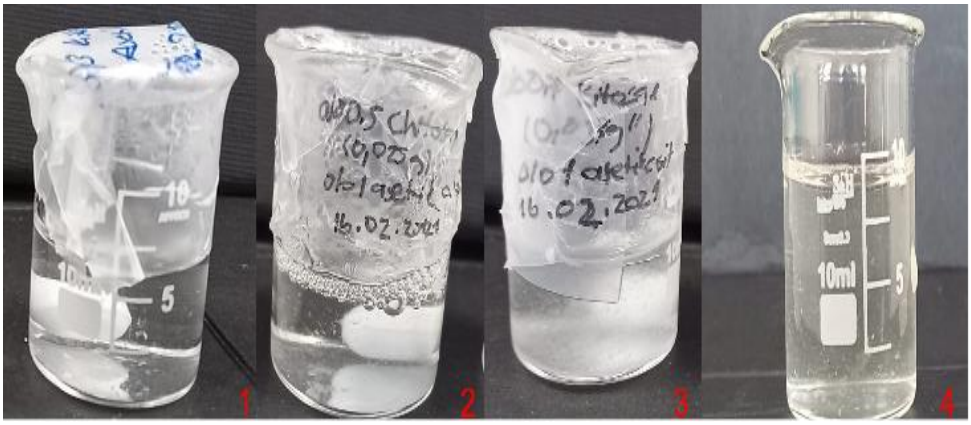

Figure 4. 5. Chitosan concentrations were optimized for polymeric chitosan solutions 0.3% w/v CS-1% v/v AA, 2. 0.5% w/v CS-1% v/v AA 3. 0.7% w/v CS-1% v/v AA 4. 1% w/v CS-1% v/v AA.

4.2. Results of Physicochemical Characterization of Chitosan-Based Solutions

The physicochemical properties of the different polymeric solutions possess key importance on microfluidic foam forming. Properties such as density, viscosity and surface tension of the polymeric solution influence microfluidic foam size and thus affect the diameters of the microbubbles. Viscosity changes with the variation in concentration of polymer solution. Adjusting the viscosity of solution is significant, because the microbubble size decreases with increase of polymeric solution viscosity when the flow rate of the liquid phase is kept constant. The surface tension of the polymeric solution is another important parameter to consider because microbubbles with higher surface tension cause faster film drainage.

Hence, chitosan based polymeric solutions physical characterization studies were conducted to evaluate the most proper solutions before use in microfluidic system. Determination of the physical properties of the CS solution will lead future studies of microfluidics. Table 4.1 demonstrates the density, viscosity and surface tension values of chitosan solutions at room temperature. Table 4.1 shows that an increase in CS concentration result in a increase of viscosity while keeping the AA concentration constant. In the values of density and surface tension, no significant change was observed with change of CS concentration. 0.3% w/v CS-1% v/v AA

solution had the lowest viscosity which may indicate the most proper solution in order to produce microfluidic foam.

Table 4. 1. Polymeric solution which their chitosan concentrations were optimized and their physical characterization results.

Solution	Viscosity (mPa.s)	Density (g/cm^3)	Surface Tension (mN/m)
0.3% w/v CS -%1 v/v AA	10.53	1.0048	69.04 (0.14 error margin)
0.5% w/v CS -%1 v/v AA	20.13	1.0097	69.73 (0.03 error margin)
0.7% w/v CS -%1 v/v AA	30.7	1.0095	69.73 (0.10 error margin)
1% w/v CS-%1 v/v AA	61.167	1.0056	68.98 (0.16 error margin)

4.3. Results of Optimization and Physicochemical Characterization of Boron Nitride Reinforced Nanobiocomposite Solutions

BN added nanobiocomposite solutions which contains different BN concentrations were shown in Figure 4.4. The transparency of the nanobiocomposite solution decreased with the increasing of BN concentration in nanobiocomposite solution.

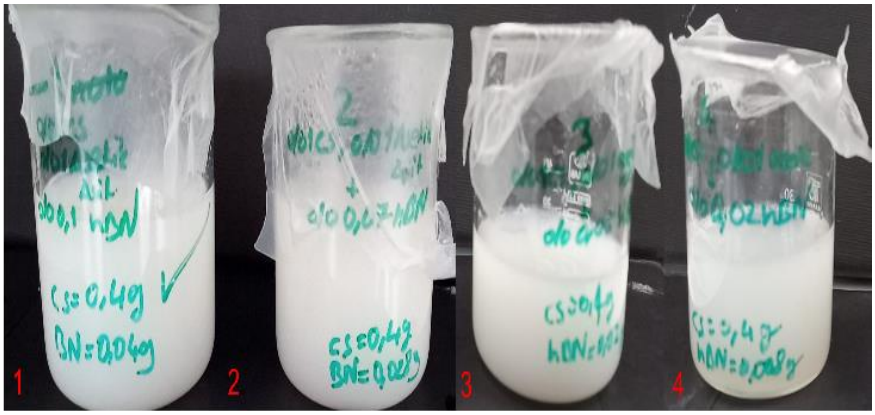

Figure 4. 6. BN concentrations were optimized BN added nanobiocomposite solutions 1. 0.1% w/v BN - %1 w/v CS- 1% v/v AA, 2. 0.07%w/v BN-1% w/v CS-1%v/v AA solution, 3. 0.05%w/v BN-1% w/v CS-1%v/v AA solution 4. 0.03%w/v BN-1% w/v CS-1%v/v AA solution.

BN added nanobiocomposite solutions physical characterization studies were conducted to evaluate the most proper nanobiocomposite solution before use in microfluidic system. Determination of the physical properties of the BN added nanobiocomposite solutions will lead future studies of microfluidic nanobiocomposite foam production. Properties such as density, viscosity and surface tension of the BN added nanobiocomposite solutions influence the foam size and thus affect the diameters of the microbubbles. Table 4.2 shows the density, viscosity and surface tension values of BN added chitosan solutions at room temperature.

Table 4.2. BN concentration optimized nanobiocomposite solution and their results of physical characterizations.

Solution	Viscosity (mPa.s)	Density (g/ cm^3)	Surface Tension (mN/m)
0.3% w/v CS - 1% v/v AA	10.53	1.0048	69.04 (0.14 error margin)
0.5% w/v CS - 1% v/v AA	20.13	1.0097	69.73 (0.03 error margin)
0.7% w/v CS - 1% v/v AA	30.7	1.0095	69.73 (0.10 error margin)
1% w/v CS- 1% v/v AA	61.167	1.0056	68.98 (0.16 error margin)

Table 4.2. shows that a higher concentration of BN in the BN added CS solutions clearly decreased viscosity and surface tension values. No significant change was observed with change of BN concentration in the BN added CS solutions as shown in Table 4.2. 0.1% BN- 1% w/v CS-1% v/v AA solution had the lowest viscosity and surface tension which may indicate the most proper solution in order to produce microfluidic foam.

4.4. Results of the Chitosan and Boron Nitride/Chitosan Nanobiocomposite Bubbles Generated via T-shaped Microfluidic Device Technique

Figure 4.5 and Figure 4.6 shows the digital images and optical microscopy images of CS and CS-BN nanobiocomposite microbubbles. As seen from Figure 4.5 and Figure 4.6, CS bubbles and nanobiocomposite bubbles were produced as contact with each other. However, the diameters of the chitosan microbubbles were not similar with each other. At the same time, BN added nanobiocomposite microbubbles with the same diameter were seen as shown in Figure 4.6. All of the obtained bubbles maintained their shapes as spherical. Sadly, the desired uniformity was not achieved.

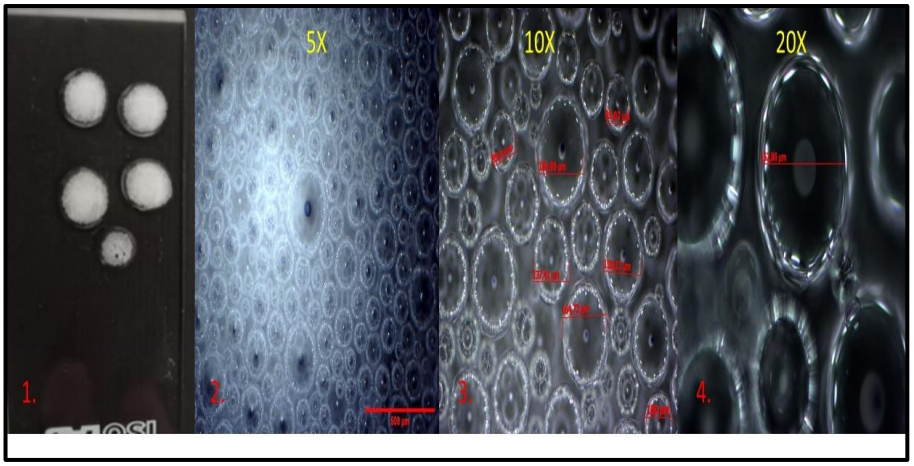

Figure 4. 7. Chitosan bubbles that were produced with using T-Shaped microfluidic and 1. Digital images, 2., 3., 4., and 5. Appearance in optical microscopy at different resolutions.

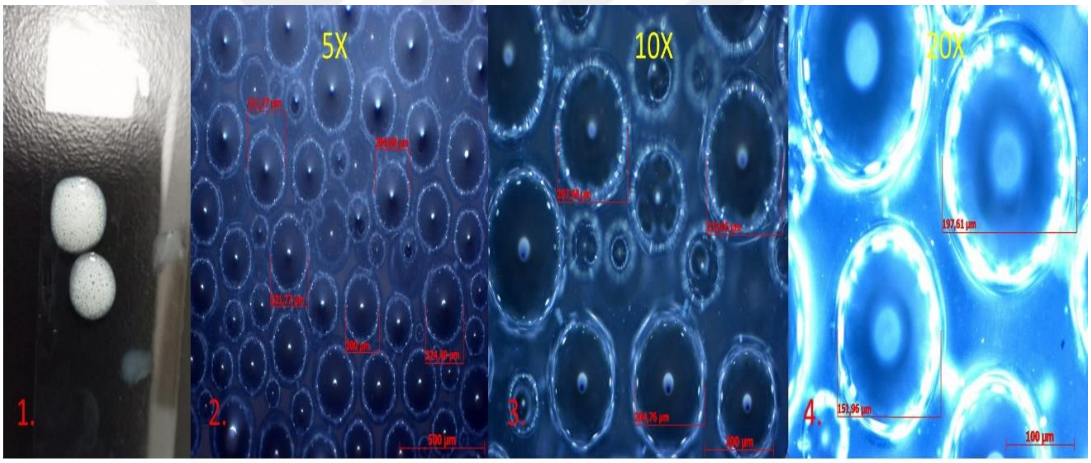

Figure 4. 8. Chitosan-BN nanobiocomposite bubbles that were produced using T-Shaped microfluidic and: 1. digital images; 3., 4., 5. appearance in optical microscopy at different resolutions.

Also using with Image J program, we calculated the radius and sizes of the bubbles. And with this data, we produced a histogram graph of the dispersion of polymeric bubbles. And we calculated their polydispersity index.

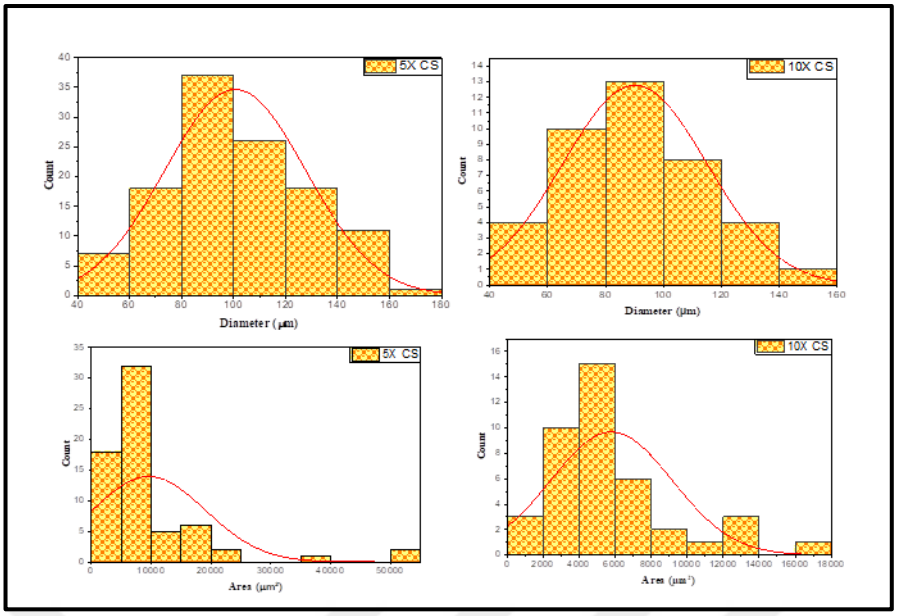

Figure 4.7. Histogram of chitosan microbubbles diameter and areas.

Figure 4.7 shows histogram results of chitosan microbubbles diameter and areas. The most observed CS microbubbles diameter are changing between 80-120 µm. The smaller CS microbubbles that possess between range of 40-80 µm diameter and the bigger CS microbubble that possess 120-180 µm were observed. In the concept of the area distribution, most of CS bubbles have area which between in 4000-6000 μm^2. When increase of resolution of microscopy number of bubbles were decreased. Also polydispersity index of CS bubbles were calculated 5X CS as 27%, 10X CS as 27%.

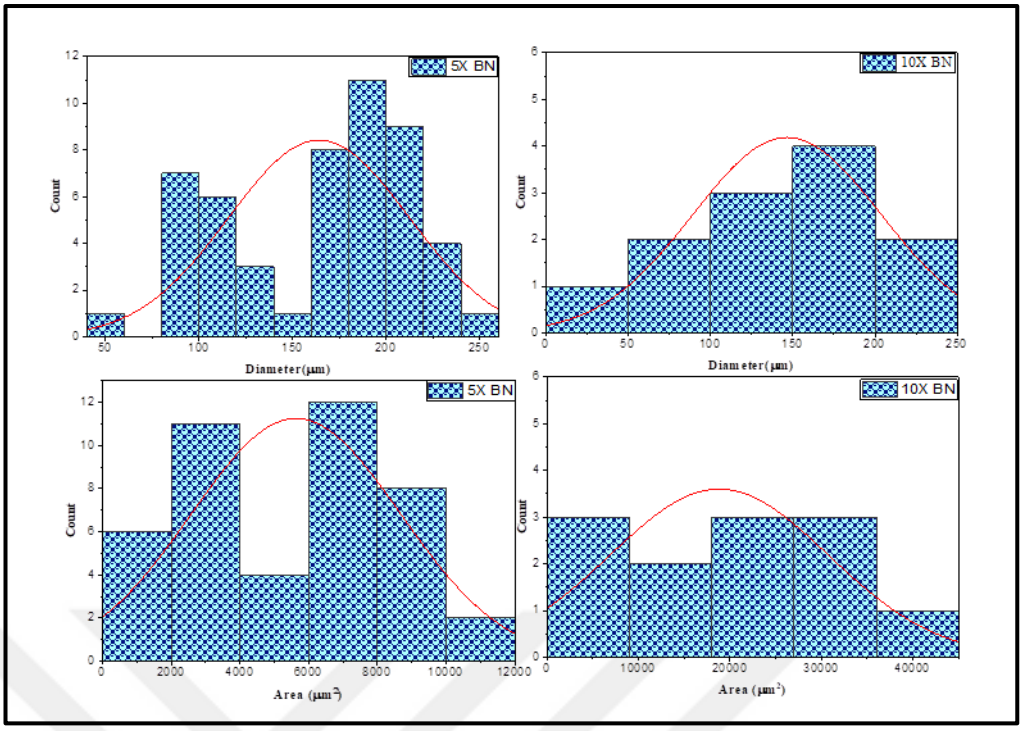

Figure 4. 9. Histogram of BN-CS microbubbles diameter and areas.

Figure 4.8 shows histogram results of BN-CS microbubbles diameter and areas. The most observed BN-CS microbubbles diameter are changing between 150-200 µm. The smaller BN-CS microbubbles that possess between range of 50-100 µm diameter and the bigger BN-CS microbubble that possess 200-250 µm were observed. PDI of 5X BN-CS microbubbles calculated as 6.2%

BN-CS bubbles, most of this bubbles diameter between range in 150-200 µm was observed. Besides there were also a few BN-CS bubble which have smaller or bigger diameter between range in 50-100 µm and 200-250 µm. PDI values were 6.2% for 5X BN-CS microbubbles and 29% for 10X BN-CS microbubbles.

4.5. Produced, Boron Nitride /Chitosan Nanobiocomposite and Chitosan Polymeric Hydrogels

Figure 4.9 shows digital image of both conventional and MF CS hydrogels and BN added CS nanobiocomposite hydrogels. In both conventional and traditional CS hydrogels, yellow colour of these hydrogels increased with the increasing

concentration of gluteradehiyde (GA). Also these hydrogels were in sponge like appearance after freeze- drying.

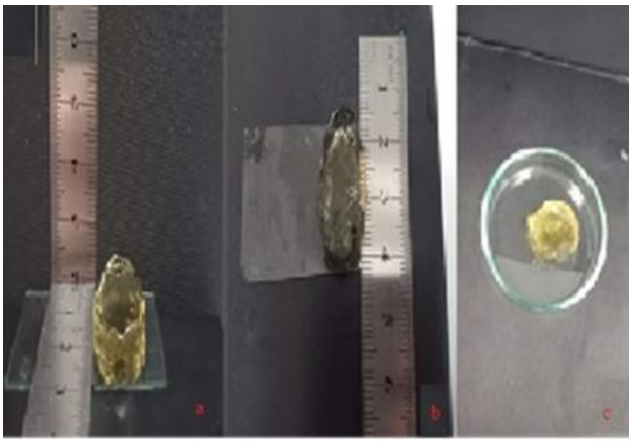

Figure 4.9. a) Polymeric hydrogels which were produced with solvent casting method; b.) 0.5% w/v CS-0.5% v/v AA-2% v/v GA Hydrogels, c) 0.5% w/v CS-0.5% v/v AA- 0.5% v/v GA Hydrogels

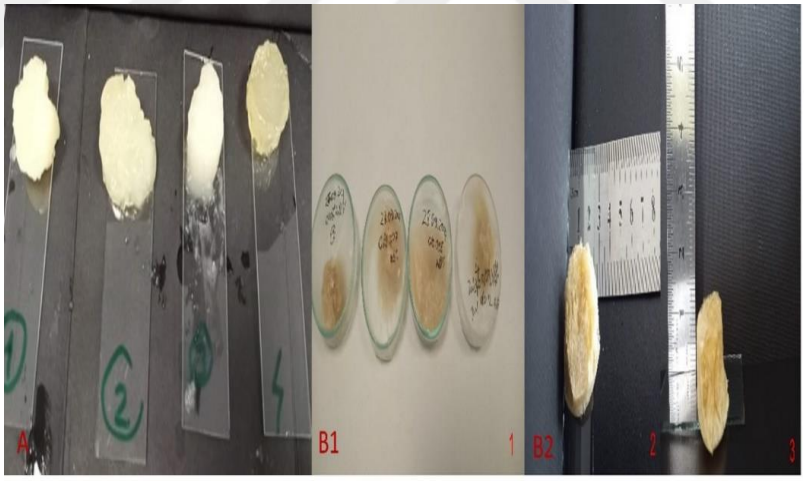

Figure 4.10. Nanobiocomposite hydrogels which BN concentrations were optimized. A 1. 0.05% w/v BN- 0.5% w/v CS- 0.5% v/v AA-0.5% v/v GA, A 2. 0.035% w/v BN- 0.5% w/v CS- 0.5% v/v AA-0.5% v/v GA, A 3. 0.025% w/v BN-0.5% w/v CS-0.5% v/v AA-0.5% v/v GA, A 4. 0.01% w/v BN-0.5% w/v CS- 0.5% v/v AA-0.5% v/v GA.

Figure 4.11 shows digital images of CS hydrogel which were produced with T-Shaped microfluidic system. As see in Figure 4.11 the CS hydrogel were white before stove process due to crosslinked CS foam. Destroyed CS foam had pale yellow appearance. After stove process, the colour of MF CS hydrogel turned from white to yellow. The colour changing may related with degassing process in stove or nature coarsening mechanism of foam. Also, disappearing of whiteness may evaluated due to resistance of CS foam to against pressure is weak. The freeze dried hydrogel had sponge like appearance.

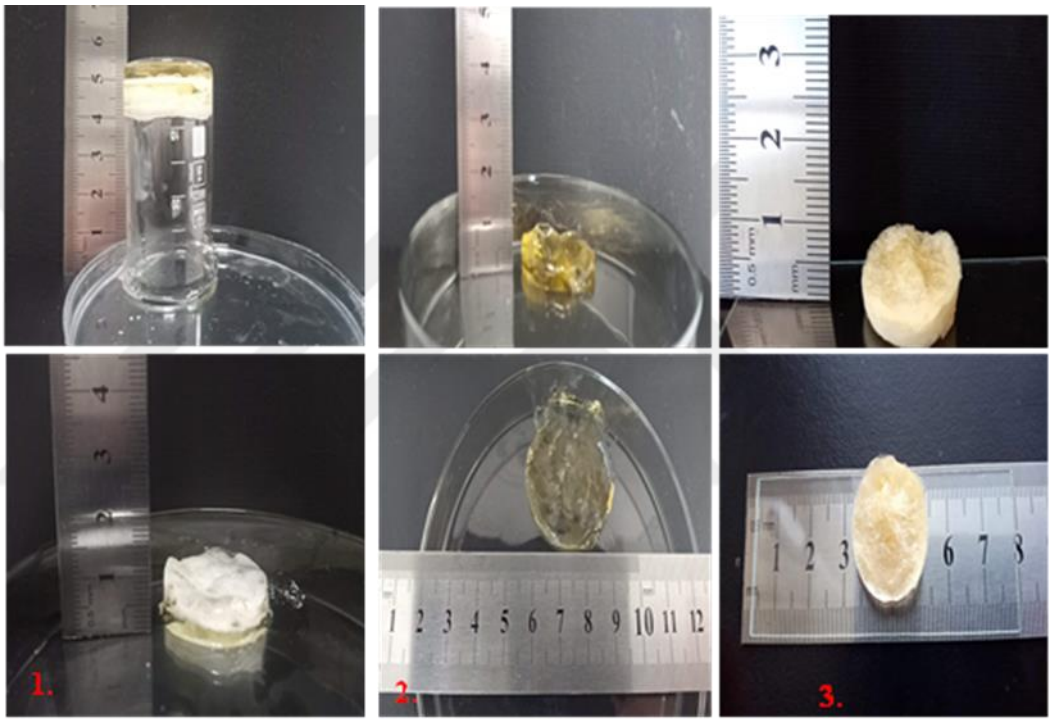

Figure 4. 10. Polymeric 0.5% w/v CS-0.5% v/v AA-2% GA hydrogel which were produced with T-Shaped microfluidic (1. Before stove process, 2. After stove process, 3. After lyophilization.)

Figure 4.12 shows digital images of novel nanobiocomposite hydrogel. As seen in Figure 4.12 the nanobiocomposite hydrogel were white. Clour of the nanobiocomposite hydrogel was not changed in both before and after stove process. When Figure 4.12 compared with Figure 4.11, it can be said that BN addition increased resistency of CS microbubbles against to external pressure. Also, the MF hydrogels

were possess more transparent and bright appearance than the traditional hydrogels as seen in Figure 4.9, Figure 4.10, Figure 4.11 and Figure 4.12.

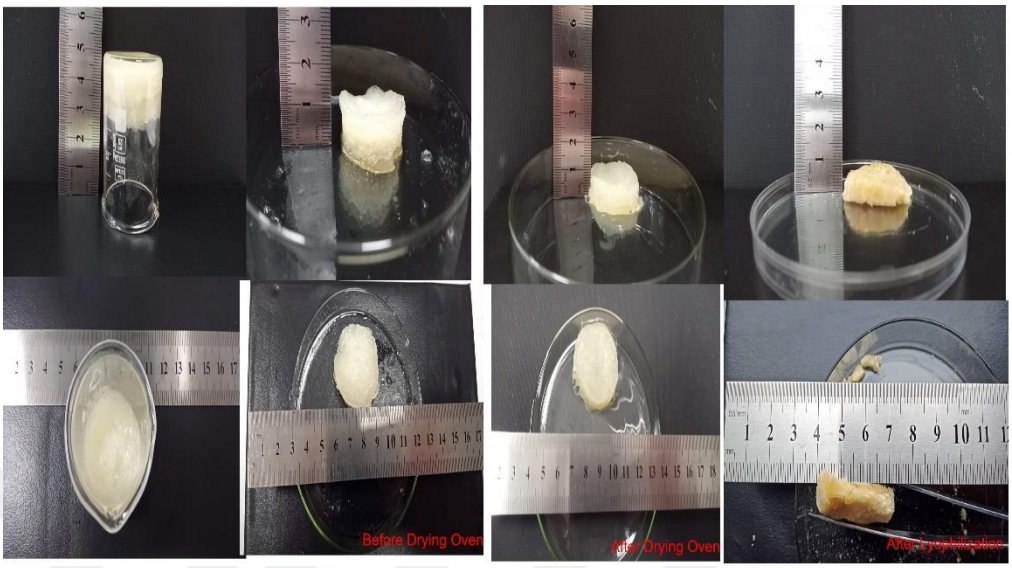

Figure 4.11. Produced BN-added nanobiocomposite with T-Shaped microfluidics. 0.05% w/v BN- 0.5% v/v CS-0.5% v/v AA-2% v/v GA hydrogel.

4.6.Characterisation Results of The Resultant Nanocomposite Hydrogel Structures

In this part, produced results from characterization studies are presenting; raw materials which we used, and polymeric chitosan and BN/CS nanobiocomposite solutions, and hydrogels which we produced.

4.6.1. FTIR Results of The Raw Materials Used And The Resultant Nanocomposite Hydrogels Achieved

In this part, result of FTIR analyses studies are explaining; raw materials which we used, and polymeric chitosan and BN/CS nanobiocomposite solutions, and hydrogels which were produced.

4.6.1.1. FTIR Results of the Raw Materials

The FTIR spectra of raw materials which PBN, PCS, AA and GA were shown in Figure 4.13. In literature, the FTIR wavelength of the B-N bond of BN ceramics is in the range of 1000-1400 cm^{-1} [97,102]. As result of FTIR analyse, PBN showed peaks at 757cm^{-1}, 1315 cm^{-1} . When AA was analysed, peaks were observed at 1234 cm^{-1} , 1288 cm^{-1} ,1400 cm^{-} 1, 1707cm^{-1} and 2972 cm^{-1} wave length. Strong sharp peak at 1707 cm^{-1} indicate that main functional group of acetic acid which is the carboxyl group (-COOH)[103]. In the GA FTIR spectrum, the repeating peaks at 1000 cm^{-1} - 1500 cm^{-1} and a broad peak at 3316 cm^{-1} were observed. The broad peak at 3316 cm^{-1} may shows hydroxy (-OH) stretching of GA bond [104].

In literature, shrimp sourced CS powder possess FTIR peaks around at 1024 cm^{-1},1050 cm^{-1}, 1065 cm^{-1}, 1260 cm^{-1}, 1377 cm^{-1}, 1426 cm^{-1}, 1375 cm^{-1}, 1574, 1630-1580 cm^{-1}, 1645, 2890 cm^{-1}, 2920 cm^{-1} and 3600-3100 cm^{-1}. The peaks at 1024 cm^{-1}, 105O cm^{-1}, 1065 cm^{-1} indicates C-O-C vibration, 1260 cm^{-1} indicates C-N vibration and carbonyl group (C=O), 1377 cm^{-1}-1426 cm^{-1} indicates C-H stretching. 1574 cm^{-1} indicates imidogen (N-H) vibration and protonated amine, 1630-1580 cm^{-1} indicates NH bond, 1645 cm^{-1} indicates C=O vibration and secondary amide, 2890 cm^{-1} indicates C-H symmetric stretching 2920 cm^{-1} indicates C-H vibration, 3600-3100 cm^{-1} indicates -OH bond[105, 106]. The FTIR spectra of PCS had peaks at 750 cm^{-1}, 1060 -1151 cm^{-1}, 1311 cm^{-1}, 1550-1648 cm^{-1}, 2876-2922 cm^{-1} and 3281-3361 cm^{-1}. The peak at 750 cm^{-1} may indicate C-H 1,2-Disubstitution (ortho) bond[113], 1060 cm^{-1} may indicate C-O vibrations, 1151 cm^{-1} may indicate asymmetric stretching of C-O-C bond, 1311 cm^{-1} may indicate amide III bond, 1550-1648 cm^{-1} may indicate NH bond, 2876 cm^{-1} may indicate C-H symmetric stretching, 2922 cm^{-1} may indicate C-H vibration and 3281-3361 cm^{-1} may indicate OH bond. The FTIR results of PCS good match with literature[105,106].

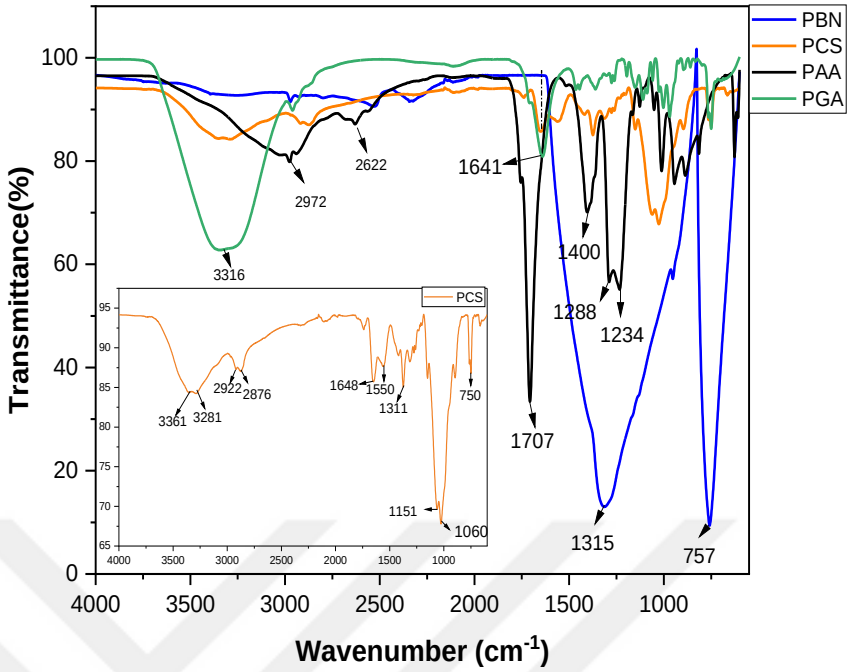

Figure 4.13. FTIR result of PBN, PCS, PAA, PGA samples.

4.6.1.2. FTIR Results of Chitosan Solution, Conventional Chitosan Hydrogels and Microfluidic Hydrogels Materials

The FTIR analyses results of resultant chitosan solution (CG), conventional CS hydrogels (CS1 and CS4) and microfluidic CS hydrogel (GMCS4) were showed in Figure 4.14. As seen in Figure 4.14, the peaks which belongs CG were observed at 750 cm^{-1}, 1639 cm^{-1} and 3307 cm^{-1}. The peak at 750 cm^{-1} may indicate C-H 1,2-Disubstitution (ortho) bond [107]. The medium and sharp peak at 1639 cm^{-1} may correspond with amid and open imino formation [108]. The broad and distinct peak at 3307 cm^{-1} may indicate -OH bond [109]. The peaks which belongs CS1 were observed at 750 cm^{-1}, 1032 cm^{-1},1262 cm^{-1}, 1450 cm^{-1}, 1563 cm^{-1}, 1656 cm^{-1}, 2865 cm^{-1}, 2938 cm^{-1} and 3321 cm^{-1}. The peak at 750 cm^{-1} may indicate C-H 1,2-Disubstitution (ortho) bond and also transmittance of this peak decreased when compared with FTIR spectrum of CG [107]. The medium broad peak at 1032 cm^{-1} in the band range between 800 cm^{-1}-1225 cm^{-1} may corresponds with C-O cyclical stretches in CS. The weak peak at 1262 cm^{-1} may indicate absorption of O-H bonds [110]. The weak symmetric

peak at 1450 cm^{-1} corresponds with common C bond in polysaccharides [117].The scissors type like peaks at 1563 cm^{-1} may indicate amide II of C=C bond and 1656 cm^{-1} may indicate amide I respectively. These peaks does not appear at FTIR spectrum of CG. This issue may indicate that CS crosslinked with glutaraldehyde. The peaks at 2865 cm^{-1} may indicate -CH bond and 2938 cm^{-1} may indicate C-H stretching respectively. The peaks at 3321 cm^{-1} may indicates -OH[104].

In the FTIR spectrum of CS4, the peaks were observed at 750 cm^{-1},1040 cm^{-1}, 1110 cm^{-1}, 1255 cm^{-1}, 1455 cm^{-1}, 1565 cm^{-1}, 1668 cm^{-1}, 1720 cm^{-1}, 2867 cm^{-1}, 2938 cm^{-1} and 3362 cm^{-1}. The peak of CS4 at 750 cm^{-1} have lower transmittance according to CG and CS1 and it may related with C-H 1,2-Disubstitution (ortho) bond forming [107]. The intense peak at 935 cm^{-1} may indicate non-planar bonding vibrations of H-C, 1040 cm^{-1} and 1110 cm^{-1} may indicate and -C-O-C-glycosidic bond respectively [111]. These peaks transmittance increased with GA concentration. The peak at 1255 cm^{-1} may indicate deformation of the $-CH_3$ group in the Si- CH_3 chain which may show silicate contamination [112]. The peak at 1455 cm^{-1} may indicate presence of C-H bending vibrations and the peak at 1565 cm^{-1} may indicate C-O stretching of amide II. 1668 cm^{-1} may indicate C=O stretching of amide I bond. The peak at 1720 cm^{-1} may indicate carbonyl bond of aldehyde. The distinct peaks at 2867 cm^{-1} and 2933 cm^{-1} may indicate C-H stretching of the methylene group. The medium broad peak at 3362 cm^{-1} may indicate -OH bond forming. GMCS4 had similar peaks with CS4 except peak at 935 cm^{-1} which may means that MF method does not change molecular structure and molecular interaction of the chitosan hydrogel. These results may show that the covalent crosslinking between chitosan and glutaraldehyde formed successfully [113].

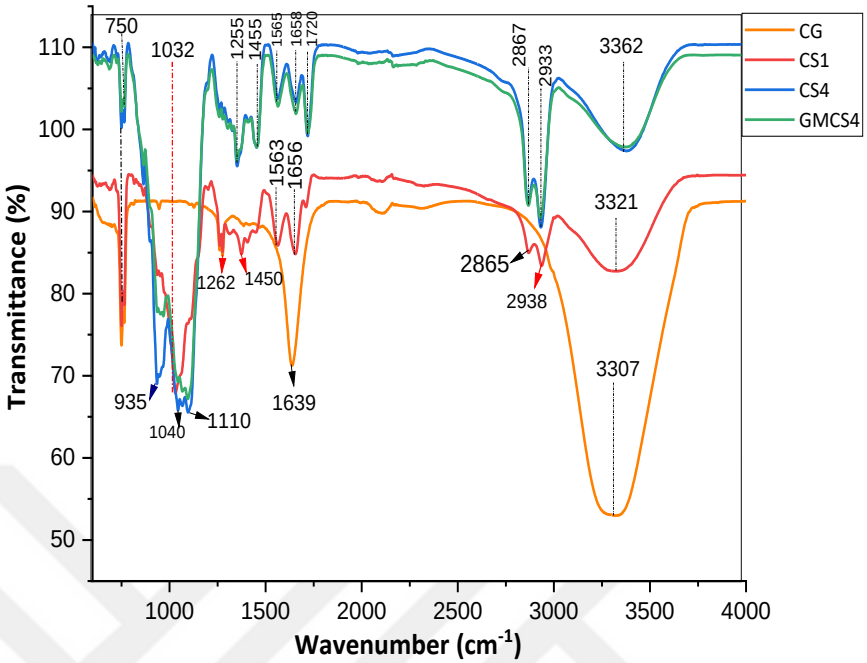

Figure 4.14. FTIR results of CG, CS2, CS4, GMCS4 samples.

4.6.1.2.FTIR Results of Nanobiocomposite Solution and Conventional Nanobiocomposite Hydrogels Microfluidic

The FTIR spectra of nanobiocomposite solution (SBN), conventional nanobiocomposite hydrogels (BC1, BC2, BC3, BC4) were showed in Figure 4.15. SBN had peaks at 671 cm^{-1}, 1638 cm^{-1}, 2136 cm^{-1} and 3310 cm^{-1}. The weak peak at 671 cm^{-1} may indicate $CaSO_4$ contamination [124]. The sharp peak at 1638 cm^{-1} may indicate C=O formation of CS. The weak and broad peak at 2136 cm^{-1} may indicate C-N vibration. The distinct broad peak at 3310 cm^{-1} may indicates B-OH forming [107,115].

The conventional nanobiocomposite hydrogel had showed peaks at 750 cm^{-1},950 cm^{-1}, 1032-1130 cm^{-1}, 1574 cm^{-1}, 1655 cm^{-1}, 2874 cm^{-1}, 2934 cm^{-1}, 2970 cm^{-1} and 3316 cm^{-1}. The sharp and distinct peak that does not seen at SBN at 750 cm^{-1} may indicate C-H 1,2-Disubstitution (ortho) bond forming. The very sharp peak at 950 cm^{-1} may indicate Si-OH stretching vibration which may show as Silicate contamination. The peaks at 1032-1130 cm^{-1} may indicate C-N stretching and at 1378 cm^{-1} may

indicate CH_3 deformation respectively. The fork type peaks at 1564 cm^{-1} and 1655 cm^{-1} may indicate formation of amide I and amide II bonding respectively [107]. The peaks at 2874 cm^{-1}, 2934 cm^{-1} and 2970 cm^{-1} may indicate C-CH_3 stretching vibrations [116]. The medium broad peak at 3316 cm^{-1} which does not seen at SBN may indicate NH bond stretching [104].

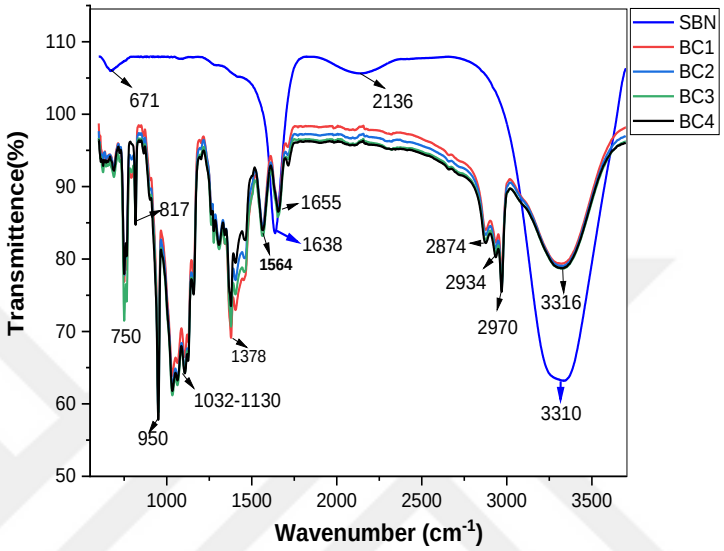

Figure 4.15. FTIR results of SBN, BC1, BC2, BC3, BC4 samples**.**

4.6.2. DSC Results of the Raw Materials Used and The Resultant Polymeric And Nanocomposite Hydrogels

DSC analysis was carried out with pure CS (9.8 mg), pure BN (4.12 mg), the resultant polymeric (CS1 (1.8 mg), CS4 (0.34 mg), GMCS4 (1.33 mg)) and nanobiocomposite hydrogels (BC1 (1.04 mg), BC2 (0.8mg), BC3 (0.94mg) and BC4 (1.08mg)), and obtained graphs are shown in Figure 4.16 and Figure 4.17. The important thermal parameters obtained from the analysis measurement are listed in Table 4.3. To indicates the onset temperature of the degradation, Tp indicates melting temperature and Te indicates to the temperature at the maximum rate of degradation. As summarised in Table 4.3, it was seen that the higher the GA content, the higher To, Tp, ΔH and Te of the chitosan hydrogels, thus better thermal stability was obtained.

Table 4.3. Thermal transitions of pure BN, pure CS, chitosan hydrogels and BN added nanobiocomposite hydrogels according to DSC results of machine graphs.

Sample	Endoterm I (°C)				Endoterm II (°C)				Endoterm III (°C)			
	To	Tp	Te	ΔH(J g^{-1})	To	Tp	Te	ΔH(J g^{-1})	To	Tp	Te	ΔH(J g^{-1})
PBN	63.3	63.8	65.9	3.87E-02	78.7	79.47	81.1	3.50E-02	238.5	238.8	240.7	0.26
PCS	50.5	109.4	160.1	211.9								
CS1	32.4	68.11	97.41	92.55	107.6	126.4	152.4	-21.1				
CS4	214.9	222	229	6.13								
GMCS4	160.1	163.4	166.7	11.97								
BC1	29.9	56.5	78.7	24.8								
BC2	37.5	65.8	91.7	56.25	169.6	182.8	196.3	7.84				
BC3	32.13	56.8	75.7	16.8	160.5	183.01	204.8	-8.62				
BC4	48.3	82.6	95.9	30.52	150.1	174.3	196.1	67.5	218.6	220	224.45	80.6

Figure 4.16. shows the DSC thermogram of PBN and PCS. The results show a broad endothermic peak around 109.4°C, which may be related to the evaporation of residual water from the CS; the enthalpy required to release these polymer was 211.9J/g as seen in Table 4.3. The endothermic peak started at 50.5°C, -4mW and ended at 160.1°C, 4 mW. Stable heat flow in the PCS was observed at 3 mW between temperature ranges of -16-6°C and 160-245°C. Stable temperature and heat flow in the PBN was also observed. The heat flow was higher than PCS. These results were similar when compared with other studies [98,117].

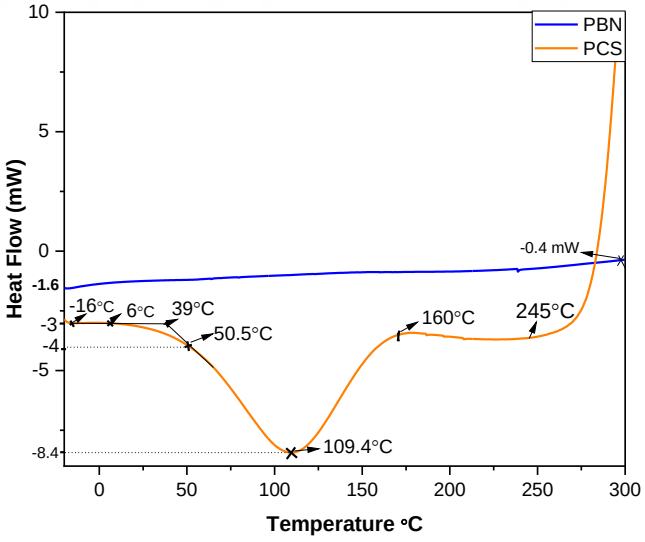

Figure 4.26. DSC analysis result of raw materials (PBN, PCS).

Figure 4.17 shows the DSC thermogram of CS hydrogel and BN added nanobiocomposite hydrogels. The DSC curve of CS1 showed an endothermic peak at

between 32-97.4°C and -1.5 - -1.9 mW. The heat flow of CS1 was stable at -1.26 mW between -19-9.7°C. Tg value of CS1 is 9.7°C. When the temperature value of CS1 reached at 32°C the heat flow suddenly start to drop at -1.9mW as for -19°C with 68°C temperature, heatflow was observed at -0.7mW as more slow. Additionally, at 68-300°C, it showed increasment as 0.3 mW. The DSC curve of BC1 showed an endothermic peak at between 30-79°C and -1 mW. The heat flow of BC1 increased from -1.26 mW to -1 mW at -19°-30°C. Additionally, at 30-253°C the heat flow increased from -1 mW to 0.8 mW. The DSC curve of BC2 showed endothermic peaks at between 30-92°C and 170-196°C. Just like DSC curve of BC1, the heat flow increased from -1.26 mW to -1 mW at -19°-30°C. Additionally, at 30-300°C the heat flow increased from -1 mW to 0 mW. The DSC curve of BC3 showed endothermic peaks between at 32-76°C and 160-205°C. The heat flow of BC3 increased from -1.26 mW to -0.7 mW at -19°-23°C. When the sample temperature reach at 23°C, the heat flow has begun stable at -0.7 mW until 53°C. After the sample temperature reach at from 53°C to 235°C, the heat flow increased from -0.7 mW to 0.5 mW and it was stable between 253°C to 300°C. The DSC curve of BC4 showed endothermic peaks between at 48-90°C, 150-196°C and 219-224°C. The heat flow of BC4 increased from -1.5 mW to -1 mW at -19°-37°C. When the sample temperature reach at 37°C, the heat flow has began stable at -1 mW until 79°C. From 79°C to 102°C the heat flow increased from -0.9 mW to -0.5 mW and also, from 102°C to 150°C the heat flow increased from -0.5 mW to -0.2 mW slowly. The second endothermic peak was around at -6 mW and the third endothermic peak was around at -3.5 mW in the DSC curve of BC4. The DSC thermograms of nanobiocomposite hydrogels was similar in different studies [25, 26, 98].

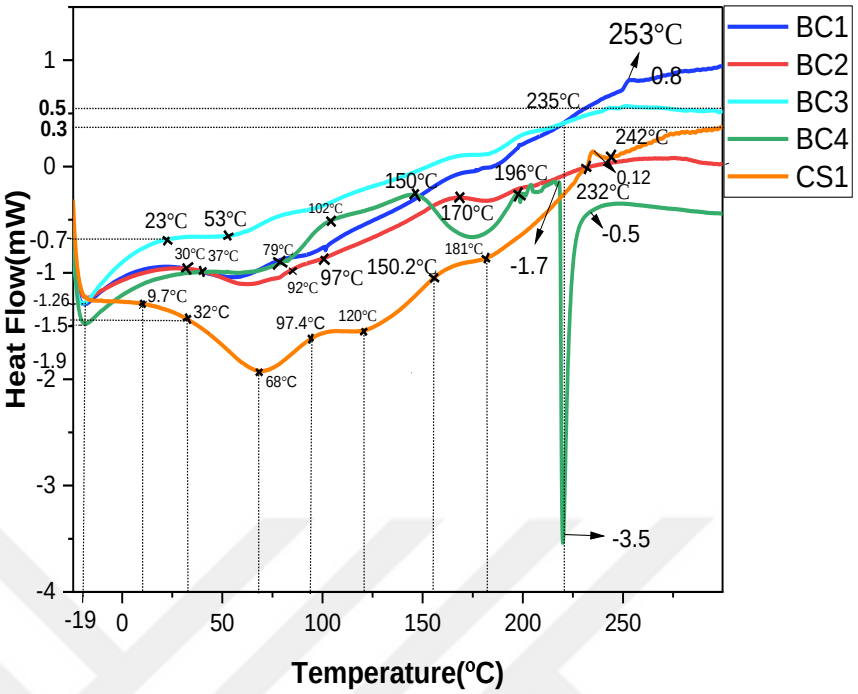

Figure 4.17. DSC results of the polymeric and nanocbiocomposite hydrogel structures formed.

Figure 4.18 shows the DSC thermogram of conventional CS hydrogel (CS4) and microfluidic hydrogel (GMCS4). The heat flow of CS4 was changed from 2 mW to 0 mW between at -34.8- -26.6°C. From 0 mW to -1.6 mW, the temperature was changed from -26.6°C to 118.8°C. An endothermic peak was observed between at 168.4-212.7°C in the CS4 curve. The heat flow of GMCS4 changed 0 mW to 2 mW between at -34.8^{o} C. From -34.8°C to 60.2°C the heat flow changed between at 0 mW to 2.5 mW and from 60.2°C to 160°C the heat flow changed between at 2.5 mW to 3.5 mW. An endothermic peak was observed between at 160°C to 166.7°C. The DSC curve of GMCS4 showed more broad endothermic peak when compared with CS4. The DSC curve of CS4 and GMCS4 was similar in different studies [118, 119].

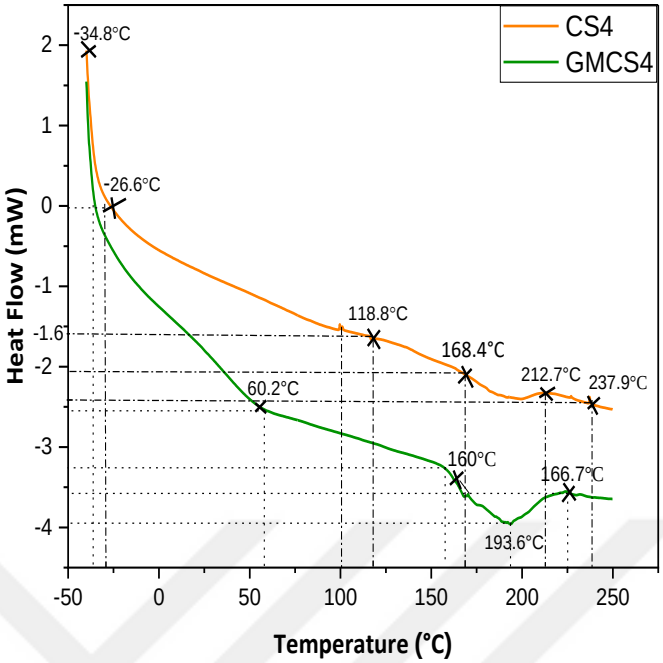

Figure 4.18. DSC results of conventional and microfluidic hydrogel structures.

4.6.3. TGA Results of The Raw Materials Used and The Resultant Nanocomposite Hydrogels Achieved

TGA analysis was carried out with pure CS (8.27 mg), pure BN (11.7 mg), the resultant polymeric (CS1 (1.8 mg), CS4 (0.81 mg), GMCS4 (2.1 mg)) and nanobiocomposite hydrogels (BC1 (3.1 mg), BC2 (2 mg), BC3 (1 mg), BC4 (1.6 mg), GMBC (1.1 mg)), and obtained thermograms are shown in Figure 4.19. As apparent from the TGA thermogram of PBN, no weight loss was observed until 700°C which a higher level of thermal stability. Additionally, PCS has revealed a 9% weight loss between 99-295°C, which may be indicate loss of residual water and adsorbed moisture [120]. The major weight loss (37%) in PCS is observed at 295-327°C which may be indicated to the decomposition of ethereal groups, glucosamine moieties or ring opening reactions [120]. Also, slow mass loss (23%) was observed at 327-700°C.

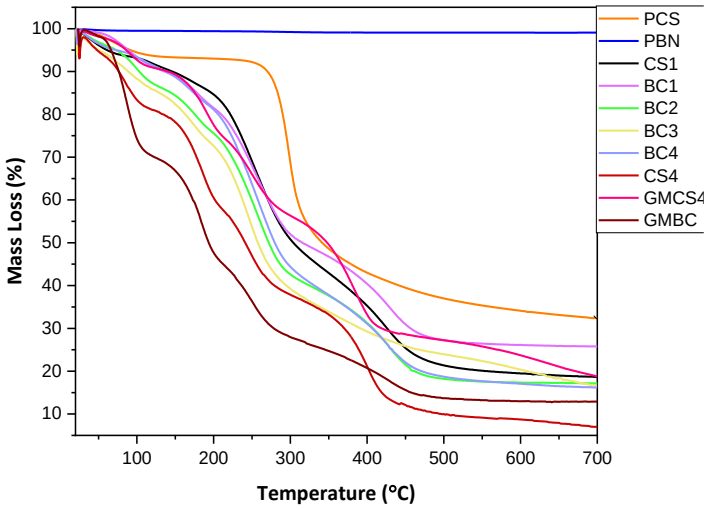

Figure 4. 19. TGA results of raw materials which are BN powder (PBN), CS powder (PCS), conventional chitosan hydrogels (CS1, CS4), microfluidic chitosan hydrogel (GMCS4), conventional BN added nanobiocomposite hydrogels (BC1, BC2, BC3, BC4) and microfluidic BN added nanobiocomposite hydrogel (GMBC).

In Figure 4.20 the thermograms of polymeric hydrogels (CS1, CS4, GMCS4) were presented in more detail. CS1 has revealed a 15% weight loss between 35-206°C, which may be indicate loss of residual water and adsorbed moisture. The major weight loss (33%) in CS1 is observed at 206-307°C which may be indicated to the decomposition of ethereal groups, glucosamine moieties or ring opening reactions. Also the more slow weight loss (28%) was observed at 307-485°C and the weight loss of CS1 was almost stable between 485-700°C. CS4 has revealed a 20% weight loss between 35-121°C. The major weight loss (40%) in CS4 is observed at 121-274°C. Slower weight loss (27%) was observed at 274-436°C. From 436°C to 700°C, 5% weight loss was observed in CS4. In microfluidic CS hydrogel (GMCS), 7% weight loss was observed at 35-107°C. The major weight loss (33%) in CMCS4 was observed at 107-273°C. GMCS4 has revealed a 29% weight loss between 273-419°C. Also the more slow weight loss (11%) was observed at 419-700°C. As summary the weight loss decreased with increasing GA concentration. The microfluidic method did not changedthermal stability of CS hydrogel as clearly seen in Figure 4.20.

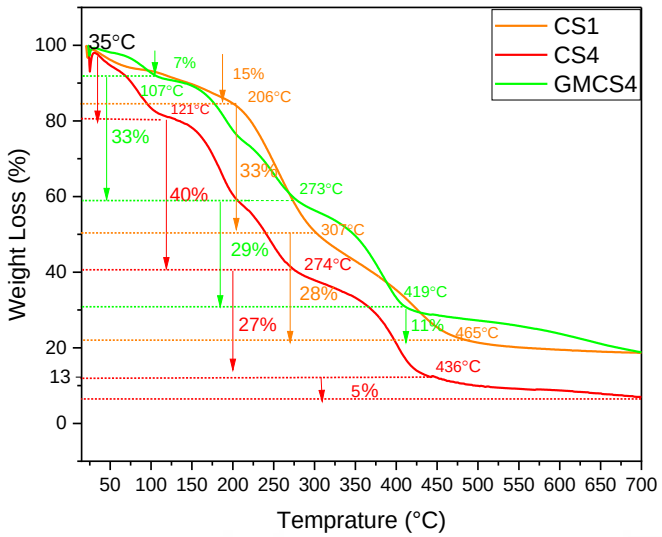

Figure 4.20. TGA thermograms of conventional chitosan hydrogels (CS1 and CS4) and microfluidic chitosan hydrogel (GMCS4).

In Figure 4.21 the thermograms of BN added conventional nanobiocomposite hydrogels (BC1, BC2, BC3, BC4) and BN added microfluidic (GMCS4) were presented in more detail. BC1 has revealed a 7% weight loss between 28-104°C, which may be indicate loss of residual water and adsorbed moisture. The major weight loss (41%) in BC1 is observed at 104-308°C which may be indicated to the decomposition of ethereal groups, glucosamine moieties or ring opening reactions. Slower weight loss (22%) was observed at 307-490°C and the weight loss of BC1 was almost stable between 490-700°C. BC2 has revealed a 13% weight loss between 28-121°C. The major weight loss (44%) in BC2 is observed at 121-301°C. Slower weight loss (22%) was observed at 301-471°C. From 471°C to 700°C, the weight loss was stable as 20% in BC2. BC3 has revealed a 16% weight loss between 28-138°C. The major weight loss (42%) in BC3 is observed at 138-301°C . Slower weight loss (24%) was observed at 301-700°C. BC4 has nearly same the thermogram with BC2. GMBC has revealed a 19% weight loss between 28-110°C, which may be indicate loss of residual water and adsorbed moisture. The major weight loss (23%) in GMBC is observed at 110-200°C which may be indicated to the decomposition of ethereal groups, glucosamine moieties or ring opening reactions. Slower weight loss (17%) was observed at 277-468°C. From 277°C to 468°C, the weight loss was 16%. From 468°C to 700°C, the weight loss was stable as 16%. As sum up, thermal stability of the nanobiocomposite

increased with increasing BN concentration. Microfluidic method did not enchancent thermal stability of the nanobiocomposites.

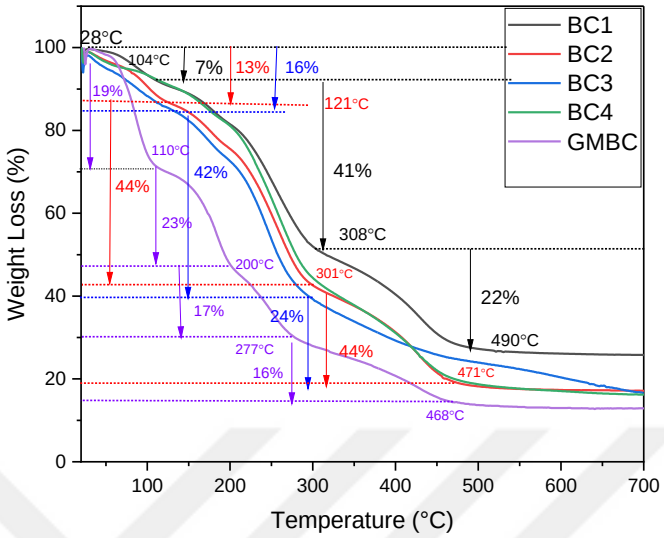

Figure 4.21. TGA thermograms of BN added conventional nanobiocomposite hydrogels (BC1, BC2, BC3, BC4) and microfluidic BN added nanobiocomposite hydrogel (GMBC).

4.6.4. XRD Results of The Raw Materials Used and The Resultant Nanobiocomposite and Polimeric Hydrogels Achieved

XRD patterns of PBN and PCS were shown in Figure 4.22. The XRD pattern of PCS shows the characteristic crystalline peaks at around 2θ= 9° and 2θ= 20.1°. The PBN shows peaks at 2θ= 26.8°, 2θ= 41.7° and 2θ= 43.8°, 55.1°. The sharp and distinct peak at 2θ= 26.8° indicates that PBN more crystalline than PCS. Also more narrow peaks at 2θ= 41.7° and 2θ= 43.8°, 55.1° may confirms that high crystallinity of PBN. These obtained results were similar with other similar studies [98, 106,121].

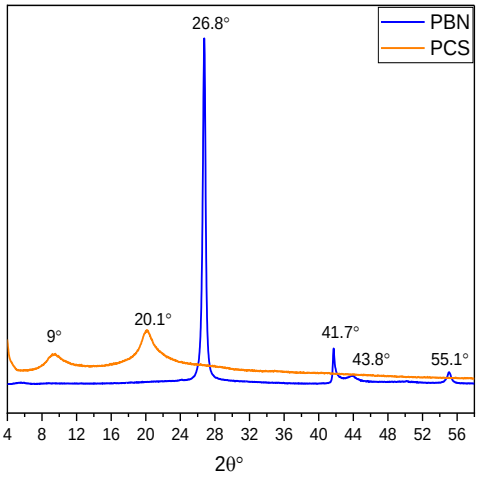

Figure 4.22. XRD patterns of BN powders (PBN) and CS powders (PCS).

XRD patterns of conventional and microfluidic hydrogels were shown in Figure 4.23. Generally, the XRD patterns of BN added nanobiocomposite hydrogels and CS hydrogels shows peaks at around 2θ=21°, 2θ=23° and 2θ=26°. CS4 has more sharp and intense peak at 2θ=21.3° when compared with CS1 and GMCS. The XRD pattern of GMBC similar with CS4. Additionally, CS1 has no peak at around 2θ=23° and 2θ=26°. These results showed that increasing GA concentration increases crystallinity of CS hydrogels. Also microfluidic method did not changed crystallinity of CS hydrogels. In regard to XRD patterns of nanobiocomposite hydrogels, the more broad peak at 2θ=26.8° was observed at BC1. BC4 has more broad and distinct peak at 2θ=21.17°. This shows that BC4 has more crystalline structure.

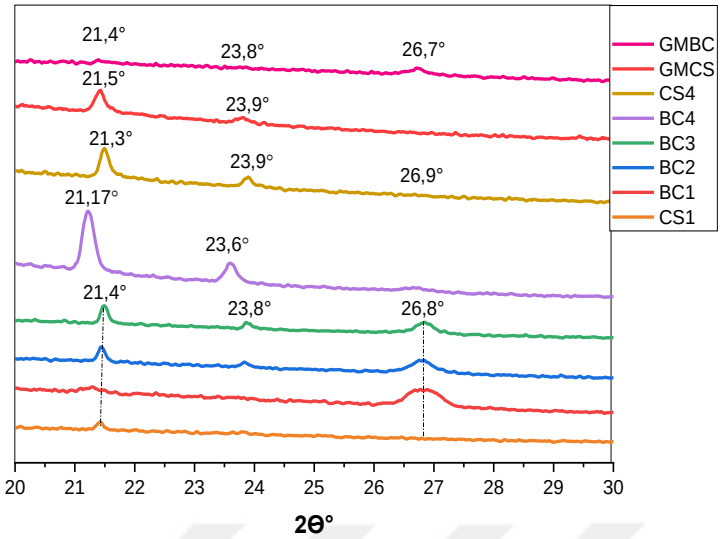

Figure 4.23. XRD results of produced BN-added and non-added nanobiocomposite hydrogels.

These obtained XRD results are similar with studies in literature. For instance, in the study of producing BN added chitosan composite material which were done by Chen and co-workers, the peaks were observed in the 2θ=26.74°, 2θ= 20° and around. These peaks also observed in our produced hydrogels XRD patterns [28]. Also, similar peaks were observed in the XRD results of another work which Dyanavel co-worker produced a cross-linked CS-BN nanobiocomposite [103].

4.6.5. Scanning Electron Microscopy Results of the Raw Materials Used and the Resultant Nanocomposite Hydrogels Achieved

SEM images of BN added nanobiocomposite hydrogels and chitosan hydrogels which were produced as result of this thesis study are shown in Figure 4.24. Also raw materials were presented in Figure 4.24.

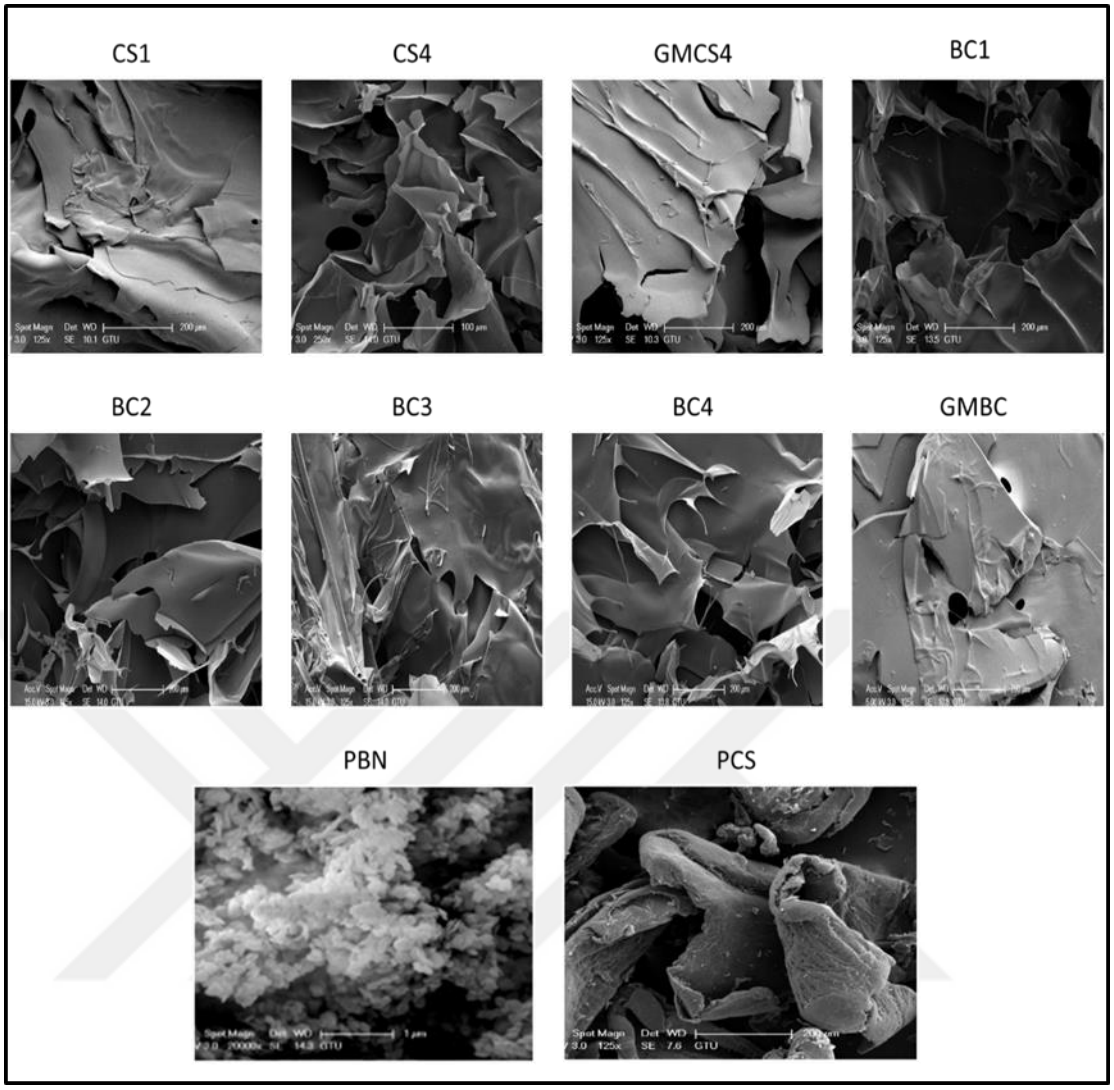

Figure 4.24. SEM images of BN powder (PBN), CS powder (PCS), and resultant polymeric hydrogels (CS1, CS4, GMCS4) and nanobiocomposite hydrogels.

Figure 4.24. shows that surface morphology of PCS presented heterogeneous rocks structures and small number of white points were on its. This SEM image of PCS similar with a study which done by Kandile and co-workers [111]. The surface morphology of PBN showed that the powders have sheet-like morphology. This SEM image of PBN similar with a study which done by Nadeem and co-workers [133].

As seen from Figure 4.24 the porous structure was not observed chitosan hydrogels (GMCS4, CS4, CS1) which were produced by both microfluidic and conventional method. Eventhough as in unregular and undesired, the porous-like black hole structures were observed in the morphology of BN added nanobiocomposite hydrogels (BC1, BC2, BC3, BC4 and GMBC). The sizes of porous-like black holes

increased with increasing BN concentration in the surface morphology of nanobiocomposites. Also, Figure 4.24 shows that the smallest porous-like black holes was observed in the surface morphology of the microfluidic nanobiocomposite hydrogel (GMBC). As sum up of SEM results which shown in Figure 4.24, the desired surface morphology of well-ordered porous structures were not obtained. Because, drawbacks of coronavirus pandemic in the realization of experimental studies, lived financial difficulties and existent budget was restricted. Focusing on optimization studies on BN added CS nanobiocomposite hydrogels pore sizes with T-Shaped microfluidic was found as a notable result.

5.CONCLUSION

In this study which were carried out, chitosan hydrogel scaffolds and BN added nanobiocomposite tissue scaffolds were produced with T-Shaped microfluidic system for the first time. The characterization studies of these unique structures were done successfully.

The study began by determining the production parameters for both chitosan solution and BN added nanobiocomposite chitosan solution. Following this, the solutions were characterized to determine the physical properties. The chitosan powder was found to be best dissolved in 1% v/v AA solution. The viscosity of CS solution increased as the CS concentration increased, and the viscosity and surface tension decreased when the BN concentration increased. The whiteness of BN added conventional nanobiocomposite hydrogels increased when the BN concentration increased.

In the study which were done, 1% w/v CS – 1% v/v AA and 0.1% w/v BN- 1% w/v CS – 1% AA solutions were determined suitable in order to use in the microfluidic as result of optimization, physical characterization and optimization studies. With these solution, polymeric and BN added nanobiocomposite foams were produced with using T-Shaped microfluidic system at 200±10 µl/minute flow and 10 psi pressure. The polymeric and BN added nanobiocomposite foams gelled with 4% v/v GA solution well and sponge-like hydrogel tissue scaffolds were produced successfully.

The obtained characterization results are similar to the characterization results in the literature. As a result of XRD analysis of BN addition in CS hydrogel, it was observed that the nanobiocomposite was more higher than pristine CS hydrogel.

As result of SEM as for that smaller porous like structures were detected at the microfluidic hydrogel. In order to produce porous structures which have same volume and contact with each other, necessary to focusing on hydrogel producing with produced CS-BN/CS foam with microfluidic and correctly take sample form these hydrogels.

During this studies when noticing also durability of produced porous structures from lyophilization device, also necessity of showing sensitivity issues on optimization of drying medium is drawing attention.

REFERENCES

[1] Echeverria Molina, M. I., Malollari, K. G., Komvopoulos, K., (2021), "Design Challenges in Polymeric Scaffolds for Tissue Engineering", Frontiers in Bioengineering and Biotechnology, 9, 617141.

[2] Israni, A. K., Zaun, D., Hadley, N., Rosendale, J. D., Schaffhausen, C., McKinney, W., Synder J.J., Kasiske, B. L., (2020), "OPTN/SRTR 2018 Annual Data Report: deceased Organ donation", American Journal of Transplantation, 20, 509-541.

[3] Şantaş G., Şantaş F., (2018), "Türkiye'de organ bağışının mevcut durumu ve organ bağışında stratejik iletişimin önemi", Süleyman Demirel Üniversitesi Sağlık Bilimleri Dergisi, 9 (2), 163-168.

[4] Zhao P., Gu H., Mi H., Rao C., Fu J., Turng L.S., (2018), "Fabrication of scaffolds in tissue engineering: A review", Frontiers of Mechanical Engineering, (13) 107–119.

[5] Dhandayuthapani B., Yoshida Y., Maekawa T., Kumar DS., (2011), "Polymeric scaffolds in tissue engineering application: a review", International journal of polymer science, 2011.

[6] Pina, S., Ribeiro, V. P., Marques, C. F., Maia, F. R., Silva, T. H., Reis, R. L., Oliveira, J. M., (2019), "Scaffolding strategies for tissue engineering and regenerative medicine applications", Materials, 12 (11), 1824.

[7] Huang, G. Y., Zhou, L. H., Zhang, Q. C., Chen, Y. M., Sun, W., Xu, F., & Lu, T. J. (2011), "Microfluidic hydrogels for tissue engineering",. Microfluidic hydrogels for tissue engineering. Biofabrication, 3 (1), 012001.

[8] Zhong, Q., Ding, H., Gao, B., He, Z., Gu, Z., (2019), "Advances of microfluidics in biomedical engineering",. Advanced materials technologies, 4 (6), 1800663.

[9] Chung B.G., Lee K.H., Khademhosseini A., & Lee, S. H., (2012), "Microfluidic fabrication of microengineered hydrogels and their application in tissue engineering",. Lab on a Chip, 12 (1), 45-59.

[10] Li Y., Liu X., Huang Q., Ohta, A. T., Arai, T., (2021), "Bubbles in microfluidics: an all-purpose tool for micromanipulation",. Lab on a Chip, 21 (6), 1016–1035.

[11] Zhao P., Wang J., Li Y., Wang, X., Chen, C., Liu, G., (2020), "Microfluidic technology for the production of well-ordered porous polymer scaffolds", Polymers, 12 (9), 1863.

[12] Kucuk I., Yilmaz N.F., Sinan A., (2018), "Effects of junction angle and gas pressure on polymer nanosphere preparation from microbubbles bursted in a combined microfluidic device with thin capillaries", Journal of Molecular Structure, 1173, 422–427.

[13] Hernandez J.L., Woodrow K.A., (2022), "Medical Applications of Porous Biomaterials: Features of Porosity and Tissue-Specific Implications for Biocompatibility", Advanced Healthcare Materials, 11 (9), 2102087.

[14] Urbanczyk M., Layland S.L., Schenke-Layland K., (2020), "The role of extracellular matrix in biomechanics and its impact on bioengineering of cells and 3D tissues",. Matrix Biology, 85, 1-14.

[15] Andrieux S., Quell A., Stubenrauch C., Drenckhan W., (2018), "Liquid foam templating – A route to tailor-made polymer foams", Advances in Colloid and Interface Science, 256, 276-290.

[16] Testouri A., Honorez C., Barillec A., Langevin, D., Drenckhan, W., (2010), "Highly structured foams from chitosan gels", Macromolecules, 43(14), 6166-6173.

[17] Djemaa I.B., Auguste S., Drenckhan-Andreatta W., Andrieux S., (2021), "Hydrogel foams from liquid foam templates: Properties and optimisation", Advances in Colloid and Interface Science, 294, 102478.

[18] Rafieian S., Mirzadeh H., Mahdavi H., Masoumi M.E., (2019), "A review on nanocomposite hydrogels and their biomedical applications", Science and Engineering of Composite Materials, 26 (1), 154-174.

[19] Spicer C.D., (2020), "Hydrogel scaffolds for tissue engineering: The importance of polymer choice", Polymer Chemistry, 11 (2), 184–219.

[20] Tonti, O. R., Larson, H., Lipp, S. N., Luetkemeyer, C. M., Makam, M., Vargas, D., Wilcox S.M., Calve S., (2021), "Tissue-specific parameters for the design of ECM-mimetic biomaterials", Acta biomaterialia, 132, 83-102.

[21] Li, P., Zhao, J., Chen, Y., Cheng, B., Yu, Z., Zhao, Y., Yan X., Tong Z., Jin S., (2017), "Preparation and characterization of chitosan physical hydrogels with enhanced mechanical and antibacterial properties", Carbohydrate polymers, 157, 1383-1392.

[22] Fu J., Yang F., Guo Z., (2018), "The chitosan hydrogels: from structure to function", New Journal of Chemistry, 42 (21), 17162–17180.

[23] Jiao J., Huang J., Zhang Z., (2019), "Hydrogels based on chitosan in tissue regeneration: How do they work? A mini review",. Journal of Applied Polymer Science, 136(13), 47235.

[24] Emanet M., Kazanç E., Çobandede Z., Çulha M., (2016), "Boron nitride nanotubes enhance properties of chitosan-based scaffolds",. Carbohydrate polymers, 151, 313-320.

[25] Kisku, S.K., Swain S.K., (2012), "Synthesis and characterization of Chitosan/Boron nitride composites",. Journal of the American Ceramic Society, 95 (9), 2753–2757.

[26] Chen J., Shang J., Xue F., Wei, Q., Xu, N., Ding, E., (2019), "Preparation and characterization of h-BN nanosheets / chitosan microspheres",. Journal of Polymer Research, 26, 1-9.

[27] Zhang, J., Chen, H., Zhao, M., Liu, G., Wu, J. (2020). "2D nanomaterials for tissue engineering application". Nano Research, 13, 2019-2034.

[28] Farshid, B., Lalwani, G., Mohammadi, M. S., Sankaran, J. S., Patel, S., Judex, S., Simonsen, J., Sitharaman, B., (2019), "Two-dimensional graphene oxide-reinforced porous biodegradable polymeric nanocomposites for bone tissue engineering", Journal of Biomedical Materials Research Part A, 107 (6), 1143–1153.

[29] Zhang, K., Feng, Y., Wang, F., Yang, Z., & Wang, J., (2017), "Two dimensional hexagonal boron nitride (2D-hBN): Synthesis, properties and applications", Journal of Materials Chemistry C, 5 (46), 11992-12022.

[30] Merlo, A., Mokkapati, V. R. S. S., Pandit, S., Mijakovic, I., (2018), Boron nitride nanomaterials: biocompatibility and bio-applications" Biomaterials science, 6 (9), 2298-2311.

[31] Farshid B., Lalwani G., Shir Mohammadi M., Simonsen, J., Sitharaman, B., (2017), "Boron nitride nanotubes and nanoplatelets as reinforcing agents of polymeric matrices for bone tissue engineering", Journal of Biomedical Materials Research Part B: Applied Biomaterials, 105 (2), 406-419.

[32] Kıvanç M., Barutca B., Koparal A. T., Göncü, Y., Bostancı, S. H., Ay, N., (2018), "Effects of hexagonal boron nitride nanoparticles on antimicrobial and antibiofilm activities, cell viability", Materials Science and Engineering : C, 91, 115-124.

[33] Zhuge W., Liu H., Wang W., Wang J., (2022), "Microfluidic bioscaffolds for regenerative engineering", Engineered Regeneration, 3, 110–120.

[34] Danie Kingsley J., Ranjan S., Dasgupta N., Saha P., (2013), "Nanotechnology for tissue engineering: Need, techniques and applications",. Journal of pharmacy research, 7(2), 200-204.

[**35**] Eltom A., Zhong G., Muhammad A., (2019), "Scaffold Techniques and Designs in Tissue Engineering Functions and Purposes: a Review", Advances in materials science and engineering, 2019.

[**36**] Bandzerewicz A., Gadomska-Gajadhur A., (2022), "Into the Tissues: Extracellular Matrix and Its Artificial Substitutes: Cell Signalling Mechanisms", Cells, 11 (5), 914.

[**37**] Codrea C.I., Croitoru A.M., Baciu C.C., Melinescu, A., Ficai, D., Fruth, V., Ficai, A., (2021), "Advances in osteoporotic bone tissue engineering", Journal of Clinical Medicine, 10 (2), 253.

[**38**] Roseti L., Parisi V., Petretta M., Cavallo, C., Desando, G., Bartolotti, I., Grigolo, B., (2017), "Scaffolds for Bone Tissue Engineering: State of the art and new perspectives", Materials Science and Engineering C, 78, 1246-1262.

[39] Wade , R. J., Burdick, J. A., (2012), " Engineering ECM signals into biomaterials ", Materials Today, 15 (10), 454-459.

[40] Frantz C., Stewart K.M., Weaver V.M., (2010), "The extracellular matrix at a glance", Journal of cell science, 123 (24), 4195-4200.

[41] Akhmanova, M., Osidak, E., Domogatsky, S., Rodin, S., & Domogatskaya, A., (2015), "Physical, Spatial, and Molecular Aspects of Extracellular Matrix of in Vivo Niches and Artificial Scaffolds Relevant to Stem Cells Research", Stem cells international, 2015.

[42] Crawford L., Wyatt M., Bryers J., Ratner B., (2021), "Biocompatibility evolves: phenomenology to toxicology to regeneration ", Advanced healthcare materials, 10 (11), 2002153.

[43] Mutlu, B. (2019). Doku mühendisliği uygulamaları için mikroakışkan sistemi kullanarak sodyum aljinat film üretimi (Master's thesis, Bursa Teknik Üniversitesi).

[44] Martín C., Kostarelos K., Prato M., Bianco A., (2019), "Biocompatibility and biodegradability of 2D materials: Graphene and beyond", Chemical communications, 55 (39), 5540-5546.

[45] Morsada, Z., Hossain, M. M., Islam, M. T., Mobin, M. A., Saha, S., (2021), "Recent progress in biodegradable and bioresorbable materials: From passive implants to active electronics", Applied Materials Today, 25, 101257.

[46] Chan, B. P., & Leong, K. W., (2008), "Scaffolding in tissue engineering: General approaches and tissue-specific considerations",. European Spine Journal, 17, 467-479.

[47] Sanchez-Salvador, J. L., Balea, A., Monte, M. C., Negro, C., & Blanco, A., (2021), "Chitosan grafted/cross-linked with biodegradable polymers: A review",. International Journal of Biological Macromolecules, 178, 325–343.

[48] Zhao, H., Li, L., Ding, S., Liu, C., Ai, J., (2018), "Effect of porous structure and pore size on mechanical strength of 3D-printed comby scaffolds", Materials letters, 223, 21-24.

[49] Jahir-Hussain, M. J., Maaruf, N. A., Esa, N. E. F., Jusoh N., (2021), "The effect of pore geometry on the mechanical properties of 3D-printed bone scaffold due to compressive loading", In IOP Conference Series: Materials Science and Engineering (Vol. 1051, No. 1, p. 012016). IOP Publishing.

[50] Zhang, Z., Feng, Y., Wang, L., Liu, D., Qin, C., Shi, Y., (2022), "A review of preparation methods of porous skin tissue engineering scaffolds", Materials Today Communications, 104109.

[51] Xie, C., Gao, Q., Wang, P., Shao, L., Yuan, H., Fu, J., Chen W., He Y., (2019), "Structure-induced cell growth by 3D printing of heterogeneous scaffolds with ultrafine fibers", Materials & Design, 181, 108092.

[52] Hasanzadeh, R., Azdast, T., Mojaver, M., Darvishi, M. M., Park, C. B., (2022), "Cost-effective and reproducible technologies for fabrication of tissue engineered scaffolds: The state-of-the-art and future perspectives", Polymer, 124681.

[53] Jansson E., Tengvall P., (2004), "Adsorption of albumin and IgG to porous and smooth titanium", Colloids and Surfaces B: Biointerfaces, 35 (1), 45-51.

[54] Richert, L., Variola, F., Rosei, F., Wuest, J. D., Nanci, A., (2010), "Adsorption of proteins on nanoporous Ti surfaces", Surface Science, 604 (17-18), 1445-1451.

[55] Garg, K., Pullen, N. A., Oskeritzian, C. A., Ryan, J. J., Bowlin, G. L., (2013), "Macrophage functional polarization (M1/M2) in response to varying fiber and pore dimensions of electrospun scaffolds", Biomaterials, 34 (18), 4439-4451.

[56] Capuana, E., Lopresti, F., Carfì Pavia, F., Brucato, V., La Carrubba, V., (2021), " Solution-based processing for scaffold fabrication in tissue engineering applications: A brief review ", Polymers, 13 (13), 2041.

[57] Çeper, B. (2021). Metal katkılı bifazik kalsiyum fosfat/kitosan esaslı doku iskelelerinin üretimi ve karakterizasyonu (Master's thesis, BTÜ, Lisansüstü Eğitim Enstitüsü).

[58] Rahmati, M., Mills, D. K., Urbanska, A. M., Saeb, M. R., Venugopal, J. R., Ramakrishna, S., Mozafari, M., (2021), "Electrospinning for tissue engineering applications", Progress in Materials Science, 117, 100721.

[59] Pou KRJ., Raghavan V., Packirisamy M., (2022), "Microfluidics in smart packaging of foods", Food Research International, 111873.

[60] Lai X., Yang M., Wu H., Li D., (2022), "Modular Microfluidics: Current Status and Future Prospects", Micromachines, 13 (8), 1363.

[61] Musile, G., Agard, Y., Wang, L., De Palo, E. F., McCord, B., Tagliaro, F., (2021), "Paper-based microfluidic devices: On-site tools for crime scene investigation", TrAC - Trends in Analytical Chemistry, 143, 116406.

[62] Gao, Y., Ma, Q., Cao, J., Wang, Y., Yang, X., Xu, Q., Liang, Q., Sun, Y., (2021), "Recent advances in microfluidic-aided chitosan-based multifunctional materials for biomedical applications", International Journal of Pharmaceutics, 600, 120465.

[63] Alrifaiy A., Lindahl O.A., Ramser K., (2012), "Polymer-based microfluidic devices for pharmacy, biology and tissue engineering", Polymers, 4 (3), 1349–1398.

[64] Huerre A., Miralles V., Jullien MC., (2014), "Bubbles and foams in microfluidics", Soft matter, 10 (36), 6888-6902.

[65] Maimouni, I., Cejas, C. M., Cossy, J., Tabeling, P., Russo, M.., (2020), " Microfluidics mediated production of foams for biomedical applications ", Micromachines, 11 (1), 83.

[66] Hill C., & Eastoe J., (2017), "Foams : From nature to industry ",. Advances Colloid Interface Science, 247, 496–513.

[67] Yang, C. N., Liang, L. S., Lin, K. H., Jang, W. Y., (2019), "The mechanical properties of monodisperse foam scaffolds", Composites Part B: Engineering, 164, 517-523.

[68] Etemad, S., Kantzas, A., Bryant, S., (2022), "A systematic analysis of foam drainage: Experiment and model" Results in Engineering, 15, 100551.

[69] Van Der Net A., Drenckhan W., Weaire D., Hutzler S., (2006), "The crystal structure of bubbles in the wet foam limit", Soft Matter, 2 (2), 129-134.

[70] Hutzler, S., Dunne, F. F., Kraynik, A. M., Weaire, D., (2020), "The energy of fcc and hcp foams", Soft Matter, 16 (35), 8262-8271.

[71] Unal, A. Z., West, J. L., (2020), "Synthetic ECM: Bioactive Synthetic Hydrogels for 3D Tissue Engineering", Bioconjugate Chemistry, 31 (10), 2253-2271.

[72] Mantha S., Pillai S., Mantha, S., Pillai, S., Khayambashi, P., Upadhyay, A., Zhang, Y., Tao, O., Pham H.M., Tran, S. D., (2019), "Smart hydrogels in tissue engineering and regenerative medicine", Materials, 12 (20), 3323.

[73] Mergen, Ö. B., Arda, E., Evingür, G. A., (2020), " Electrical, optical and mechanical properties of chitosan biocomposites ", Journal of Composite Materials, 54 (11), 1497-1510.

[74] Azmana, M., Mahmood, S., Hilles, A. R., Rahman, A., Arifin, M. A. B., Ahmed, S., (2021), "A review on chitosan and chitosan-based bionanocomposites : Promising material for combatting global issues and its applications", International journal of biological macromolecules, 185, 832–848.

[75] Mohan, K., Ganesan, A. R., Ezhilarasi, P. N., Kondamareddy, K. K., Rajan, D. K., Sathishkumar, P., Conterno, L., (2022), "Green and eco-friendly approaches for the extraction of chitin and chitosan: A review", Carbohydrate Polymers, 119349.

[76] Silva, A. O., Cunha, R. S., Hotza, D., Machado, R. A. F., (2021), "Chitosan as a matrix of nanocomposites: A review on nanostructures, processes, properties, and applications", Carbohydrate Polymers, 272, 118472.

[77] Pieklarz K., Galita G., Tylman, M., Maniukiewicz, W., Kucharska, E., Majsterek, I., & Modrzejewska, Z., (2021), "Physico-chemical properties and biocompatibility of thermosensitive chitosan lactate and chitosan chloride hydrogels developed for tissue engineering application", Journal of Functional Biomaterials, 12 (2), 37.

[78] Pinto, R. V., Gomes, P. S., Fernandes, M. H., Costa, M. E., Almeida, M. M., (2020), "Glutaraldehyde-crosslinking chitosan scaffolds reinforced with calcium phosphate spray-dried granules for bone tissue applications", Materials Science and Engineering: C, 109, 110557.

[79] Sacco, P., Furlani, F., De Marzo, G., Marsich, E., Paoletti, S., Donati, I., (2018), "Concepts for Developing Physical Gels of Chitosan and of Chitosan Derivatives", Gels, 4 (3), 67.

[80] Akakuru, O. U., Isiuku, B. O., (2017), "Chitosan Hydrogels and their Glutaraldehyde-Crosslinked Counterparts as Potential Drug Release and Tissue Engineering Systems - Synthesis, Characterization, Swelling Kinetics and Mechanism", Journal of Physical Chemistry & Biophysics, 7 (3), 1-7.

[81] Xu, T., Liu, K., Sheng, N., Zhang, M., Liu, W., Liu, H., Dai, L., Zhang, X., Si, C., Du, H., Zhang K., (2022), "Biopolymer-based hydrogel electrolytes for advanced energy storage/conversion devices: Properties, applications, and perspectives", Energy Storage Materials.48, 244–262.

[82] Qu, B., Luo, Y., (2020), "Chitosan-based hydrogel beads: Preparations, modifications and applications in food and agriculture sectors – A review", International Journal of Biological Macromolecules, 152, 437-448.

[83] Manzoor, A., Dar, A. H., Pandey, V. K., Shams, R., Khan, S., Panesar, P. S., Kennedy J.F., Fayaz, U., Khan, S. A.., (2022), "Recent insights into polysaccharide-based hydrogels and their potential applications in food sector: A review", International Journal of Biological Macromolecules, 213, 987-1006.

[84] Jiao J., Huang J., Zhang Z., (2019), "Hydrogels based on chitosan in tissue regeneration: How do they work? A mini review", Journal of Applied Polymer Science, 136 (13), 47235.

[85] Murali, A., Lokhande, G., Deo, K. A., Brokesh, A., Gaharwar, A. K., (2021), "Emerging 2D nanomaterials for biomedical applications", Materials Today, 50, 276-302.

[86] Rasul, M. G., Kiziltas, A., Arfaei, B., Shahbazian-Yassar, R., (2021), "2D boron nitride nanosheets for polymer composite materials", npj 2D Materials and Applications, 5 (1), 56.

[87] Gonzalez-Ortiz D., Salameh C., Bechelany M., Miele P., (2020), "Nanostructured boron nitride–based materials: synthesis and applications", Materials Today Advances, 8, 100107.

[88] Ertuğ B., Addemir O., (2017), "Hegzagonal bor nitrür seramik tozlarının temel endüstriyel üretim yöntemleri" İTÜ Kimya-Metalurji Fakültesi, Metalurji Dergisi, 136, 54-58.

[89] Matveev, A. T., Permyakova, E. S., Kovalskii, A. M., Leibo, D., Shchetinin, I. V., Maslakov, K. I., Golberg, D.V., Shtansky, D.V., Konopatsky, A. S., (2020), "New

insights into synthesis of nanocrystalline hexagonal BN", Ceramics International, 46 (12), 19866-19872.

[90] Emanet, M., Sen, Ö., Taşkin, I. Ç., Çulha, M., (2019), "Synthesis, Functionalization, and Bioapplications of Two-Dimensional Boron Nitride Nanomaterials", Frontiers in Bioengineering and Biotechnology, 7, 363.

[91] Wang, J., Zhang, L., Wang, L., Lei, W., & Wu, Z. S.., (2022), "Two-dimensional Boron Nitride for Electronics and Energy Applications",. Energy and Environmental Materials, 5 (1), 10-44.

[92] Turhan, E. A., Pazarçeviren, A. E., Evis, Z., Tezcaner, A., (2022), "Properties and applications of boron nitride nanotubes", Nanotechnology, 33 (24), 242001.

[93] Zheng, Y., Hong, X., Wang, J., Feng, L., Fan, T., Guo, R., Zhang, H., (2021), "2D Nanomaterials for Tissue Engineering and Regenerative Nanomedicines: Recent Advances and Future Challenges", Advanced healthcare materials, 10 (7), 2001743.

[94] Lu, T., Wang, L., Jiang, Y., Huang, C., (2016), "Hexagonal boron nitride nanoplates as emerging biological nanovectors and their potential applications in biomedicine", Journal of Materials Chemistry B, 4 (36), 6103-6110.

[95] Lima, D. M., Chinellato, A. C., & Champeau, M., (2021), "Boron nitride-based nanocomposite hydrogels: preparation, properties and applications", Soft Matter, 17(17), 4475-4488.

[96] Li, B., Luo, Y., Zheng, Y., Liu, X., Tan, L., & Wu, S., (2022), "Two-dimensional antibacterial materials", Progress in Materials Science, 100976.

[97] Dhanavel, S., Sivaranjani, T., Sivakumar, K., Palani, P., Gupta, V. K., Narayanan, V., Stephen, A., (2021), "Cross-linked chitosan/hydroxylated boron nitride nanocomposites for co-delivery of curcumin and 5-fluorouracil towards human colon cancer cells",. Journal of the Iranian Chemical Society, 18, 317-329.

[98] Zou, Q., Xiong, S. W., Jiang, M. Y., Chen, L. Y., Zheng, K., Fu, P. G., Gai, J. G., (2021), "Highly thermally conductive and eco-friendly OH-h-BN/chitosan nanocomposites by constructing a honeycomb thermal network", Carbohydrate Polymers, 266, 118127.

[99] Quade, B. N., Parker, M. D., Occhipinti, R., (2021), "The therapeutic importance of acid-base balance", Biochemical Pharmacology, 183, 114278.

[100] Savitri, E., Juliastuti, S. R., Handaratri, A., Roesyadi, A., (2014), "Degradation of chitosan by sonication in very-low-concentration acetic acid", Polymer Degradation and Stability, 110, 344-352.

[101] Pardo-Castaño C., Bolaños G., (2019), "Solubility of chitosan in aqueous acetic acid and pressurized carbon dioxide-water: Experimental equilibrium and solubilization kinetics", The Journal of Supercritical Fluids, 151, 63-74.

[102] Aydin H., (2018), "Nanoyapılı Hegzagonal Bor Nitrür Üretimi ve Karakterizasyonu",. Fırat Üniversitesi Mühendislik Bilimleri, 30 (2), 269-275.

[103] Colomer, M. T., (2013), "Straightforward synthesis of Ti-doped YSZ gels by chemical modification of the precursors alkoxides", Journal of sol-gel science and technology, 67, 135-144.

[104] Islam N., Wang H., Maqbool F., Ferro V., (2019), "In vitro enzymatic digestibility of glutaraldehyde-crosslinked chitosan nanoparticles in lysozyme solution and their applicability in pulmonary drug delivery", Molecules, 24 (7), 1271.

[105] Kandile, N. G., Zaky, H. T., Mohamed, M. I., Nasr, A. S., & Ali, Y. G. (2018), "Extraction and Characterization of Chitosan from Shrimp Shells", Open Journal of Organic Polymer Materials, 8 (3), 33-42.

[106] de Queiroz Antonino, R. S. C. M., Lia Fook, B. R. P., de Oliveira Lima, V. A., de Farias Rached, R. Í., Lima, E. P. N., da Silva Lima, R. J., Peniche, Covas, C.A., Lia Fook, M. V., (2017), "Preparation and characterization of chitosan obtained from shells of shrimp (Litopenaeus vannamei Boone)", Marine drugs, 15 (5), 141.

[107] Nandiyanto ABD., Oktiani R., Ragadhita R., (2019), "How to read and interpret ftir spectroscope of organic material", Indonesian Journal of Science and Technology, 4 (1), 97-118.

[108] Elella, M. H. A., Shalan, A. E., Sabaa, M. W., Mohamed, R. R., (2022), "One-pot green synthesis of antimicrobial chitosan derivative nanocomposites to control foodborne pathogens",. RSC advances, 12 (2), 1095-1104.

[109] Barth A., (2007), "Infrared spectroscopy of proteins", Biochimica et Biophysica Acta (BBA)-Bioenergetics, 1767 (9), 1073-1101.

[110] Norouzi, Z., Abdouss, M., Tajiki, A., Rezaei, S. M., Nahooji, M. K., (2018), "Application of chitosan/PVA nanofibrous composite for molecular capture", 7 (3), 221-226.

[111] Queiroz, M. F., Teodosio Melo, K. R., Sabry, D. A., Sassaki, G. L., Rocha, H. A. O., (2014), "Does the use of chitosan contribute to oxalate kidney stone formation?", Marine drugs, 13 (1), 141-158.

[112] Lenza, R. F., Vasconcelos, W. L., (2001), "Structural evolution of silica sols modified with formamide", Materials Research, 4, 175–179.

[113] Ghosh B., Bhattacharya D., Mukhopadhyay M., (2021), "Fabrication of natural polysaccharide based hydrogel with utility to entrap pollutants", In Journal of Physics: Conference Series, Vol. 1797, No. 1, p. 012060.

[114] Kiefer J., Strk A., Kiefer AL., Glade H., (2018), "Infrared spectroscopic analysis of the inorganic deposits from water in domestic and technical heat exchangers", Energies, 11 (4), 798.

[115] Hu, X., Liu, J., He, Q., Meng, Y., Cao, L., Sun, Y. P., Chen, J., Lu, F., (2016), "Aqueous compatible boron nitride nanosheets for high-performance hydrogels", Nanoscale, 8 (7), 4260-4266.

[116] Boota M., Chen C., Yang L., Kolesnikov, A.L., "Probing Molecular Interactions at MXene-Organic Heterointerfaces", Chemistry of Materials, 32 (18), 7884-7894.

[117] Goycoolea, F. M., Argüelles-Monal, W. M., Lizardi, J., Peniche, C., Heras, A., Galed, G., Díaz, E. I., (2007), "Temperature and pH-sensitive chitosan hydrogels: DSC, rheological and swelling evidence of a volume phase transition", Polymer Bulletin, 58, 225–234.

[118] Kittur, F. S., Prashanth, K. H., Sankar, K. U., Tharanathan, R. N., (2002), "Characterization of chitin, chitosan and their carboxymethyl derivatives by differential scanning calorimetry", Carbohydr polymers, 49 (2), 185-193.

[119] Mukheem A., Shahabuddin S., Akbar, N., Miskon, A., Muhamad Sarih, N., Sudesh, K., Ahmed, Khan., Saidur, R., Sridewi, N. (2019), "Boron nitride doped polyhydroxyalkanoate/chitosan nanocomposite for antibacterial and biological applications", Nanomaterials, 9 (4), 645.

[120] Li, S., Lu, X., Lou, Y., Liu, K., Zou, B., (2021), "The Synthesis and Characterization of h-BN Nanosheets with High Yield and Crystallinity", ACS Omega, 6 (42), 27814-27822.

[121] Nadeem, A., Raza, M. A., Maqsood, M. F., Ilyas, M. T., Westwood, A., & Rehman, Z. U., (2020), "Characterization of boron nitride nanosheets synthesized by boron-ammonia reaction", Ceramics International, 46 (12), 20415-20422.

[122] Web 1, (2022),), https://www.news-medical.net/life-sciences/What-are-DNA-Nanomachines.aspx (Accessed Date: 10/05/2022)
[123] Web 2, (2022),), https://www.news-medical.net/life-sciences/What-are-DNA-Nanomachines.aspx (Accessed Date: 10/05/2022)
[124] Web 3, (2022),) https://www.biolinscientific.com/blog/biomaterials-vs-tissue-engineering-what-is-the-difference (Accessed Date: 10/05/2022)
[125] Web 4, (2022),) https://www.thoughtco.com/how-many-atoms-in-human-cell-603882 (Accessed Date: 10/05/2022)

BIOGRAPHY

Burak ERAYHAN is currently a MSc student in the programme of Nanoscience and Nanoengineering in Institute of Nanotechnology at Gebze Technical University (GTU). He received his Bachelor's Degree in Bioengineering from Gaziosmanpasa University in Turkey. He internship for 20 working day in the molecular biotechnology laboratory of the Faculty of Agriculture at Tokat Gaziosmanpasa University and 20 working-day summer internship at the BioMEMS - BioNEMs laboratory affiliated with the Electrical and Electronics Engineering department at Kayseri AGU University. He has successfully completed the 'Experimental Animal Use Certificate' training organized by GTU-Hadyek between 12-21 December 2022 and entitled to receive a Group A Certificate. He also attended and presented a presentation at Internatıonal Marmara Sciences Congress on December 09, 2022.